UNIVERSITÀ DEGLI STUDI DI PADOVA

SCUOLA DI SCIENZE

Dipartimento di Geoscienze
Direttore Prof.ssa Cristina Stefani

TESI DI LAUREA MAGISTRALE IN GEOLOGIA E GEOLOGIA TECNICA

VERY-HIGH RESOLUTION SEISMO-ACOUSTIC AND MORPHOLOGIC INVESTIGATIONS OF A HOLOCENE TRANSGRESSIVE SYSTEM IN THE NORTHERN ADRIATIC SHELF

Relatore: Dott. Alessandro Fontana
Correlatore: Dott.ssa Annamaria Correggiari

Laureando: Livio Ronchi

ANNO ACCADEMICO 2014 / 2015

Contents

Abstract

The Adriatic Sea has been characterized by a progressive sea-level increase since the end of the Last Glacial Maximum, about 20 ka ago; in that period the sea-level was situated roughly 120 m below the present one, and the Adriatic Sea was completely enclosed in the Mid Adriatic Depression. During the last 20 000 years the rising sea induced a north-shifting of the coastal environments and of the rear alluvial plain, thus producing a characteristic and well-recognizable pattern in the sedimentary succession, which is constituted by a constant aggradation and by the overlapping of coastal and marine deposits on the previous alluvial plain deposits.

The reconstruction of the various steps of the sea-level rise, in addition to the academic interest, can be useful in many application areas, such as the seek for exploitable sand bodies and the study of the evolution of a coastal environment under condition of sea transgression.

In this work several seismo-acoustic profiles are analyzed, along with other geophysical data from a 45 km^2 area of the northern Adriatic Sea; the majority of these data were collected during the CNR-ISMAR Bologna ASCI14 marine survey, onboard of the R/V Urania.

Through the analysis of these profiles three detailed 3D paleo-surfaces were reconstructed, representing different moments during the sea-level rise. The combination of data inferred by paleo-morphologies and sedimentary structures allows to hypothesize the evolution of the study area approximately during the last 10 000 years: the depositional environment gradually shifts from an alluvial plain, characterized by meandering-pensile rivers, to a lagoon-brackish swamp, which was then drowned and covered by prodelta-offshore deposits.

The area is characterized by the presence of a deep erosive scour, which has been interpreted as a tidal inlet on a stratigraphic and geomorphological basis. This information has interesting implications on the interpretation of the numerous similar erosive features of the northern Adriatic basin. The presence

of the tidal inlet represents a clear indicator of the sea-level position and allows to estimate the age of the linked lagoon-brackish swamp deposits which, basing on the observed sea-level rise curve for the Adriatic Sea, is likely comprised between 9 800 and 9 850 years BP. The further comparison of this inferred age with a geophysical model for the sea-level rise in the northern Adriatic Sea allows to estimate a subsidence of 0.02 cm/year for the area, which is well-comparable to other data from published works.

This work concludes with the presentation of some paleo and present analogous morphologies and stratigraphies, which may be compared to the study area in order to obtain some important information about their evolutionary history.

The Adriatic area is characterized by a huge amount of geophysical data and cores collected during various campaigns; this high-resolution analysis may be therefore performed in other areas, in order to better understand the recent evolutionary history of the Adriatic basin.

Sommario

L'evoluzione tardo quaternaria del bacino Adriatico è strettamente legata alla risalita del livello marino; durante l'ultimo massimo glaciale (Last Glacial Maximum, LGM), conclusosi approssimativamente 20 000 anni fa, la superfice d'acqua era completamente confinata nella depressione medio-Adriatica (MAD). Con il successivo aumento di temperatura e progressivo scioglimento dei ghiacciai continentali il livello marino cominciò a risalire, andando quindi progressivamente ad occupare porzioni sempre maggiori della pianura alluvionale del LGM, sino ad arrivare all'attuale estensione del Mare Adriatico.

La risalita del livello marino ha segnato profondamente la successione sedimentaria Adriatica, andando a costituire dei corpi dalle caratteristiche ben riconoscibili. Queste unità, in questo lavoro come in altri riguardanti il bacino Adriatico, sono state analizzate con gli strumenti della stratigrafia sequenziale, distinguendo quindi:

- Un corpo comprendente FSST e LST, costituito dai depositi di piana alluvionale legati alla precedente regressione marina e alla fase di stazionamento basso del mare;
- Un corpo corrispondente alla TST, costituito da depositi aggradanti di piana alluvionale, depositatisi durante la trasgressione marina distale, e da depositi lagunari-costieri-marini, afferenti all'effettiva ingressione marina nell'area considerata;
- Un corpo corrispondente alla HST, depositatosi in ambiente sommerso.

Il lavoro di tesi si è basato essenzialmente sulla raccolta, l'elaborazione e l'interpretazione di dati geomorfologici e stratigrafici provenienti da un'area dell'Adriatico settentrionale in cui affiorano depositi tardo quaternari, situata circa 30 km al largo di Comacchio, ad una profondità compresa tra i -30 e -35 m slm.

I dati sono stati raccolti durante la crociera oceanografica ASCI14, realizzata tra il 30/09 ed il 13/10 2014 dal CNR-ISMAR di Bologna (responsabile Dr.ssa A. Correggiari) in collaborazione con il Dipartimento di Geoscienze dell'Università di Padova (Dr. A. Fontana), a bordo della Nave Oceanografica Urania. Tali dati sono, per la quasi totalità, di carattere geofisico, acquisiti tramite CHIRP Sub-Bottom Profiler e Multibeam sonar: l'area in studio, la quale presenta un'estensione approssimativa di 45 km^2, è definita da 36 profili CHIRP, per una lunghezza totale di 270 km. Contestualmente ai profili CHIRP è stata acquisita anche la batimetria del fondale tramite metodologia Multibeam sonar.

Oltre ai dati di carattere geofisico, durante ASCI14 sono stati raccolti anche numerosi campioni di sedimento, mediante carotatore a gravità, vibrocarotiere e benna Van Veen. I carotaggi effettuati non ricadono all'interno dell'area considerata dalla tesi; per validare le analisi geofisiche sono quindi state utilizzate alcune carote stratigrafiche prelevate nelle vicinanze, con le medesime tecniche, durante precedenti crociere condotte dal CNR-ISMAR.

In questo lavoro il dato di principale interesse è la stratigrafia dei depositi superficiali, la quale è fornita dalle analisi CHIRP. I profili sismo-acustici acquisiti durante la navigazione sono stati processati ed analizzati mediante i software SwanPro, Kogeo, SeisPrho, LibreOffice Calc e ArcGis, con lo scopo iniziale di evidenziare alcuni riflettori corrispondenti a superfici di particolare interesse ai fini della ricostruzione dell'evoluzione dell'area in esame. Tali riflettori si distinguono per la forte risposta acustica e per la loro continuità, sia lungo il medesimo profilo che fra profili diversi.

Le tre principali superfici individuate, così come i relativi corpi sedimentari, sono state interpretate con gli strumenti della stratigrafia sequenziale. Va notato che i profili non sono stati migrati nella scala dei tempi visto il limitato miglioramento ottenibile su questa tipologia di dati.

Digitalizzando i riflettori sopra descritti si è resa possibile una ricostruzione tridimensionale delle corrispondenti superfici, le quali sono quindi state interpretate da un punto di vista geomorfologico, oltre che stratigrafico. Questa analisi ha individuato le seguenti forme:

- *TS* (*Transgressive Surface*): Tale superficie è caratterizzata da canali fluviali meandriformi con i relativi depositi di rotta fluviale; essa è inoltre contraddistinta da una vasta area erosiva canalizzata, probabilmente legata all'ingressione marina. L'ambiente in cui si è formata la *TS* è riconducibile ad una pianura alluvionale aggradante, la quale è stata

direttamente interessata da un'ingressione marina solo durante gli stadi finali della sua esposizione. Sulla base delle datazioni radiometriche disponibili per le aree circostanti, la *TS* ha un'età di $10\,955 \pm 225$ cal. a BP;

- *AS* (*A Surface*): Questa superficie si sviluppa tramite una rete di dossi fluviali appartenenti a diverse generazioni. È inoltre solcata da un importante canale erosivo, il quale arriva ad una profondità di 15 m rispetto alla quota media della *AS*; questo canale è stato interpretato come una bocca tidale, andando quindi a costituire un chiaro indicatore del livello marino. L'ambiente della *AS* è strettamente legato alla vicina presenza del mare in risalita, come testimoniato dalla bocca tidale e dai depositi lagunari che la sigillano. Questa superficie, sulla base dei dati disponibili per zone limitrofe, è datata a $10\,307 \pm 115$ cal. a BP.

- *RS* (*Ravinement Surface*): non sono individuabili particolari morfologie data la natura fortemente erosiva di questa superficie, generata dall'azione delle onde. La datazione radiometrica disponibile per tale superficie è di $9\,845 \pm 115$ cal. a BP.

Varie ulteriori analisi sono state condotte a partire da questi risultati, le quali hanno permesso di elaborare nuove informazioni sulla zona:

- La rappresentazione tridimensionale delle superfici ha permesso il calcolo dei volumi compresi fra le stesse e di volumi definiti da singole morfologie, quali i dossi fluviali. Questi dati sono di particolare interesse nel caso della ricerca di depositi sabbiosi sommersi, utilizzabili per il ripascimento costiero;

- Lo studio ha consentito di ricostruire la posizione del livello marino relativo subito dopo la formazione della *AS*. Infatti, quando era attiva la bocca tidale, essa era in connessione con una zona lagunare, a sua volta in fase con il livello marino dell'epoca. La profondità dei depositi lagunari fornita dalle linee CHIRP, individuata a -33 m slm (-2; +0,5 m), ha permesso quindi di datare questa posizione del livello marino a 9,8 cal. ka BP, e di fissare una possibile porzione di linea di costa, in buon accordo con le datazioni disponibili in letteratura nell'area al largo del Po. Per ricostruire l'età dei depositi, conoscendone la profondità attuale,

è stata impiegata la curva di risalita del livello marino per l'Adriatico. La misura dell'antico livello marino relativo è affetta da un'incertezza legata alla posizione dei depositi lagunari analizzati rispetto ad esso. Vi sono poi errori meno significativi connessi ai problemi di misura della posizione e della batimetria (es. dGPS, marea, pressione atmosferica);

- Utilizzando il dato descritto al punto precedente ed un modello geofisico per la risalita del livello marino, è stato possibile valutare la subsidenza dell'area in studio negli ultimi 10 000 anni, ottenendo un valore di 0,2-0,3 mm/anno. Tale intervallo denota un limitato sprofondamento della zona rispetto all'area costiera attuale, presso Comacchio, dove raggiunge 0,8-1,0 mm/anno;

- Si è dimostrato che la valle incisa riempita, documentata nel settore più orientale (profili AS14-AS7), corrisponde ad una bocca tidale che raggiungeva i 15 m di profondità rispetto alla superficie esterna correlata. Verso est e verso ovest, tale morfologia erosiva va scomparendo, testimoniando la limitata continuità della depressione.

  Questo ultimo punto riveste una notevole importanza a scala dell'intero Adriatico, in quanto erano state precedentemente individuate numerose altre valli incise con dimensioni simili e che si sviluppano su distanze inferiori a 1 km, assottigliandosi improvvisamente sino a scomparire. Tali forme sono in genere descritte in letteratura come segmenti di valli incise di natura fluviale. Il lavoro di questa tesi fornisce, quindi, una nuova re-interpretazione di una parte di queste morfologie, consentendo anche di riconoscere varie posizioni della linea di costa durante l'ultima trasgressione. L'evidente risposta sismo-acustica, che le rende facilmente individuabili tramite i profili CHIRP, rende ancora più interessanti queste incisioni, le quali, se studiate su ampia scala, potrebbero fornire ulteriori dettagli sulla storia evolutiva dell'Adriatico.

Chapter 1

Introduction

The following research work was developed within the frame of the CNR-ISMAR Bologna Institute and of the Geoscience Department of the Padua University areas of interest.

One of the main research topics of these authorities, related to the field of marine geology, is the reconstruction of a Holocene detailed relative sea-level rise curve for the Mediterranean basin, which is the basis for several further investigations, such as:

- The response of a coastal system affected by a rapid sea level rise, which represents a dramatically actual situation, in order to "develop adequate plans for coastal management and protection" (Amorosi et al., 2008, IPCC, 2014). The NW Adriatic coastal area is particularly vulnerable to the hazards induced by the sea-level rise, such as flooding, salt-water wedge intrusion and subsidence, due to the superposition of natural and anthropogenic processes (Bondesan et al., 1995, Amorosi et al., 2008, Lambeck et al., 2011);

- The reconstruction of the paleo-geography and -geomorphology of the area, in order to define economically exploitable resources of clean sand, used in the activity of beach nourishment. The combined action of sea-level rise and intensified storminess is the cause of the present beach erosion, which represents a huge problem both from the economic (tourism and other activities tied to the seashore) and, moreover, from the hinterland flooding hazard points of view;

- The analysis of a recent example of sea level rise affecting a peculiar

environment, such as the one of the Adriatic Sea, characterized by a very low topographic gradient, which can help to explain analogous deposits in the geological record and therefore contributing to the international research, both in the academic and oil fields.

Motivated by an interest in the field of the Quaternary and geomorphology research, I have approached the subject of marine geology and had the chance to participate to the ASCI14 oceanographic cruise, organized by the CNR-ISMAR Bologna Institute (scientific responsible Dr. A. Correggiari) with the contribute of the Geoscience Department of the Padua University (Dr. A. Fontana).

During this campaign a huge amount of data have been collected, consisting in seismic profiles, with a CHIRP Sub-Bottom Profiler, bathymetries, with a Multi Beam echosounder, and several cores. The aim of the ASCI14 was the further investigation of the themes described above, with a special focus on the analysis of the paralic transgressive sand bodies, in which the Emilia-Romagna region have interest for the production of a geodatabase as an instrument for their exploitation, and the analysis of the paleo-drainage of the Adriatic platform, once again in order to track the sandy deposits tied to the channel systems.

The data that were analyzed in this work are only a small portion of the total amount collected during the whole campaign; the main points that are described in this thesis are:

1. Contextualization of the data into a regional framework with the use of published references and data collected in other campaigns;

2. Analysis of the data, both from a geomorphological and a stratigraphical viewpoint;

3. Digitalization of the data;

4. Reconstruction of some paleo-surfaces in order to visualize and describe their morphology in the context of the Holocene relative sea-level rise;

5. Tentative to reconstruct depositional histories and environments for these surfaces;

6. Tentative to correlate the visible morphologies to the position of the paleo sea-level, in order to possibly date them within a good confidence interval,

thus reconstructing another piece of the paleo Adriatic history (Figure 2.6);

7. Assessment of the sediment volumes at stake during the sea level rise in this area;

8. Comparison between the considered case with other study cases, both in the geological record and in present environments.

Chapter 2

Overview

2.1 Study Area

The following research work is based on a portion of data collected during the ASCI14 oceanographic survey: the analyzed data are inscribed in a small rectangular-shaped area (approximately 45 km^2, 6 km width per 7.5 km height), delimited to the north by the 44.717° parallel, to the east by the 12.708° meridian, to the south by the 44.649° parallel and to the west by the 12.634° meridian (all the previous values are express in decimal degrees). This area is located in the Adriatic Sea, in the Italian territorial waters, facing the Emilia-Romagna shores and approximately 30 km offshore the Valli di Comacchio coasts (Figure 2.1).

2.2 Adriatic Sea Morphology

The Adriatic Sea is a narrow, shallow, semi-enclosed basin (approximately 200 km wide per 800 km long) which divides the Italian Peninsula from the Dinaric-Balcanic area; this basin is bordered to the southwest by the Apennines, to the north by the Alps and to the northeast by the Dinaric Alps. The Otranto strait separates the Adriatic Sea from the Ionian Sea to the south (Figure 2.2).

The Adriatic basin can be subdivided into three main morpho-bathymetrical domains (Correggiari et al., 1996, Vai & Martini, 2001, Storms et al., 2008, Trincardi et al., 2011):

1. An extended continental shelf, which occupies the northern sector of the Adriatic basin, characterized by a low topographic gradient (roughly

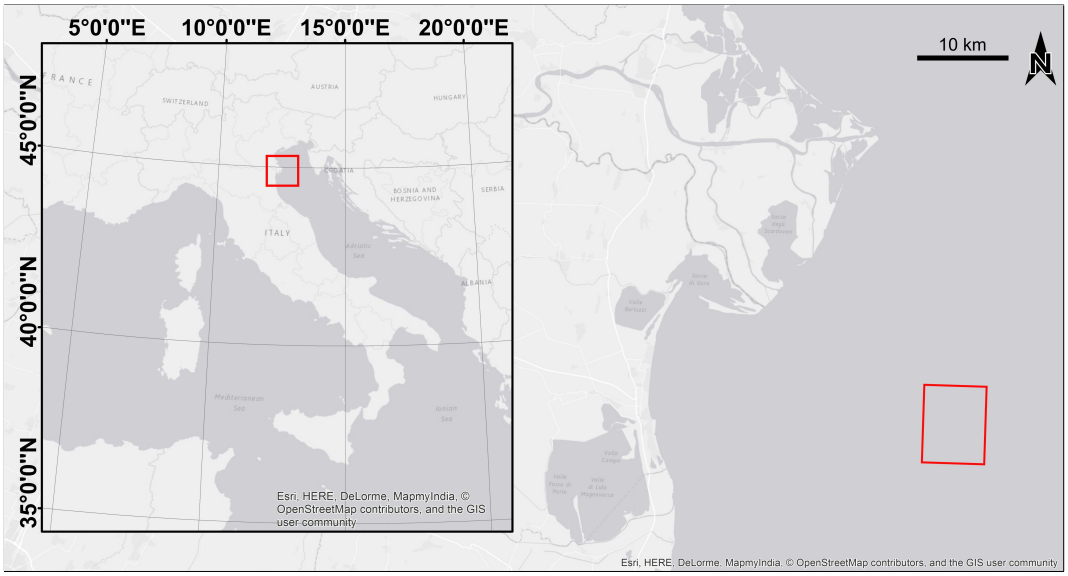

Figure 2.1: Contextualization of the study area, represented by the coloured shape.

0.02°, which corresponds to a 0.04% slope). This area shows a complex microtopography, with metric size reliefs and scours which reach a depth of 4-5 m; in proximity to the Italian shoreline the shown depth is always less than 10-14 m due to the presence of a belt composed of muddy delta deposits, whereas the Slovenian and Croatian side is characterized by a steeper topography;

2. The middle region, which comprises several slope basins, including the Meso-Adriatic Depression (MAD), a basin with a maximum depth of 255 m, characterized by a NE-SW trend and delimited by a small platform on the west and south edges, and by the structural high of the Dosso Gallignani on the east side;

3. The southern part beyond the Pelagosa isles, which reaches a depth of 1200 meters.

The Italian coasts of the north Adriatic are dominated by lagoon systems, which a total extent of about 820 km^2. The main lagoon systems are the Grado-Marano Lagoon, Venice lagoon and the lagoons and marshes in the Po Delta (e.g. Sacca di Goro, Scardovari, Canarin) (Trincardi et al., 2011).

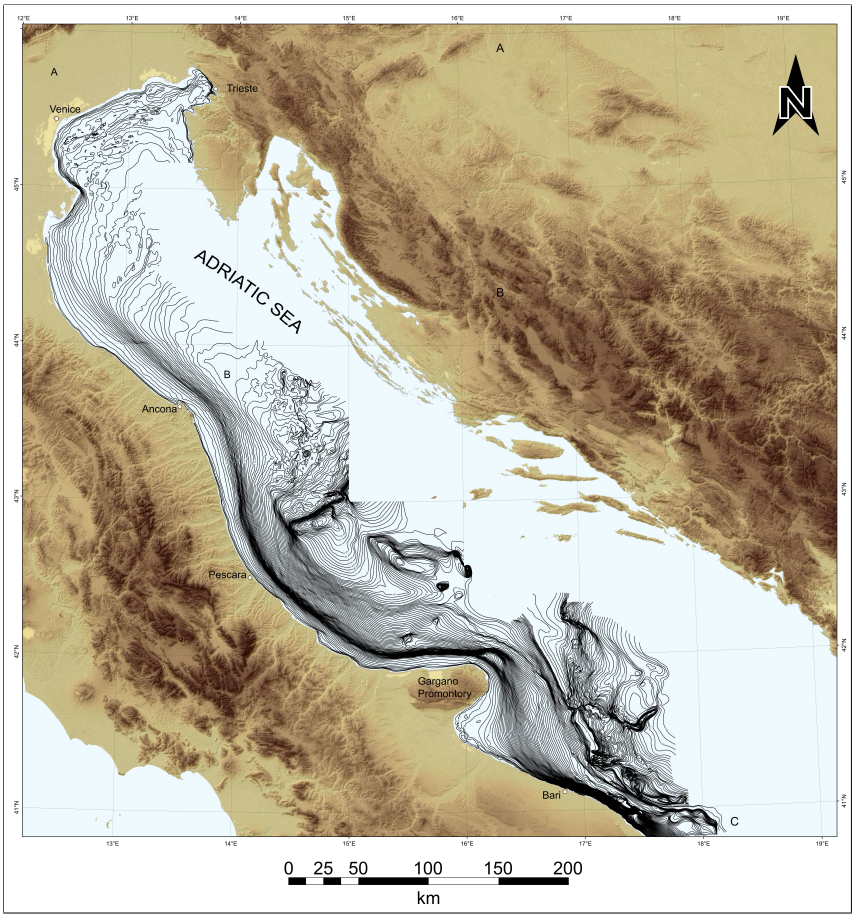

Figure 2.2: The Adriatic basin; the isobaths are drawn only for the Italian side. Modified from Trincardi et al., 2014.

2.3 Oceanography

The Adriatic Sea shows a microtidal regime, with a tidal range lower than one meter, and is dominated by a cyclonic circulation driven by thermohaline currents (Correggiari et al., 2001, Cattaneo et al., 2003). The prevailing winds are the Bora, blowing form northeast, and the Sirocco, from southeast. The wind waves show a statistical amplitude peak of about 0.5 m with a 3 to 4 seconds period. The strongest storms follow the directors of the main winds described above and storm waves can reach amplitudes of 9 m in exceptional events (Cattaneo et al., 2003).

The northern portion of the Adriatic Sea receives the higher fluvial discharge of the entire Mediterranean basin, and is very susceptible to its variations and to atmospheric conditions due to its limited depth. The Po River, with a mean discharge of 1470 m^3s^{-1} (from 1918 to 2009), supplies half of the total fluvial

discharge in the northern Adriatic (Syvitski & Kettner, 2007).

Three main water masses can be described within the Adriatic water body (Cattaneo et al., 2003, Trincardi et al., 2011):

1. A superficial body (ranging from the mean sea level to a depth of 30 meters) with an upper 10 m layer of less saline and cooler waters of coastal origin, mainly Po river runoff, prone to seasonal variability;

2. An intermediate body (LIW Levantine Intermediate Water) ranging from 30 to 130 meters depth with a salinity peak at about 80 m depth;

3. A bottom-water region which shows the maximum density values.

The Adriatic water circulation is dominated by three main forcings (Cattaneo et al., 2003, Trincardi et al., 2011):

1. River forcing, due to the 5700 m^3s^{-1} of fresh water discharge, associated to the loss of heat;

2. Wind forcing, insisting on the surface and responsible for evaporation and heat loss, with the consequent production of deep waters and seasonal circulation changes;

3. Morphologic forcing, due to the Otranto Strait (reinforced by the Sirocco wind) through which warm and salty water enters and balances the effects of the first two forcings.

In the winter periods, the Bora (a strong katabatic wind) induces two large gyres that affect the entire water column with a SE component along the Italian coast (Correggiari et al., 2001).

Other factors influencing the Adriatic circulation are bound to gravitational tides, due to resonance effects with the Ionian Sea tides, southeast wind associated seiche (*sessa* in Italian) and storm setups (Trincardi et al., 2011).

2.4 Adriatic Catchment

The Adriatic clastic sources are not evenly distributed; the major sediment loads are observed in the northern and western edges of the basin and four main regions can be described: the eastern Alpine rivers, with a solid discharge of 3 x 10^6 ta^{-1}, the Po river catchment, with a sediment load of 15 x 10^6 ta^{-1},

the Apennine rivers, which deliver 32.2 x 10^6 ta^{-1}, and the rivers south of the Gargano promontory with a solid discharge of 1.5 x 10^6 ta^{-1}. Whereas the drainage area of the eastern Apennine rivers is less than half of that of the Po river, their sediment load is greater: the eastern Apennine rivers have the highest sediment yield of the region (Cattaneo et al., 2003, Trincardi et al., 2011).

The sedimentary contribution from the Croatian margin is negligible due to the characteristic shore-parallel geological structure which acts as sedimentary traps, and also due to the little size of the rivers which drain a carbonate prevailing area dominated by karstic processes (Cattaneo et al., 2003, Trincardi et al., 2011).

These data could be considered representative for the last 5500 years (corresponding to the late-Holocene highstand) and fit with the known features of the HST muddy wedge (Cattaneo et al., 2003).

2.5 Pre-Holocene Geological Evolution

The geological evolution of the Adriatic area shows the typical features of a passive continental margin evolution, from the Permo-Triassic onset of the Tethydean ocean to the Apenninic orogenesis due to the convergence between the European and African plates (Trincardi et al., 2011); the history of the Adriatic sector has been reconstructed with the data provided by the oil wells of the western Adriatic Sea.

During the Lower Jurassic Epoch the carbonatic platform sedimentation was substituted by a pelagic carbonate sedimentation because of the subsidence and probably also in consequence of the establishment of adverse climatic conditions; only in few areas the carbonatic platform has still remained active, determining the typical platforms and basins configuration of the southern Tethys edge (Bernoulli, 2001, Allen & Allen, 2005).

The Mesozoic Era was characterized by a prevailing carbonatic deposition, which gradually turned to a prevailing silicoclastic deposition during the Cenozoic Era (Trincardi et al., 2011).

A peculiar event took place during the Messinian Age: a relative sea-level fall combined to hyperhaline conditions which affected the whole Mediterranean Sea induced the exposure of the Adriatic basin, which was exposed to subaerial erosion and evaporitic deposition (Roveri et al., 2005).

From a regional viewpoint the Adriatic Sea is an epicontinental basin superimposed on the relics of the Adria plate: the northern Adriatic basin can be identified as the pro-foreland basin of both Apennines and Dinaric thrust belts (Vai & Martini, 2001, Cattaneo et al., 2003, Allen & Allen, 2005).

2.5.1 Western Adriatic Basin

The western portion of the northern and central Adriatic corresponds to a foredeep basin, which represents the most recent of a series of westward migrating foredeep basins formed during the Apennine orogenesis (Trincardi et al., 2011). This foredeep basin is delimited in its western portion by the thrust front of the Northern Apennines, which is characterized by a subdivision into four main folded arcs: the Monferrato, Emilia and Ferrara folds, which are buried under the Po plain, and the Adriatic fold. (Castellarin, 2001, Trincardi et al., 2011) (Figure 2.3). In some zones the frontal deformation is widespread on huge areas which gradually turn into the foreland (low strain front end; Morley, 1986), whereas in other zones the deformation is focused in narrow areas sharply separated from the undeformed foreland (high strain front end; Morley, 1986).

This foredeep basin started to develop during the Pleistocene Epoch; the seismic reflector recognizable as the plio-quaternary depositional surface is bended toward the Apennine, and the surrounding strata terminate on it with an onlap geometry with a maximum depth of 6 000 meters (Structural model of Italy, 1990-1992). The Adriatic Plio-Quaternary foredeep is, on the whole, characterized by two main depocentres, linked to the minimum Bouguer anomalies (Allen & Allen, 2005) and separated by a structural high in the Ancona zone.

The Gargano area is characterized by a deformation induced by a N-S and a NE-SW stress field due to the Dinaric front push (Bertotti et al., 1999); also the Central Adriatic zone shows a similar deformation with a W-NW/E-SE trending belt of structural highs, which run from the city of Ancona to the island of Pelagosa (CADB, Central Adriatic Deformation Belt). The base of the Plio-Quaternary deposits is affected by folds aligned along this belt: seismic profiles across the CADB indicate that deformation was active during the Quaternary (Argnani et al., 1997).

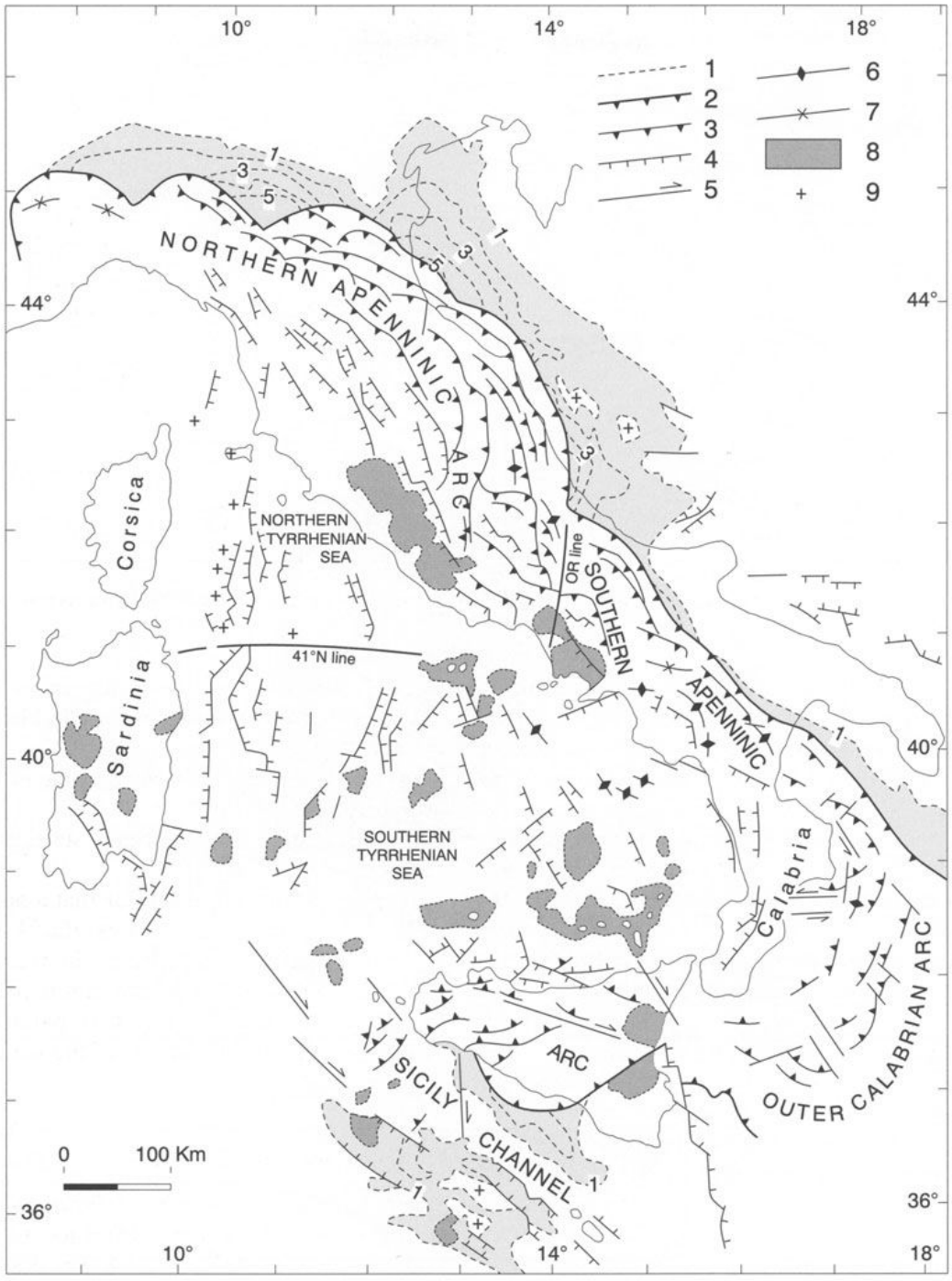

Figure 2.3: Structural map of the Apennine and surrounding seas. (1) Base of Pliocene-Quaternary isobaths in km; (2) Front of the thrust belt; (3) Major post-Tortonian thrusts; (4) Normal faults; (5) Strike-slip faults; (6) Antiforms; (7) Synforms; (8) Volcanoes; (9) Intrusive bodies. From Vai & Martini, 2001.

2.5.2 Eastern Adriatic Basin

The eastern sector of the Adriatic basin is affected by the Dinaric Alps foredeep, and shows a strong Bouguer anomaly. In the northern and central portions this foredeep is dated before the Pliocene: the Pliocene bottom is characterized by sub-horizontal dipping and little depth; underneath this surface the seismic profiles have highlighted a sedimentary wedge quickly thickening toward east, constituting the foredeep Eocene-Oligocene infilling. In the southern Adriatic, beneath the Plio-Quaternary foredeep an Oligocene-Miocene sedimentary wedge is observable, representing the infilling of the prior Dinaric-Hellenic foredeep (Trincardi et al., 2011).

The related quite undeformed foreland basin, is located in the Istrian Peninsula and in the Apulian region; those areas show poor Plio-Quaternary deposits thickness and scarce vertical tectonics.

2.6 Quaternary Evolution

2.6.1 Sea Level History - Quaternary Glacio-eusatic Cycles

The evolution of the Adriatic basin morphology has been strongly influenced by the relative sea-level position during the last millenia, and especially in the Holocene Epoch. The relative sea-level is controlled by several factors, among which can be recognized:

- The eustatic component, related to the global water volume variations (growth/melting of continental ice caps and thermal expansion of water bodies) and the ocean basins volume variations (related to the spread rate variations of mid-ocean ridges and different lithospheric plates deformation state);
- The isostatic vertical movements of the crust, which may be downward, due to overburdens (e.g. ice caps, lithosphere cooling) or upward, in consequence of mantle adjustments after the removal of the overburdens (e.g. melting of ice caps);
- The subsidence, due to compaction of sediments and expulsion of fluids, which determines a local downward shift of the sea bottom.

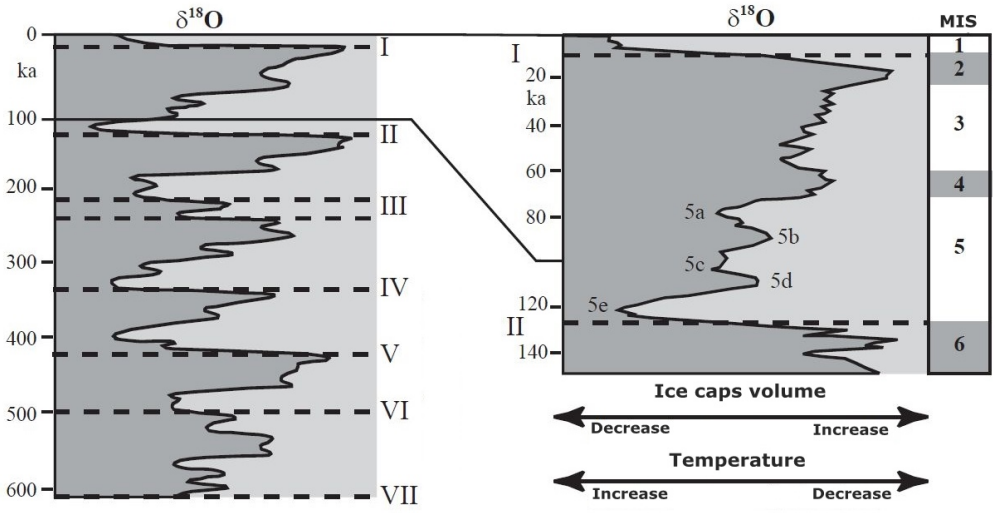

Figure 2.4: Quaternary glacial periods: the main terminations which divide glacials and interglacials periods are indicated by the Roman numeral; A more detailed time scale with the relative MIS is shown for the last glacial cycle on the right. Modified from Trincardi et al., 2011.

The glacio-eustatic cycles, during the Quaternary and particularly in the last 800 000 years, were determinant for the continental margin deposition, because of both their amplitude (up to 100 m) and frequency (Figure 2.4). During the late Quaternary period the rapid succession of glacial and interglacial periods have led to several sea-level fluctuations, characterized by long sea level falling related to the growth of ice caps and inlandsis, interrupted by sea level rises induced by the melting of ice caps and the thermal expansion of water.

The most recent glacial-interglacial cycle began with the general sea-level fall which followed the last interglacial (MIS 5e, 132 000-116 000 years BP, +6 ±3 m above MSL), intercalated by some periods of minor sea-level rise (as MIS 3, 58 000-29 000 years BP, around -60 m MSL) and with a peak corresponding to the Last Glacial Maximum, 29 000-19 000 years BP (Martinson et al., 1987, Bard et al., 1990, Ferranti et al., 2006).

The last sea-level rise, driven by the destabilization of northern hemisphere inlandsis and western Antarctic glaciers, was characterized by a complex pattern, with the alternation of sudden rise and stasis episodes (Figure 2.5) (Fleming et al., 1998, Trincardi et al., 2011).

Though several aspects are still undefined, it is widely accepted that a sequence of three melting phases occured during the last sea-level rise (Figure 2.6):

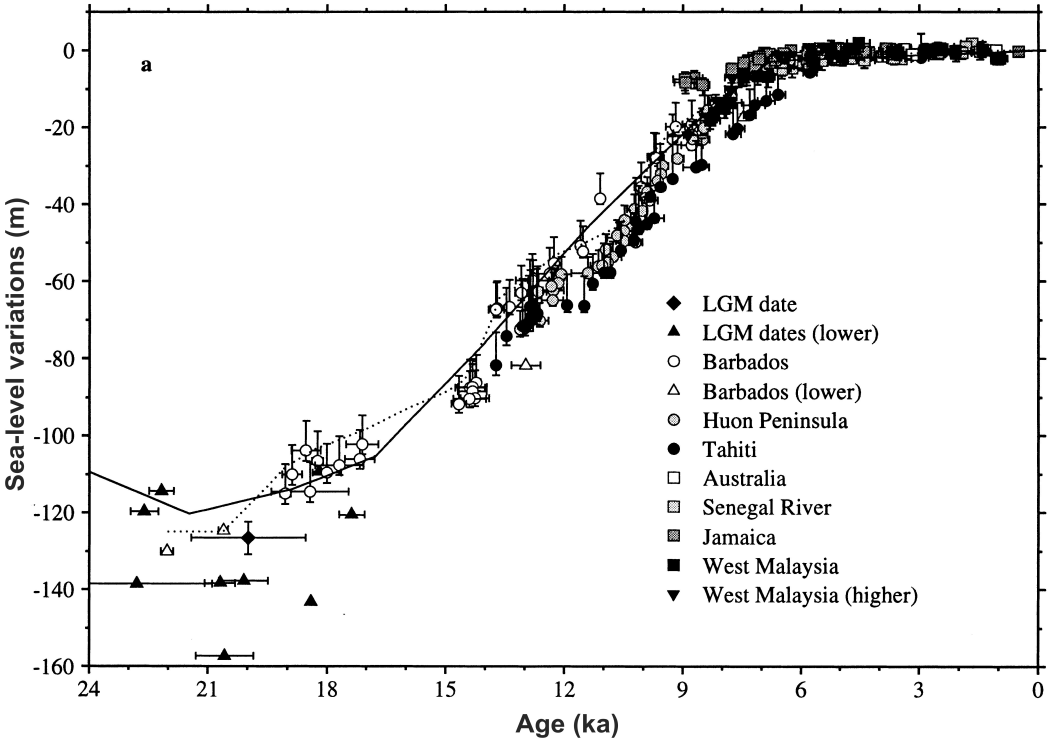

Figure 2.5: Post LGM sea-level rise curve based on data collected in several continental platform. From Fleming et al., 1998.

- the first rapid rise took place around 19 600 years ago (Hanebuth et al., 2008);

- the second high speed sea-level rise phase (about 25 m in 1500 years) took place between 14 650 and 14 310 years ago (MWP-1A, coeval to the Bølling interstadial) (Deschamps et al., 2012);

- the third strong rise coincided with the end of the cold phase of the Younger Dryas stadial (MWP-1B, 9 700 BC) (Fairbanks, 1989, Blanchon & Shaw, 1995, Asioli et al., 2001).

During the LGM the Adriatic Sea was reduced to a small, shallow and semi-enclosed basin which occupied the MAD and the southern portion of the present Adriatic Sea, whereas the northern sector was exposed to subaerial conditions (Correggiari et al., 1996). The post 18 ka relative sea-level rise described above took place over the low-gradient alluvial plain originated during the low-stand, determining a surface spread which, 5.5 ka BP, reaches up to 8 fold the lowstand surface, with a shoreline placed roughly 30 km toward the

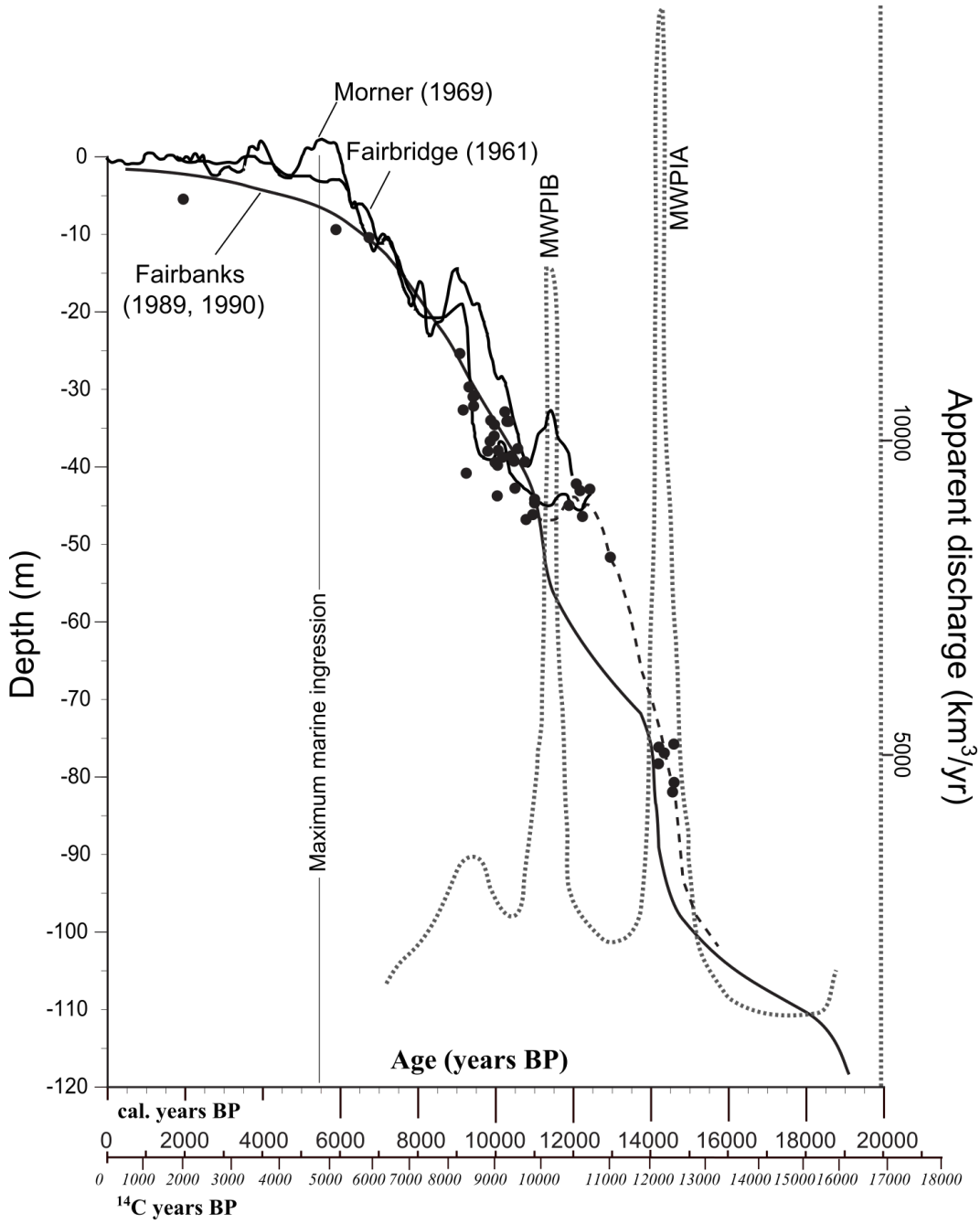

Figure 2.6: Post LGM sea-level rise curve based only on data collected in the Adriatic continental platform (black dashed line). The curves of Fairbridge (1961), Morner (1969) and Fairbanks (1989) are shown for comparison, along with the rate of meltwater discharge (dotted gray line). The points represent the data collected in the Adriatic basin. Modified from Correggiari et al., 1996

.

hinterland compared to the modern shoreline in the area of the present Po Delta (Correggiari et al., 1996, Amorosi et al., 2008) (Figure 2.7).

The sea-level rise defined a complex depositional pattern which will be described in the paragraph 2.6.4.

2.6.2 Paleo-oceanography

Storms et al., (2008) tried to reconstruct the paleo-environment of the Adriatic Sea during the sea-level rise through the implementation of some simple models; the results show a paleo tidal amplitude which gradually increased distancing from the actual shoreline (hence the tidal amplitude was higher when the sea level was lower) counterposed to a decrease of paleo wave height, distancing from the actual shoreline, due to a decrease of the fetch. (Figure 2.8)

2.6.3 Subsidence

The subsidence refers to the vertical motion of an area; it can be induced by subduction or other tectonic processes, by sediment compaction and fluids expulsion and by loading - unloading of a surface (e.g. formation and melting of ice caps). The reconstruction of the relative sea-level rise curve requires the knowledge of the subsidence history of the area.

There is no comprehensive analysis for the offshore area of the north Adriatic and, in particular, in the study area two subsidence ratios were inferred using different models: the Lambeck model shows a subsidence ratio of 0.3 mm/a for the Holocene, whereas the Spada-Stocchi model yields a ratio of 1 mm/a; according to the cores collected in the area of the Po Delta, the former datum may be the closer to the real subsidence ratio (Lambeck et al., 2004, Storms et al., 2008, Antonioli et al., 2009, Lambeck et al., 2011, Maselli et al., 2010).

2.6.4 Sequence Stratigraphy Approach and Late Quaternary Evolution

Sea level oscillations and variations of accommodation space are recorded in the sedimentary bodies of the Adriatic continental shelf; in particular, according to previous works (Trincardi et al., 2011, Trincardi & Argnani, 2011), the sequence stratigraphy approach was followed, with the distinction of Falling-Stage Systems Tract (FSST), Lowstand Systems Tract (LST), Transgressive

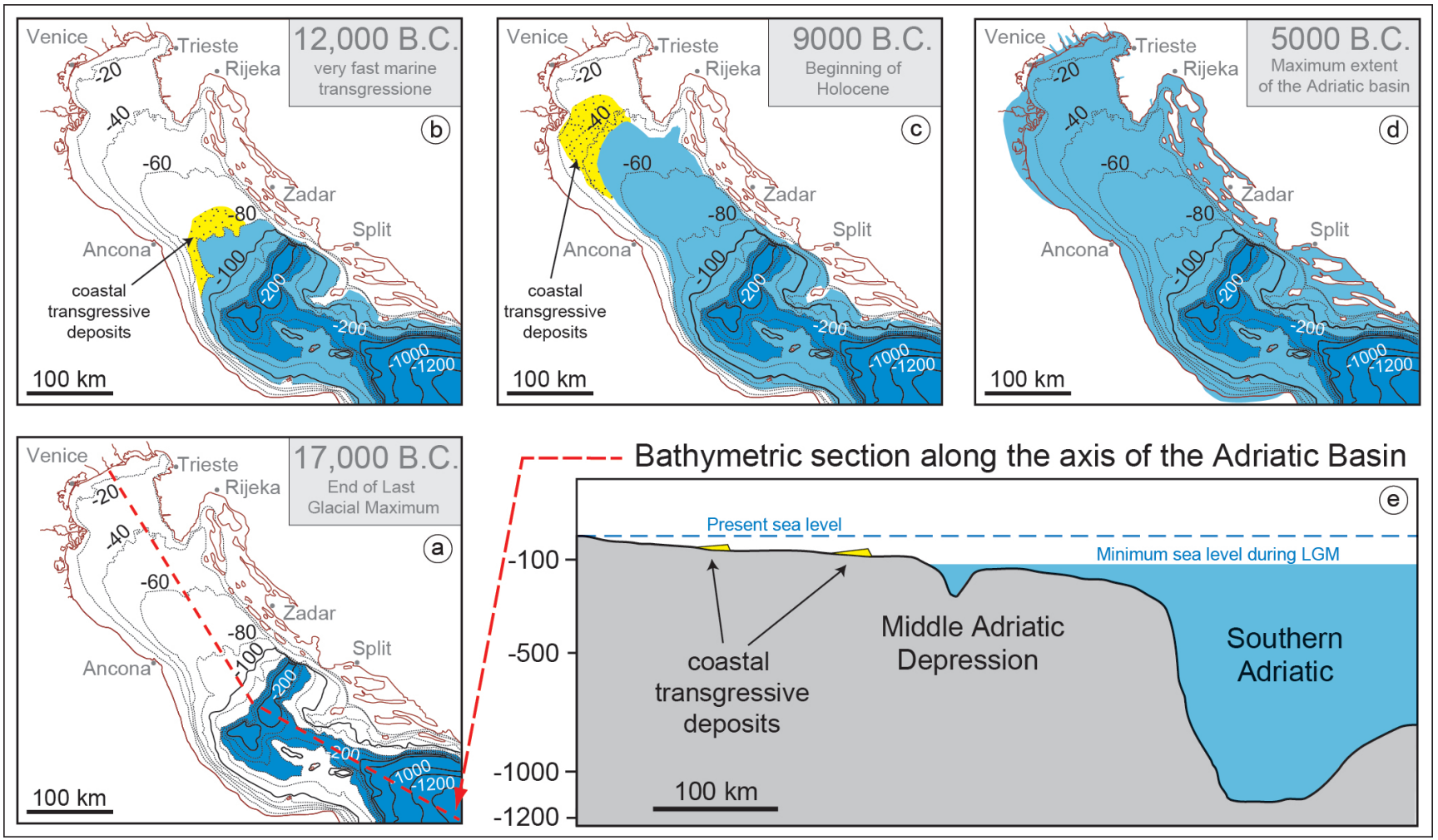

Figure 2.7: Post LGM sea-level rise phases. From Correggiari et al., 1996, modified in Fontana, Correggiari & Juračić, 2014.

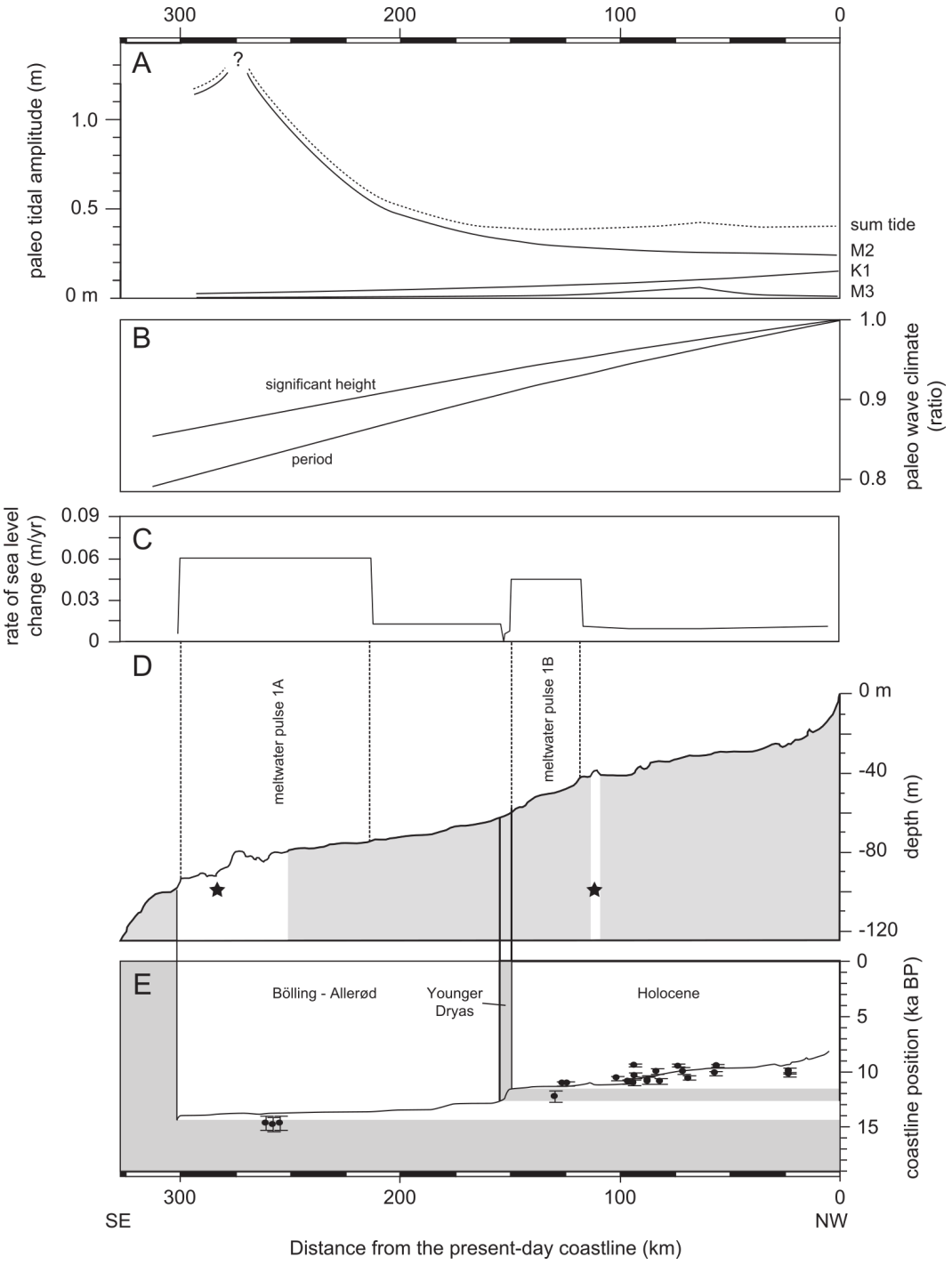

Figure 2.8: Reconstructed paleo-environmental conditions on the northern Adriatic shelf during post-glacial sea-level rise. The horizontal scale represents the coastline position during the Late Quaternary transgression. (A) Maximum cumulative tidal amplitude, (B) paleo-wave climate, (C) rate of sea-level change, (D) modern bathymetry of the Adriatic shelf, with locations of the isolated sediment bodies indicated by the white areas with black stars and (E) paleo-coastline positions based on modern bathymetry and eustatic sea-level curve shown in Figure 2.4. From Storms et al., 2008.

Systems Tract (TST) and Highstand Systems Tract (HST). The interpretation of the Systems tracts is based on stratal stacking patterns, on the position within the sequence and on the sequence boundary surface (Catuneanu, 2006).

System Tracts

FSST and LST "The falling-stage systems tract includes all strata that accumulate in a sedimentary basin during the forced regression of the shoreline; the falling-stage systems tract is bounded at the top by a composite surface that includes the subaerial unconformity, its correlative conformity, and the youngest portion of the regressive surface of marine erosion" (Catuneanu, 2006). "The lowstand systems tract is defined as the sedimentary deposits accumulated during the stage of early-rise normal regression and it is bounded by the top of the falling-stage systems tract at the base, and by the maximum regressive surface at the top" (Catuneanu, 2006).

In this work (as in Trincardi et al., 2011 and Trincardi & Argnani, 2011) these sedimentary deposits are assimilated to the same body due to the impossibility of identifying and tracking the reflector corresponding to the delimiting surface.

Generally, in the Adriatic basin, these deposits are mainly composed of yellowish-grey over-consolidated clays characterized by a typical fauna of mollusk (*Planorbidea spp., Pisidium sp., Bythinia sp.*), but peaty horizons and fine sand bodies are also present (Correggiari et al., 1996, Trincardi et al., 2011).

This unit is the product of an alluvial plain depositional environment, with the presence of fluvial channels and swamps, which represents the paleo environment of the Adriatic shelf before the marine transgression.

TST "The transgressive systems tract is bounded by the maximum regressive surface at the base, and by the maximum flooding surface at the top. This systems tract forms during the stage of base-level rise when the rates of rise outpace the sedimentation rates at the shoreline" (Catuneanu, 2006).

In the analyzed area this deposit shows a thickness up to 6 meters, and it is underlain by a peat layer dated about 11 cal. ka BP (Moscon et al., in press) and capped by the ravinement surface (Correggiari et al., 1996).

The specialized literature on the area (Correggiari et al., 1996, Trincardi et al., 2011, Trincardi & Argnani, 2011) describes the presence of different depositional environments, inferred by seismic geometries and core data: from

a lower delta plain environment, with distributary channels, bars and natural levees, to a paralic environment, passing through tidal regulated barrier-lagoon-estuary systems. Sand shoals cut by inlet channels, resembling the outer portion of the modern Po delta, mark the seaward limit of the systems; the landward side is dominated by bioturbated mud. Malacofauna indicates a fresh water to brackish environment.

HST "The highstand systems tract forms during the late stage of base-level rise, when the rates of rise drop below the sedimentation rates, generating a normal regression of the shoreline. Consequently depositional trends and stacking patterns are dominated by a combination of aggradation and progradation processes. The highstand systems tract is bounded by the maximum flooding surface at the base, and by a composite surface at the top that includes apportion of the subaerial unconformity, the basal surface of forced regression, and the oldest portion of the regressive surface of marine erosion" (Catuneanu, 2006).

According to the specialized literature (Trincardi et al., 2011, Trincardi & Argnani, 2011) this deposit is composed of a prodelta pelitic body (clay and clayey-mud), variably bioturbated and with *Turritella communis* faunas, gradually intercalated with sandy and bioclastic horizons showing a *Chamelea gallina* fauna.

In the studied area the highstand systems tract is reduced to a stratum with a maximum thickness of 2 meters.

Sequence Stratigraphic Surfaces

The boundaries between different system tracts are surfaces of sequence stratigraphic interest; these surfaces are defined from the base-level changes curve at the shoreline and from the shoreline shifts history (Catuneanu, 2006). Among all the observable surfaces described in literature, in this paragraph only the relevant surfaces for this research will be described.

- The term Transgressive Surface (TS), in this work, is used to define the most ancient recognizable surface that marks the marine transgression. This surface does not always represent the boundary between continental and marine deposits, but may also separate continental deposits which are the product of distal variations of the sea-level, as in the case of the

study area.

- The Maximum Flooding Surface (MFS) marks the maximum landward ingression of the sea; it separates the underlying retrograding strata from the prograding strata (Catuneanu, 2006);
- The Ravinement Surface (RS) is an erosive surface due to wave and tide action that superimposed on a former emerged area. Ideally this surface represents the boundary between the transgressive beach deposits and the above transgressive shoreface deposits. Typically on the RS a mixed deposit called transgressive lag can be found (Catuneanu, 2006).

Late Quaternary Evolution

In short, during the LGM the study area was an alluvial plain crossed by various fluvial channel (Storms et al., 2008 suppose the presence of a "Mega Po" river with the Alpine and Apenninic rivers as tributaries) which, with the melting of the ice caps and the sea level rising, experienced a progressive aggradation during the early Holocene (FSST and LST units). The aggradation during the FSST is in disagreement with the classical sequence stratigraphy models (e.g. Blum & Törnqvist, 2000) which predict a strong river incision; the aggradation of the Adriatic platform was probably due to the very low slope, which may have absorbed the sea regression (Fontana et al., 2008, 2014).

The end of the lowstand phase with the sea transgression marked the transgressive surface. With the on-going sea-level rise the distal alluvial plain experienced a switch to a paralic and barrier-lagoon-estuary environment; these morphologies were drowned by the progressive sea ingression and were subsequently truncated by the erosive action of the waves (ravinement surface, end of the TST deposition). In the late Holocene this area was characterized by the deposition of fine sediments related to the sedimentation of the prodelta of the Po River (HST) (Figures 2.7, 2.10 and 2.9).

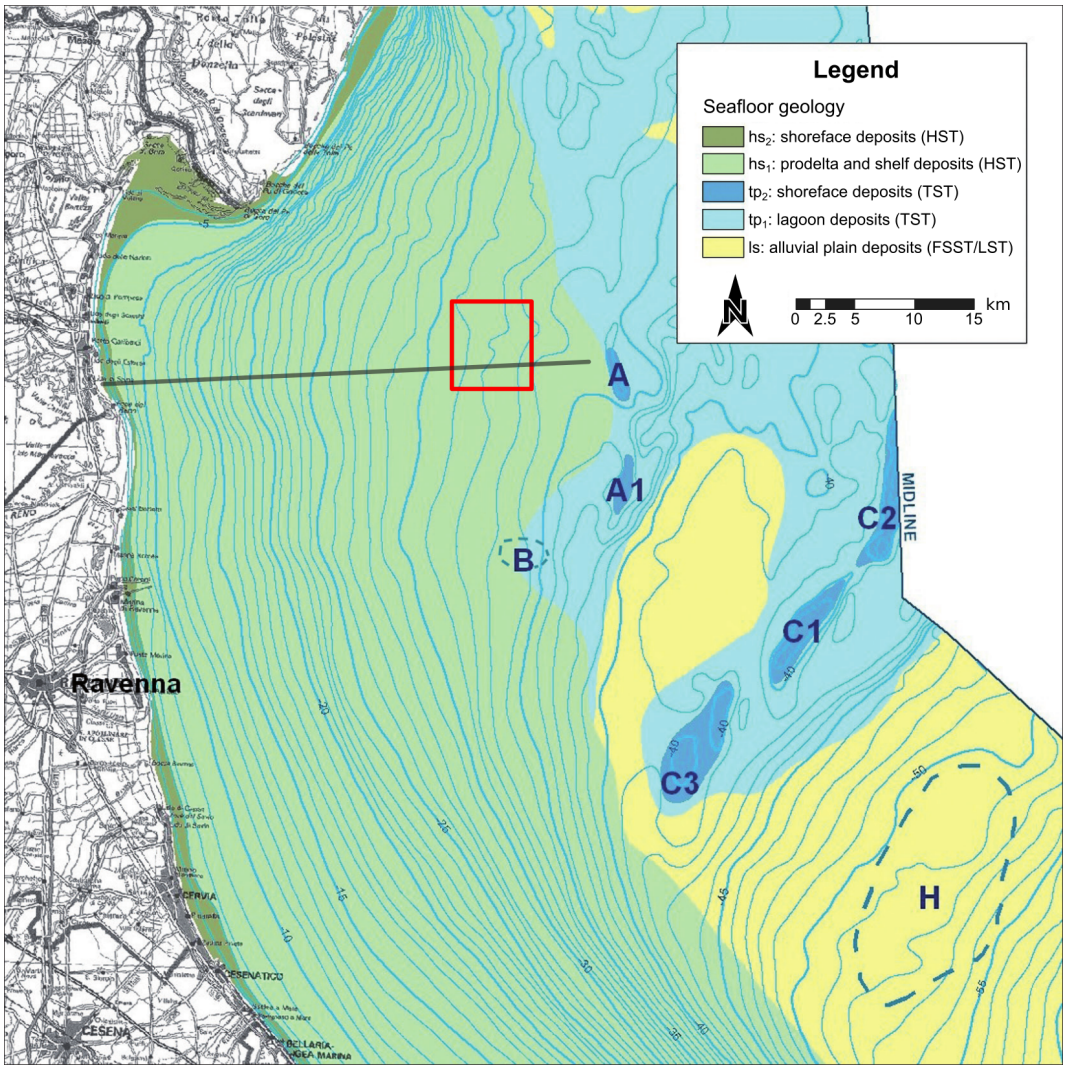

Figure 2.9: Geological map of the northern Adriatic shelf; the red rectangle indicates the study area, the grey line represents the trace of the section shown in figure 2.10. The letters indicate other areas discussed in various works; in particular the A and A1 areas are discussed in Moscon et al., (in press). From Correggiari et al., 2011.

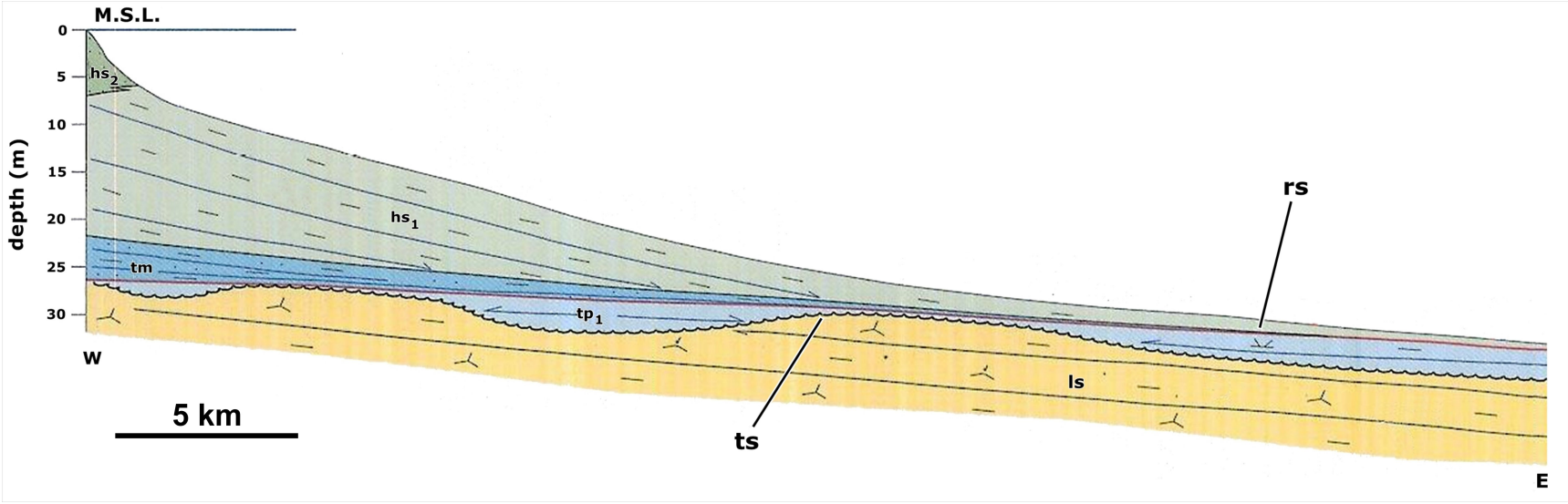

Figure 2.10: Cross section of the post LGM deposits subdivided in system tracts. *ls*: deposits of sea level fall and lowstand in a continental environment; tp_1: transgressive deposits characterized by muds and muddy sands with peat layers; *tm*: transgressive deposits made up of bioclastic sands at the base, which gradually shift to a muddy complex towards the top of the unit; hs_1: highstand deposits showing a prodelta facies; hs_2: highstand deposits showing a shoreface facies; *ts*: transgressive surface; *rs*: ravinement surface. Modified from Trincardi & Argnani, 2011.

Chapter 3

Methods

3.1 Oceanographic Cruise ASCI14

The raw data considered in this work come mostly from the data collected during the oceanographic cruise ASCI14. This survey mission, directed by the CNR-ISMAR Bologna researcher A. Correggiari, was supported and organized by the CNR-ISMAR Bologna Institute, with the collaboration of the Geoscience Department of the University of Padua (Dr. A. Fontana). The survey was carried out on board of the ship Urania, a research vessel managed by the SO.PRO.MAR. on behalf of the Italian CNR (Figure 3.1). The boat is equipped for a maximum of 36 crew members and with a series of instruments and labs on board, used for collecting data and analyzing samples; an essential characteristic of this type of vessel is the ability to perform precision manoeuvres in order to keep the position and permit the sampling procedures. The cruise took place between 30th September and 12th October 2014 and operated in the Italian territorial waters of the northern Adriatic (Figure 3.2)

The data collected during the campaign are both samples and geophysical data; all the methods and instruments are described in detail in the next paragraphs.

3.1.1 CHIRP Sonar

The CHIRP (Compressed High Intensity Radar Pulse) Sonar is a Sub Bottom Profiler which, via the emission of a modulated acoustic pulse, returns an image of the acoustic impedance structure of the first meters of a loose sediment body (Stoker et al., 1997). The CHIRP technology uses a limited bandwidth

Figure 3.1: R/V Urania; from the CNR-ISMAR website (www.ismar.cnr.it).

signal with a defined transmission length and Linear Frequency Modulation; the resolution is proportional to the bandwidth of the signal, therefore a long signal with a large bandwidth produces a higher resolution image (up to four times compared to the traditional Sub Bottom Profilers) and an increase in the sonar dynamic range (Correggiari et al., 2011). The horizontal resolution depends also on the technical features of the emitter, on the thickness of the water column and on the acoustic impedance of the sediment (Rossato, 2009).

A strong advantage of the SBP seismic data is that they do not need migration, because they investigate only the first few meters, and so the error deriving from the omitted migration is negligible.

During ASCI14 cruise the used CHIRP Sonar was a Teledyne Benthos CHIRP-III SBP equipped with 16 low frequency transducers (2-7 kHz) mounted on the keel. The adopted configuration was characterized by a pulse length of 5-10 ms and a trigger rate varying from 0.24 to 1.5 s, depending on the sea floor depth.

All the data were recorded in .XTF extension by the SwanPRO 1.60 software by Communication Technology, directly interfaced to the Differential GPS in order to track the exact position of the seismic profile with a centimetric to decimetric accuracy.

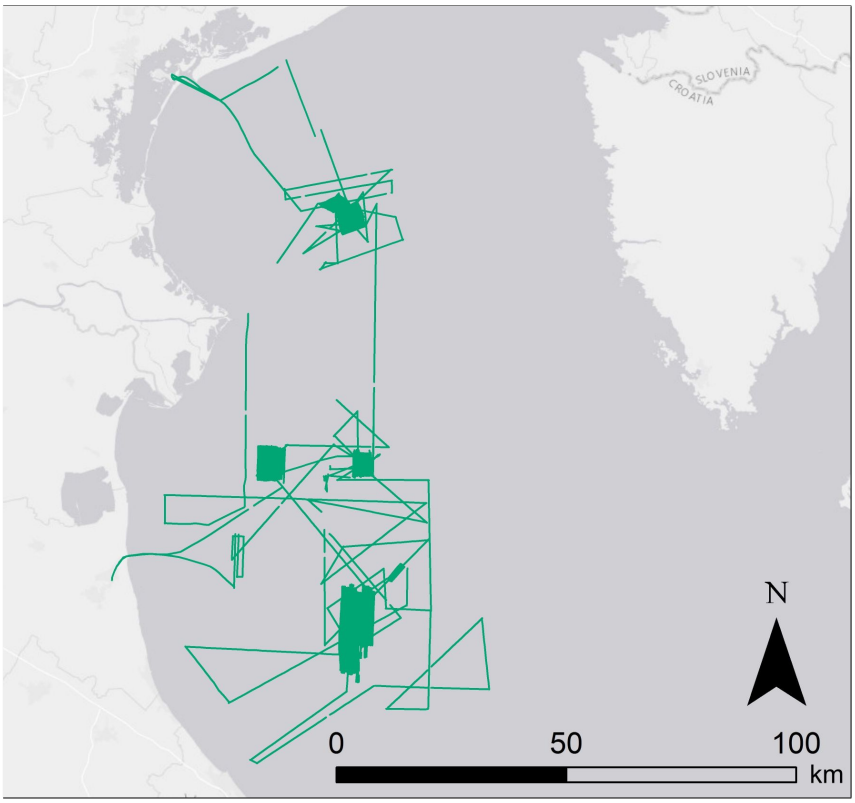

(a) The ASCI14 path.

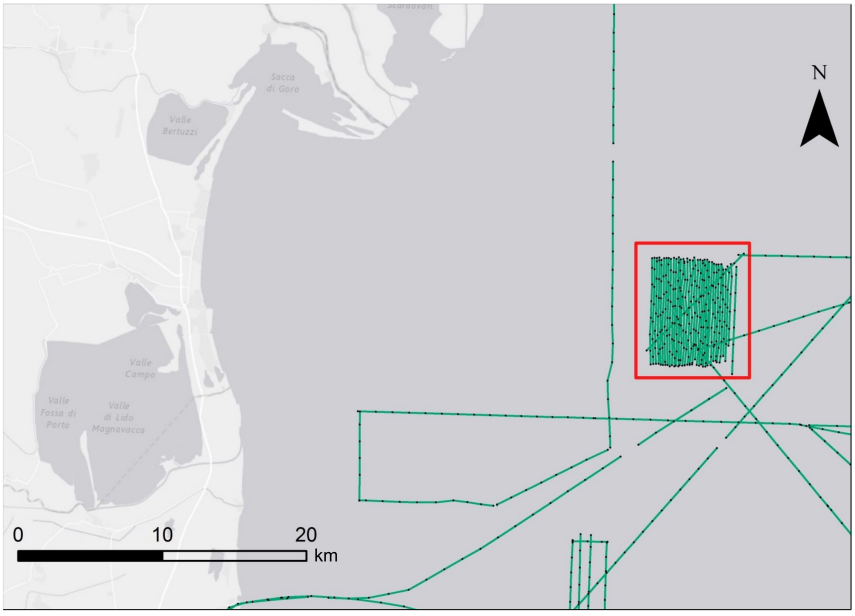

(b) A detail of the ASCI14 path; the red shape indicates the examinated area.

Figure 3.2: The path of the ASCI14 cruise and the detail of the study area.

Data Description

The collected data used here are a series of 35 north-south oriented profiles distributed on a rectangular area, and a single northeast-southwest oriented profile roughly superimposed on the rectangle diagonal. The maximum length of the NS profiles is 7.5 km; they are spaced apart by a mean distance of 160 m. The oblique profile reaches a length of 9.5 km (Figure 3.3). The overall analyzed profiles cover a length of more than 270 km.

The mean time employed in collecting data for a single line was slightly more than 30 minutes, consequently the entire area has been covered in about 24 hours (considering also the time employed for the CTD probe), between 30th September and 1st October 2014.

The obtained profiles show a good penetration for the first 8 meters, which in some points can reach more than 15 meters (e.g. in the case of filled channels Figure 3.4). Under this depth the signal becomes gradually blurry due to the loss of energy.

The collected data are of good quality, and show a decimetric range resolution.

The adjacent profiles are obviously specular one to another due to the sinuous path followed by the vessel.

3.1.2 Multibeam Echo-sounder System (MBES)

The Multibeam is an active type of sonar which measures the depth of the sea floor by generating a short pulse of sound (ping) and recording the echo of the pulse from the bottom (SeaBeam Instruments Manual, 2000); the characteristic of multibeam systems is that they can map more than one location on the sea floor with a single ping, with higher resolution than the conventional echo sounders. With this system the job of a narrow single-beam echo sounder is performed at several different locations on the bottom at once. The spots of the Multibeam are arranged in order to map a contiguous area of the bottom (called *swath*) such as a strip of points in a direction normal to the path of the survey vessel. The dimension of the swath perpendicular to the ship path is called the *swath width* (SeaBeam Instruments Manual, 2000) (Figure 3.5). In order to obtain the best result from this method the Multibeam must be calibrated with an accurate sound velocity profile of the water column (see the CTD probe paragraph for a more detailed description).

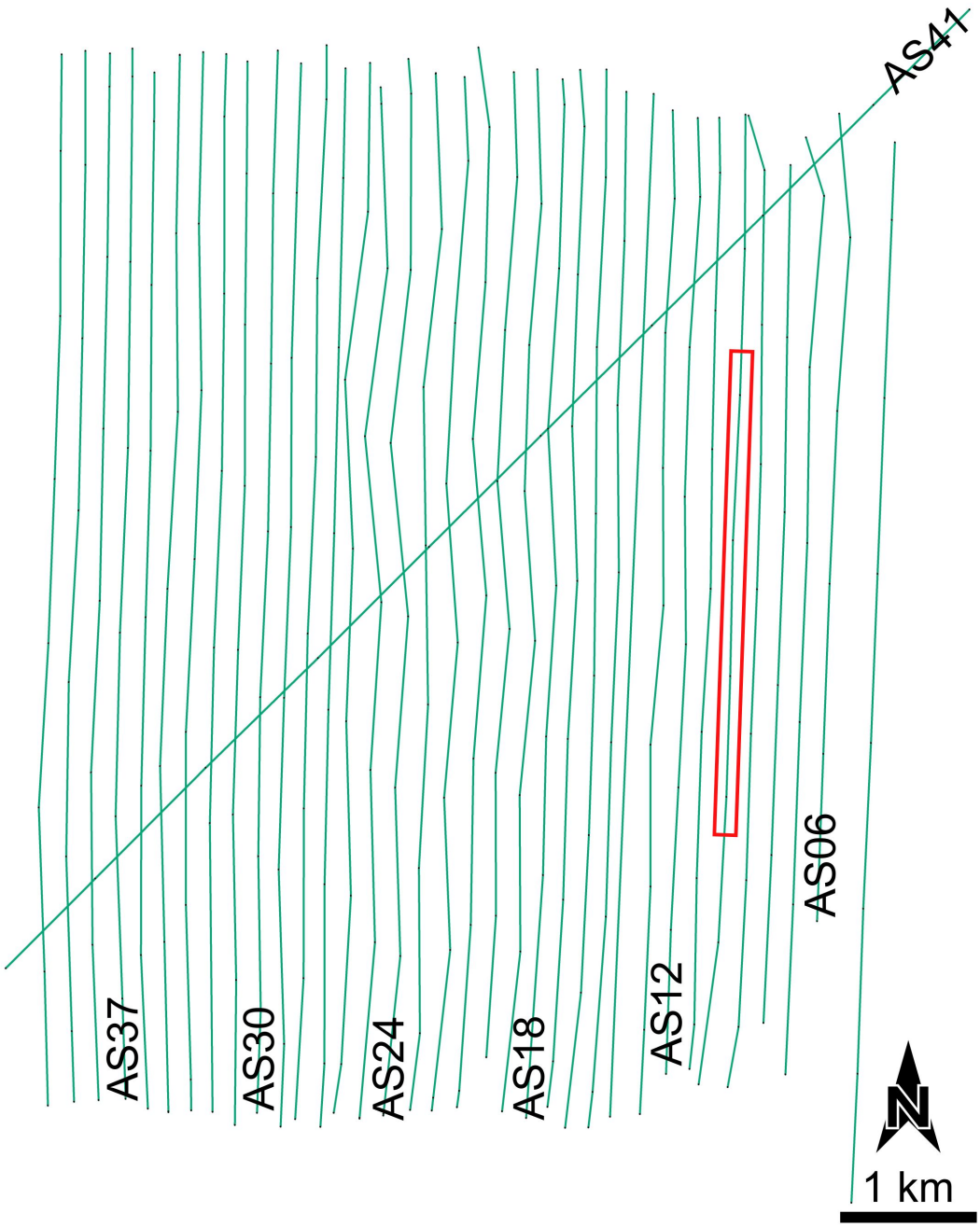

Figure 3.3: Seismic lines used in this work; the black dots represent the events recorded by the software. The red rectangle indicates the portion of data shown in Figure 3.4

.

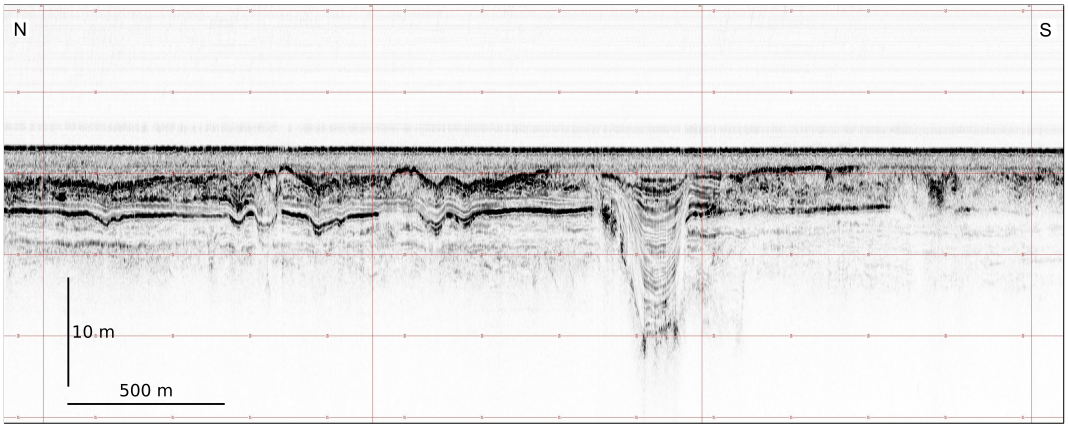

Figure 3.4: An example of the seismic data collected by the CHIRP. The red vertical lines correspond to the events shown in Figure 3.3 and occur with a time lapse of 300 seconds. The horizontal red lines correspond to the two-way time and are drawn with a 10 ms spacing; every 20 ms represent a depth of roughly 15 m.

Travelling through paths close enough to keep the swath length linked, a detailed bathymetric map can be obtained.

During the AS14 campaign a Kongsberg EM170 multibeam system was used; a DGPS was connected to the Kongsberg Seatex Seapath 200 and to the Kongsberg Seatex MRU5 motion sensors in order to exactly track the vessel path. The ping transmission frequency ranged from 70 to 100 kHz, with a swath width of 140°, resulting in a maximum effective coverage of five times the water depth.

The collection of the Multibeam data has been contextual to that of the CHIRP sonar, with the modalities explained in the previous paragraph.

The obtained bathymetry was then corrected with the CARIS software in order to remove the effect of the tidal cycle.

3.1.3 Conductivity-Temperature-Density Probe (CTD)

Sound travels in water in a moving series of pressure fronts known as a compressional wave. The specific propagation speed of these fronts is the local sound speed, which can change depending on the water conditions, such as its salinity, pressure and temperature. As stated in the previous paragraph, in order to obtain the best result from the multibeam analysis, a sound velocity profile must be realized; with this aim a CTD probe was lower to the sea floor at regular intervals (typically at the end of the lines).

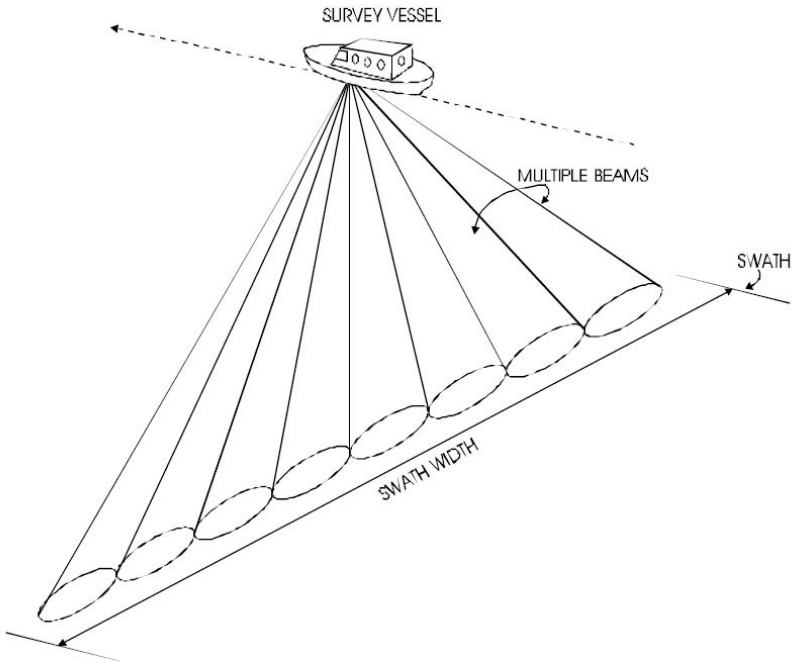

Figure 3.5: Schematic illustration of the Multibeam survey area. From SeaBeam Instruments Manual, 2000.

The CTD probe returns the values of Conductivity and Temperature at increasing Depths, from the sea surface to the bottom; with these data it is therefore possible to construct the sound velocity profiles, which are then used to calibrate the Multibeam acquisition system (Figure 3.6).

3.1.4 Cores

20 stratigraphic cores were also collected during the survey through the use of a gravity corer and a vibrocorer.

Although none of these ASCI14 samples has been taken in the area analyzed in this work, these techniques will also be explained in the following paragraphs, as the analyzed core was collected with analogous procedures during different oceanographic campaigns.

Gravity Corer

The gravity corer is used in order to core loose sediment bodies with a low resistance to penetration. The device is composed of a head, consisting of a cylindrical weight which provides the momentum necessary for the penetration of the instrument, a steel barrel, which contains a PVC liner, and a nose, which

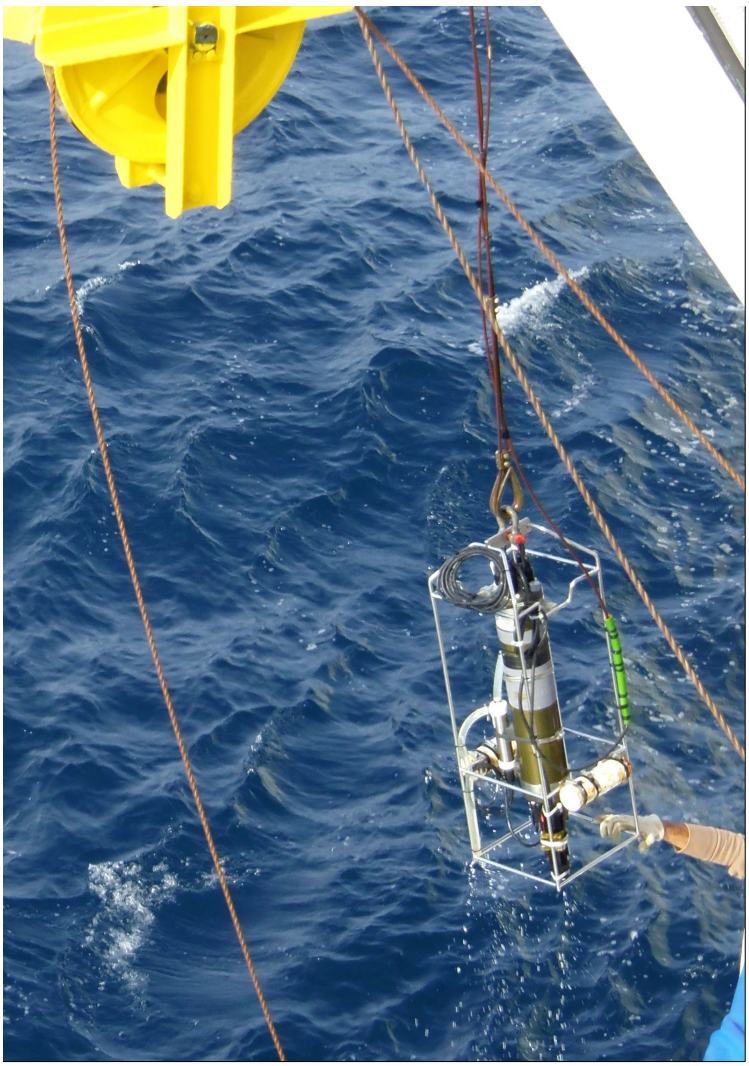

Figure 3.6: Recover of the CTD probe after the measurement; Photo by L. Ronchi, 2014.

Figure 3.7: A specimen of the gravity corer used during the AS14 campaign; photo from website of CarmaCoring s.r.l. (www.carmacoring.com/).

includes a cutter and a catcher. The cutter is constituted by a sharp edge ring which facilitates the penetration of the corer, whereas the catcher is a device designed to keep the sample inside the liner (Stoker et al., 1997) (Figure 3.7).

The used corer was equipped with a 600 kg head and a 6 m long barrel, which housed a liner with a diameter of 90 mm. Immediately after the coring procedure the liner was extracted from the barrel and sawed in sections of 1 m in length, that were immediately stored in refrigerated boxes in order to preserve them and to be analyzed later.

Vibrocorer

The vibrocorer finds application in the coring of stiff sediment bodies, in which the penetration of a standard gravity corer is difficult or even impossible. The concept that lies behind the vibrocorer is that, due to the vibrations, a thin layer of sediment is mobilized, thus reducing the friction and permitting an easier penetration of the corer. The vibrocorer is characterized by the same components of a gravity corer, except for the heavy head, which is substituted by the vibrohead, that is the engine which produces the vibration. The vibrocorer device is completed by a base platform and some buoys, which assure the uprightness of the barrel (Figure 3.8).

The barrel and the nose used with this coring device are the same of the gravity corer, as also the procedure for the core recovering and storage.

3.2 Software and First Analysis

In order to manage all the collected geophysical data little software was used, some with the aim of modifying the data type and reading and printing them, other with the aim of elaborating these data and producing surfaces used in the geomorphological interpretation of the area. For a logical presentation of the work, all the software described below is listed in the order it has been used during the research.

3.2.1 SwanPRO v. 2.00

The first software used was SwanPRO v. 2.00 by Communication Technology (http://www.comm-tec.com/Prods/mfgs/CommTech/swanpro/SwanPro.html), that is a piece of commercial software which is the same that was employed

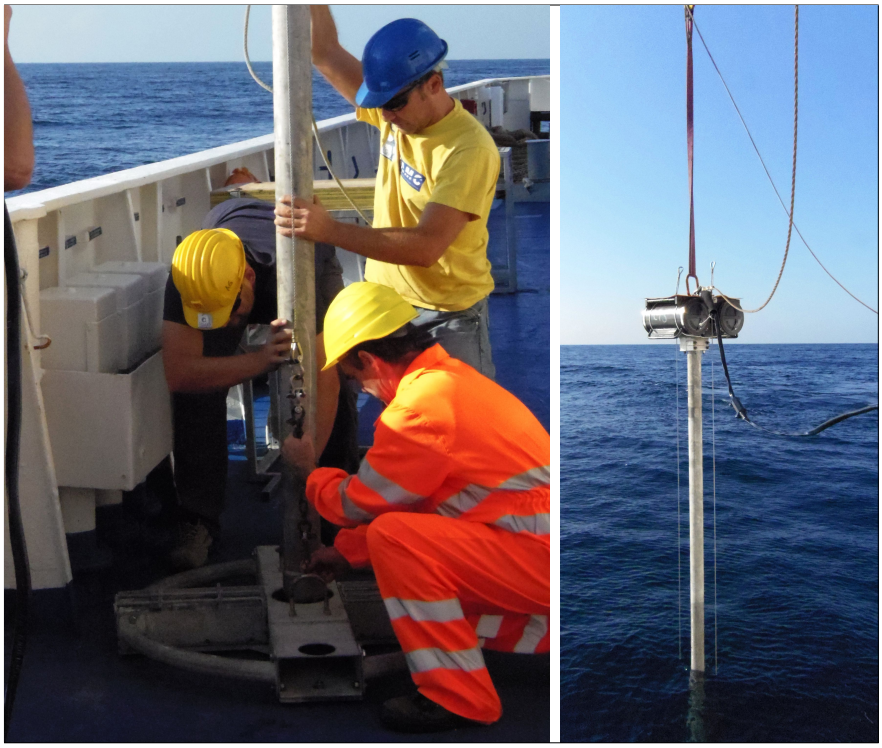

Figure 3.8: Preparation and lowering of the vibrocorer. On the left: fastening of the basal platform; on the right: lowering of the vibrocorer. Photos by L. Ronchi, 2014.

on board for the data collection. This software has been essential for the data format conversion: all the data were recorded with a .XTF extension type, which is an intellectual property of the Triton Imaging Inc., whereas the other employed software only reads the .SEGY extension type, which is an open standard file format.

The obtained .SEGY files were also converted into .TIFF images and then printed on A0 pages. These printed images were used in the first approach to the work, which consisted in the analysis of every profile in order to pinpoint the sedimentary structure and the patterns of the different deposits and to highlight and follow few selected surfaces (Figure 3.9).

In this phase, due to their specular nature (Paragraph 3.1.1), the odd profiles were flipped, in order to obtain an easily readable data.

3.2.2 Kogeo v. 2.7

Kogeo v. 2.7 (http://www.kogeo.de/) is a piece of open software developed by the Institute for Biogeochemistry and Marine Chemistry of the University of

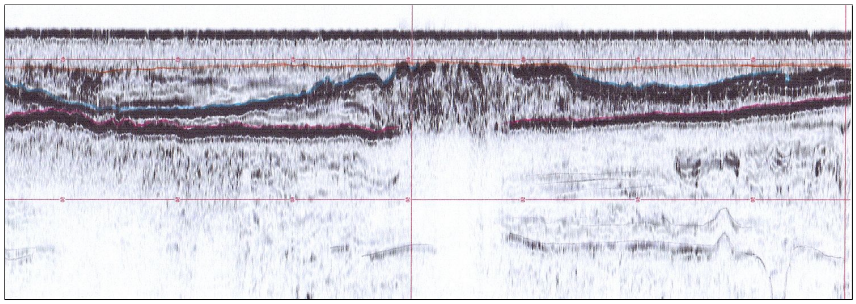

Figure 3.9: Example of the preparatory work; the three main surfaces were marked with coloured pencils.

Hamburg. The main purpose in the use of this software is the visualization and stretching of the profiles, in order to compare the printed and the digital profile versions. Kogeo is also useful for the application of filters on the data, such as amplitude filters, which will be briefly described in 3.3 (Figure 3.10).

3.2.3 SeisPrho

SeisPrho (Gasperini & Stanghellini, 2009) is a piece of software for the processing and interpretation of high-resolution seismic reflection profiles. This software is open and has been developed by the ISMAR-CNR institute (http://software.bo.ismar.cnr.it/seisprho).

After the recognizing work, all the identified surfaces were digitalized by picking, with an average of 1000 point for every profile, in order to reproduce a highly detailed surface. The files obtained by the picking are text files with a .dgt format, from which the coordinates and the two-way time of every picked point were extracted (Figure 3.11).

3.2.4 Libre Office Calc

Libre Office Calc (https://it.libreoffice.org/) is free software which allows to manage and elaborate huge amounts of numerical data; its operating principles and layout are very similar to the classical Microsoft Excel software.

The .dgt files were extracted and the coordinates and the two-way time of every profile were then joined in order to produce a single file which contains the points pertaining to a surface; this work was then reproduced for every different surface.

In this phase the two-way time was converted to the real depth value, using

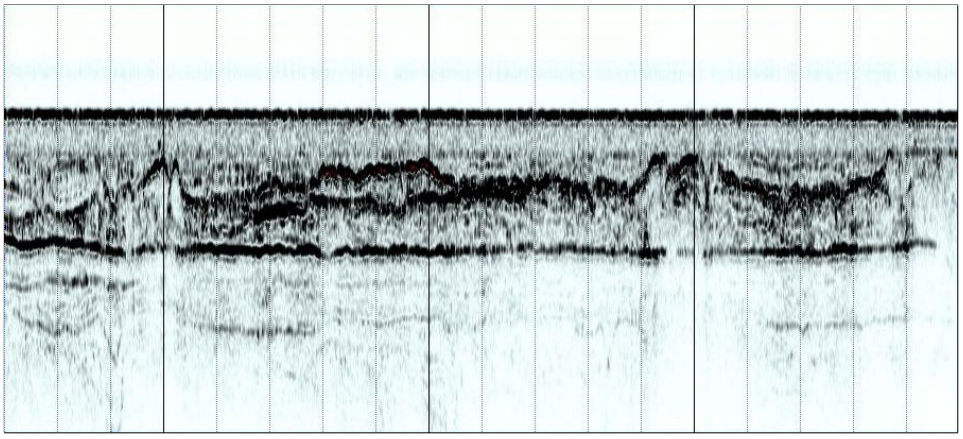

(a) Raw seismic datum.

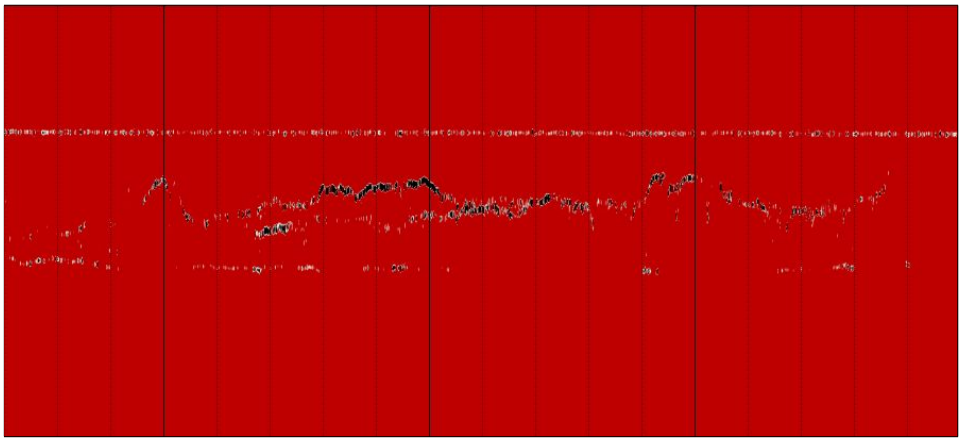

(b) *Absolute amplitude* filtered datum.

Figure 3.10: The comparison between the raw seismic data in picture 3.10a and the same data processed with the *absolute amplitude* filter provided by kogeo 3.10b; the layers highlighted by this tool likely correspond to peaty layers, as explained in paragraph 3.3.

the simple relation:

$$z = -3.5 + \frac{twt}{2} * -1.5$$

Where *twt* represents the two-way time expressed in *ms*. This relation is obtained by considering a mean sound velocity through the sediment of 1500 m/s, and a mean immersion of the hull of 3.5 m. Using a SBP like the CHIRP there is no point in the migration of a seismic record, which refers only to few meters, so a mean sound velocity through the sediment is adopted, as stated above; anyway it must be noticed that some features may appear steepest than they really are.

The obtained files were then converted to a .csv file (Comma Separated

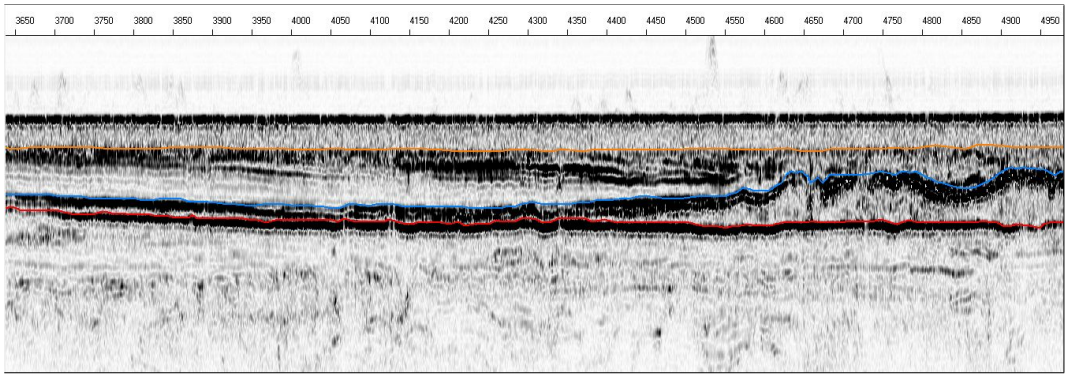

Figure 3.11: Digitalization of the surface with SeisPrho; the drawn colored lines represent the interpolation of the points which mark the surfaces.

Values), an ASCII file easily readable by the GIS software.

3.2.5 ArcGIS 10.2.1

A GIS (Geographic Information System) allows the acquisition, recording, analysis and the visualization of geographical data. The GIS software used in this work was ArcGIS (http://www.arcgis.com/features/), which is a commercial GIS implemented by ESRI. ArcGIS was used in order to obtain raster and TIN models of the analyzed surfaces.

The .csv files were first transformed into shape files with the Arc Catalog software: these shape files contain all the points obtained by the picking work, which are characterized by the longitude, latitude and elevation parameters (Figure 3.12). The chosen coordinate system is the WGS84, whereas the Trieste height datum[1] has been used for the altitude.

The *twt*s are necessarily linked to the position of the sea-level during the measurement, so the whole elevation contains an intrinsic error, due to the tidal cycle, which can be estimated in a maximum of ±20 cm.

In order to obtain a DEM (Digital Elevation Model) of these surfaces, these shape files were then converted to a raster file using the *Topo to Raster*

[1]The Trieste height datum was defined with the measurements carried out only during the year 1875 by the Austro-Hungarian Empire army. This datum can be compared to the HVRST71 datum elaborated by the data collected on five tide gauges along the eastern Adriatic coast on a period of 18.6 years (from 1962 to 1981). The HVRST71 datum is 22.7 cm higher than the Trieste one. In the hypothesis that the HVRST71 datum represents a good estimate for the present sea-level, the elevation data discussed in this work should be affected by an underestimation of about 20 cm, without accounting for the height differences due to the tide. (Liker et al., 2008, Tir et al., 2013)

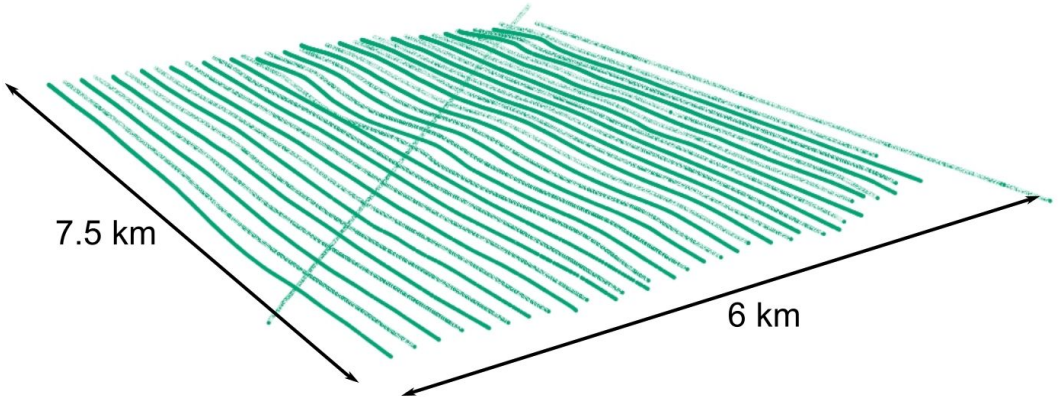

Figure 3.12: 3D representation of the picked points of the *Ravinement Surface*.

interpolation tool which belongs to the *3D Analyst tools* package. The Topo to Raster tool "interpolates a hydrologically correct raster surface from point data"; the chosen settings, which deviate from the default, used in the running of this tool are:

- *Drainage enforcement: NO_ENFORCE*, which imposes to the algorithm not to fill the sinks;
- *Primary type of input data: SPOT*, which refers to dominant type of input data.

The interpolated area was reduced to the area introduced in the Study area paragraph, in order to avoid artifacts in the zones characterized by few data.

Approaching to this phase, several interpolation methods were tried (e.g. *Kriging*, *Natural Neighbor*) but the *Topo to Raster* tool provided the best possible interpolation among them.

The obtained raster images were also refined with a low-pass filter supplied by the *Filter* tool of the *Spatial Analyst tools* package; this filter produces a smoother version of the interpolated raster, which tends to delete outlier morphologies and allows a better visualization of the paleo morphology. In order to further improve the visualization of the surfaces, semi-transparent hillshade images were overlapped to the raster images; the hillshade image, produced with the homonymous tool from the *Spatial Analyst tools* package, simulates a shaded relief with a light source with an azimuth of 315°and an altitude of 45°.

In order to calculate the deposited sediment volumes the raster files were also converted into surfaces generated by TIN (Trianguar Irregular Network;

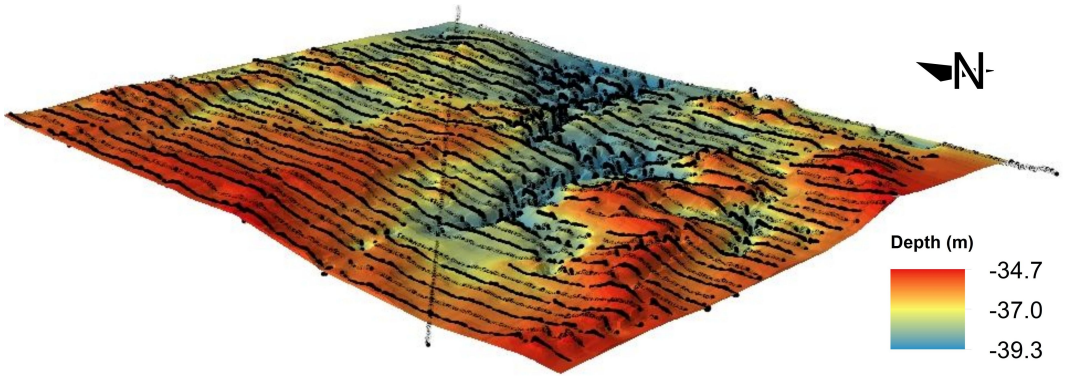

Figure 3.13: Example of a TIN surface; the black lines represent the CHIRP lines interpreted in order to obtain the depths of the surfaces.

Hengl & Reuter, 2009). The rasters were previously projected in the WGS84 UTM zone 33 coordinate system with the *Project Raster* tool of the *Data management tools* package; these files where then converted into multipoint shape files with the *Raster to multipoint* tool of the *3D Analyst tools* package and then turned into terrain datasets. Finally the terrains were used for the production of the TINs with the *Terrain to TIN* tool of the *3D Analyst tools* package (Figure 3.13).

This TIN files are essential for the evaluation of the volumes which are comprised between different surfaces (*Surface difference* and *Polygon volume* from *3D Analyst tools*).

3.3 Stratigraphic Analysis

Due to the lack of cores in the analyzed area, the stratigraphic analysis has been carried out only through the acoustic response of the chirp soundings, except for a single core which, even if is placed outside the investigated zone, is linked to the area by a regional chirp profile, provinding some ground truth evidence (Figure 3.14).

According to Stoker et al., (1997) the reflection character can be described by amplitude, frequency and continuity:

- The reflection amplitude is a function of the acoustic impedance contrast between layers; in the context of quaternary succession typical high amplitude reflectors correspond to peat layers. In this context a useful tool is provided by the absolute amplitude filter of Kogeo software, which

helps to distinguish the surfaces characterized by the higher amplitude (Figure 3.10);

- The reflection frequency is largely dependent on the layer thickness which gives a particular breadth to the signal. Vertical thickness changes can be used to identify a sequence boundary, whereas lateral variation can be the trace of a change of the facies;

- The reflection continuity is related to the continuity of the reflector layer and may be an indicator of the depositional environment; high continuity is often associable to low-energy depositional environments, whereas discontinuous reflectors are often associated to high energy environments.

It must also be considered that the reflector continuity may be affected by shallow gas deposits, which can adsorb the signal showing a blank response (acoustic blanking) on the CHIRP profile (Orange et al., 2005).

Another essential feature that has been analyzed is the reflection configuration, which represents the shape of the reflector surface and has implications for bedding patterns, depositional processes, erosion and paleo topography. (Stoker et al., 1997).

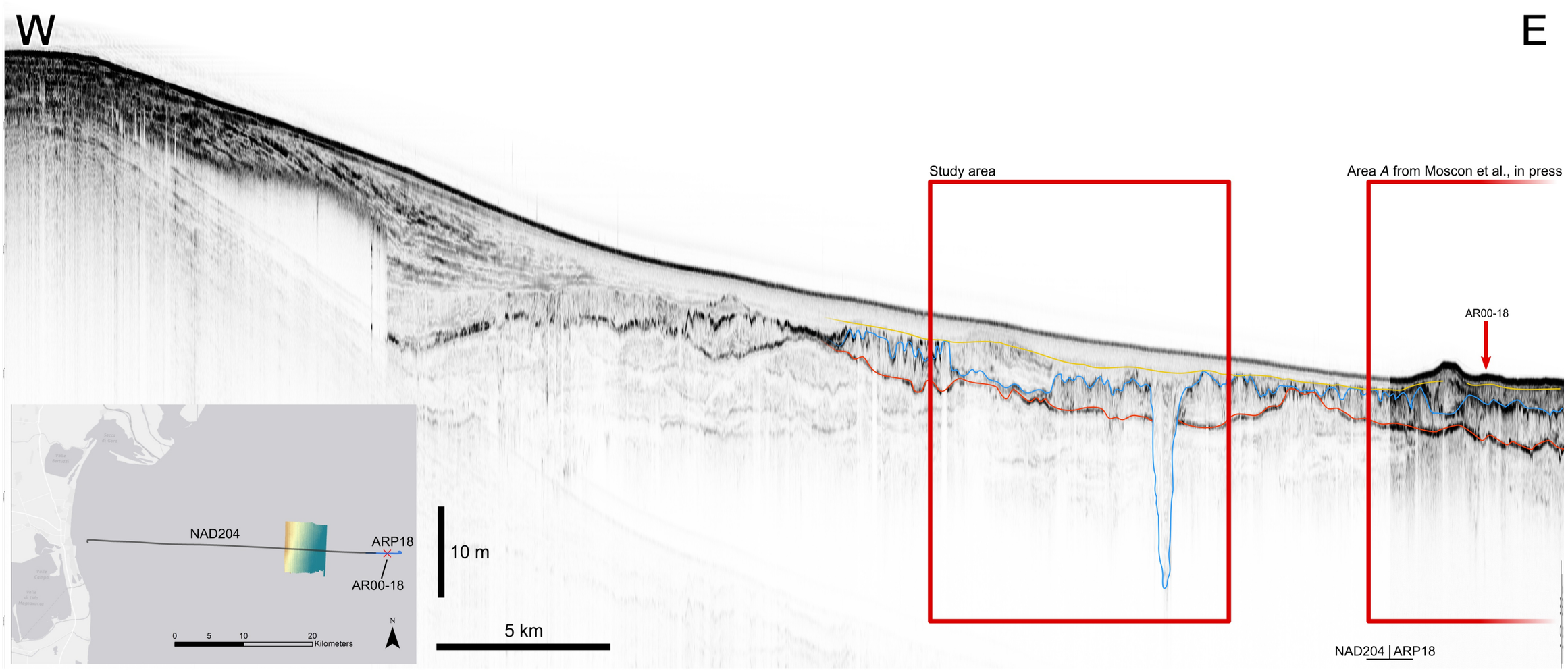

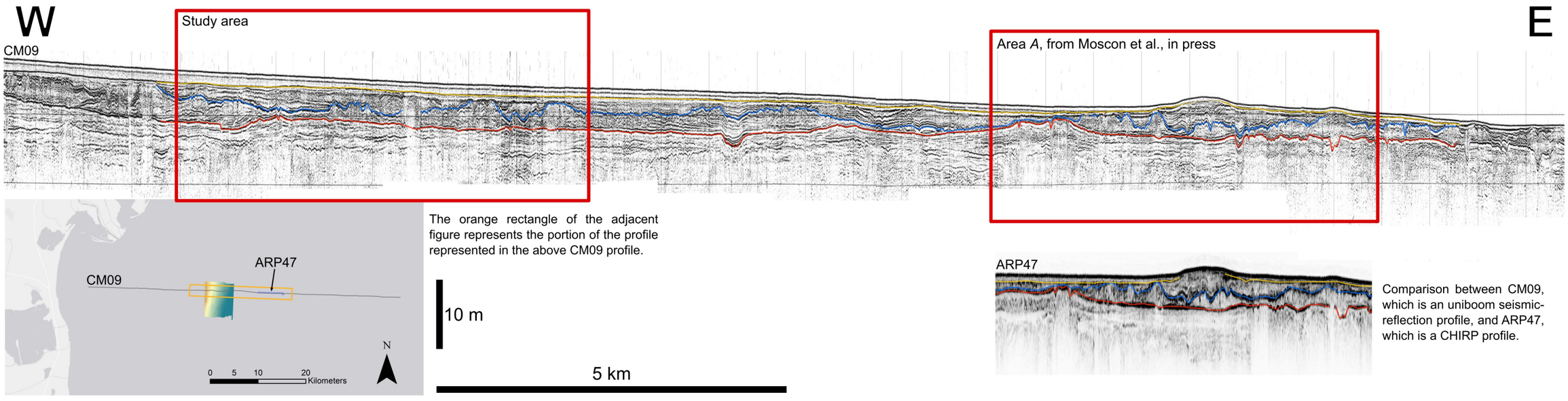

Figure 3.14: Regional profiles CM09 and NAD204-ARP18 which connect the study area to the A area analyzed in Moscon et al., in press.

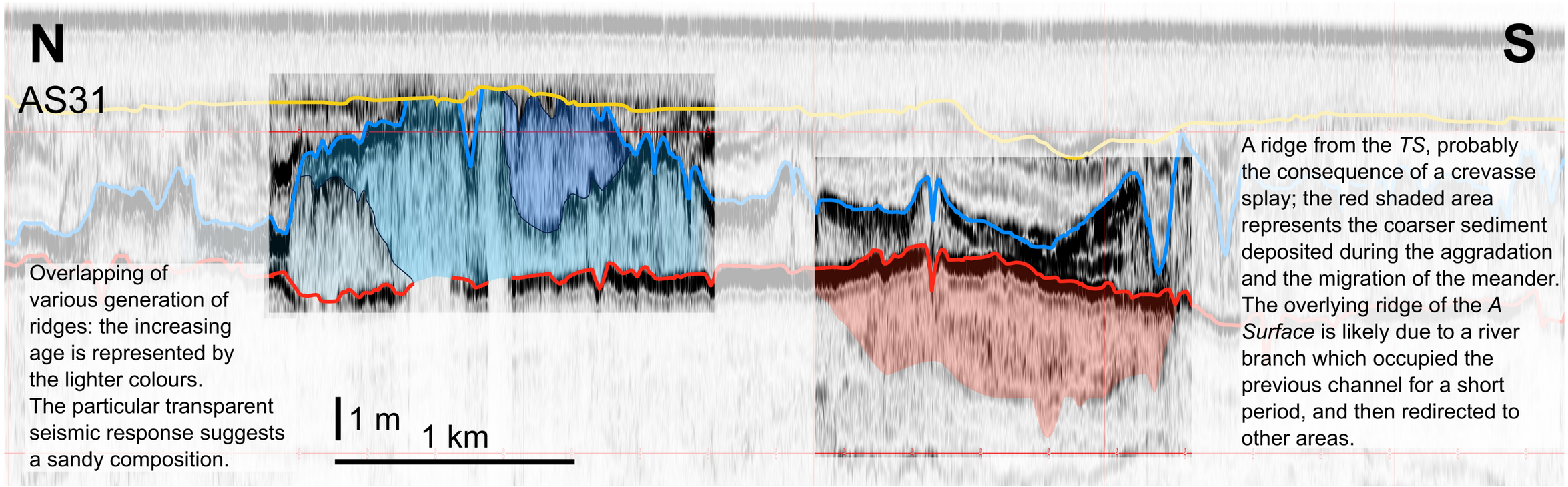

Figure 3.15: Stratigraphic examples of some peculiar morphologies.

Chapter 4

Results

4.1 Multibeam Bathymetry

The bathymetry obtained by the multibeam analysis does not show any peculiar morphology, except for a slight slope toward E-SE (0.04%); the maximum depth of the seafloor reaches -34.7 m, whereas the minimum depth is -29.6 m.

The vertical striping is only due to the partial superimposition of adjacent multibeam lines and, if necessary, can be erased with particular software procedures (Figure 4.1).

4.2 Seismic Analysis

The chirp profiles show three different acoustic responses as evidenced in some adjacent areas (Correggiari et al., 2011, Moscon et al., in press) (Figure 3.14):

- Semi-transparent bodies which tend to shield the underneath reflectors. These deposits are generally interpreted as sand bodies (Figures 4.2 & 4.21);
- Interbedded transparent facies, which are interpreted as fine-grain deposits. The onlapping on the underneath surface may suggest a low-energy depositional environment (Figures 4.20b);
- Thick and strong reflectors, which are interpreted as peaty layers.

In each profile, during the analysis of the printed data, three main surfaces have been identified due to their peculiarities, such as the continuity and the recognizability:

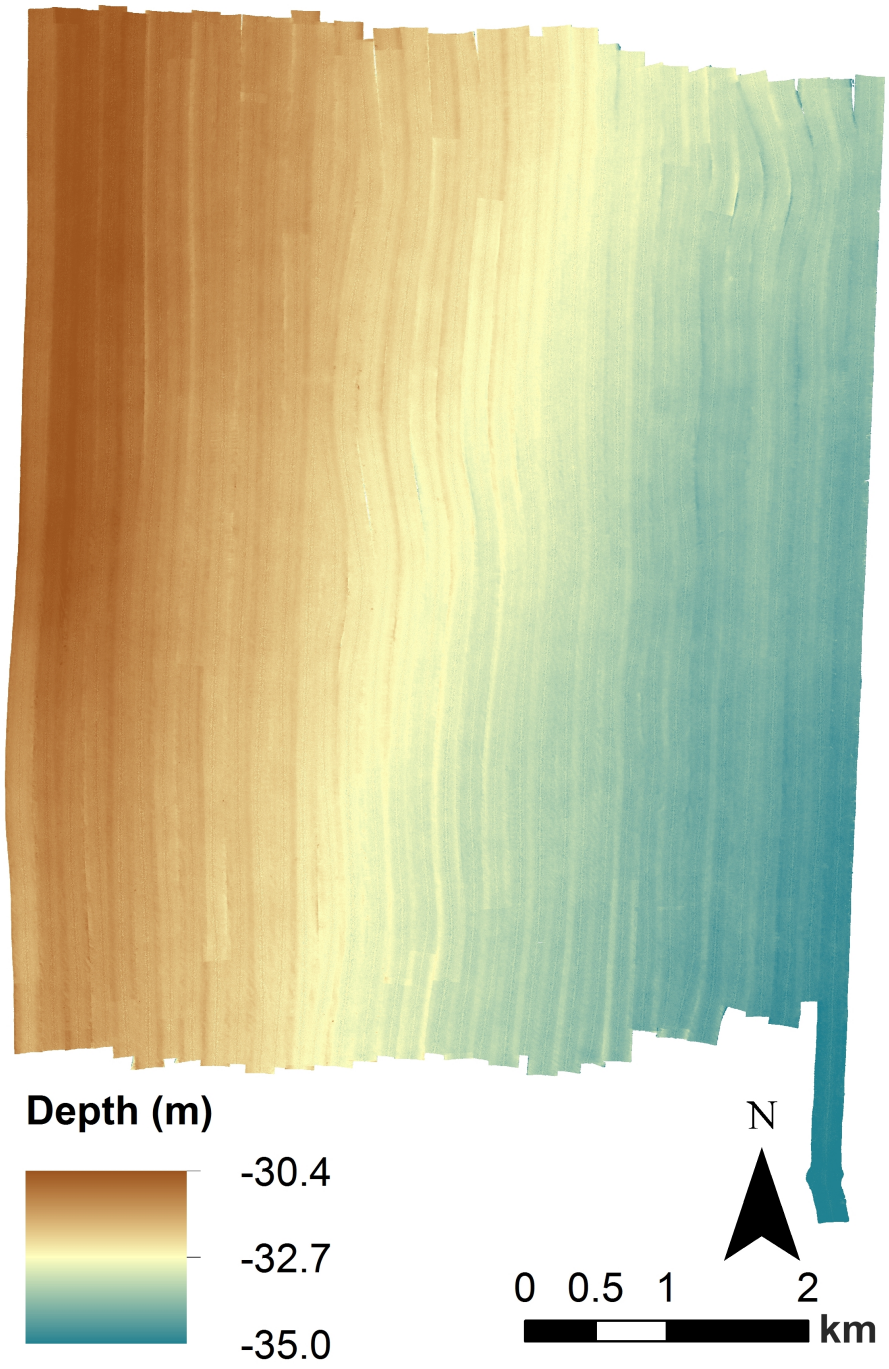

Figure 4.1: The seafloor bathymetry obtained with the multibeam.

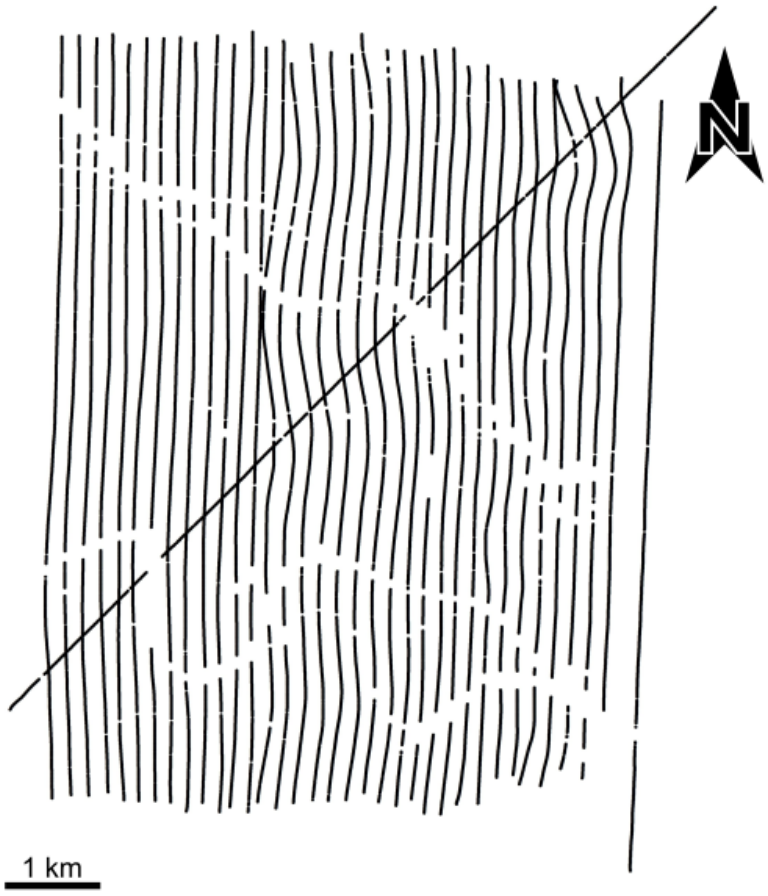

Figure 4.2: Picked point of the *Transgressive Surface*; the lack of data due to the sand deposits shielding marks sinuous patterns which resemble a fluvial path.

- The lower surface has been associated to the *Transgressive Surface*; this statement is possible thanks to Moscon et al., (in press) which defines the exact position of the *TS* dating the peat layers and compares them to the published data. The study area of this work is connected to the study area considered in Moscon et al., (in press) with some regional CHIRP profiles (AMC282, NAD204, KS062) which demonstrate the continuity of the peaty layer that marks this surface (Figure 3.14);

- The middle surface, here called *A Surface*, represents an easily traceable peat layer which rests between the *transgressive* and the *ravinement* surfaces, thus representing a snap-shot of the paleogeography during sea transgression. The sedimentary body comprised between the *TS* and the

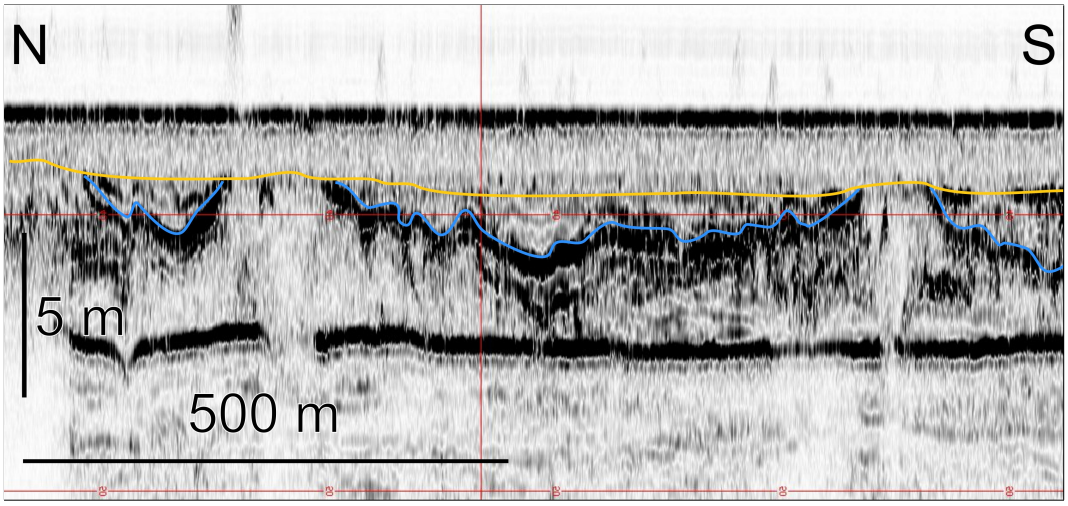

Figure 4.3: Profile AS39: the typical truncation operated by the *RS* (orange line) on the *A Surface* (blue line).

A surfaces is a composite body made up by several minor units delimited by low order surfaces (Moscon et al., in press);

- The upper surface has been recognized as the *Ravinement Surface* due to the characteristic truncation operated on the underlying morphologies (Figure 4.3).

Both the *TS* and the *A* surfaces are likely covered by a peat veneer; peat layers are due both to waterlogged soils and low minerogenic vs organic sedimentation. The peaty layers detected by the seismic survey, in addiction to a necessary depositional hiatus, may be the effect of a superficial water table recharged by a pensile fluvial system (cf. Miola et al., 2006), thus strengthening the following interpretations of the elaborated data.

Every single surface must neither be considered as built in an unique event nor to be the expression of a single, well-defined environment, but, on the contrary, can be the expression of different processes, both sedimentary and erosive, which operated in different time spans. These surfaces were, instead, most likely exposed (in subaerial or underwater conditions) in the same time interval.

4.3 Core Analysis

Despite no cores are available inside the study area, a single core, sampled with a vibrocorer during the AR00 cruise[2], is connectable by a regional CHIRP profile to the study area. (Figure 3.14) This core provides the groundtruth for the seismic facies interpretation (Figures 4.5 and 4.6). The core analysis confirmed the interpretations made through the seismic analysis: the semi-transparent bodies, characterized by a non-well-defined sedimentary pattern, are composed of sandy deposits, the transparent bodies are associated to clay and clayey-silt deposits and the strong reflectors are linked to thin peaty layers (Figure 4.4).

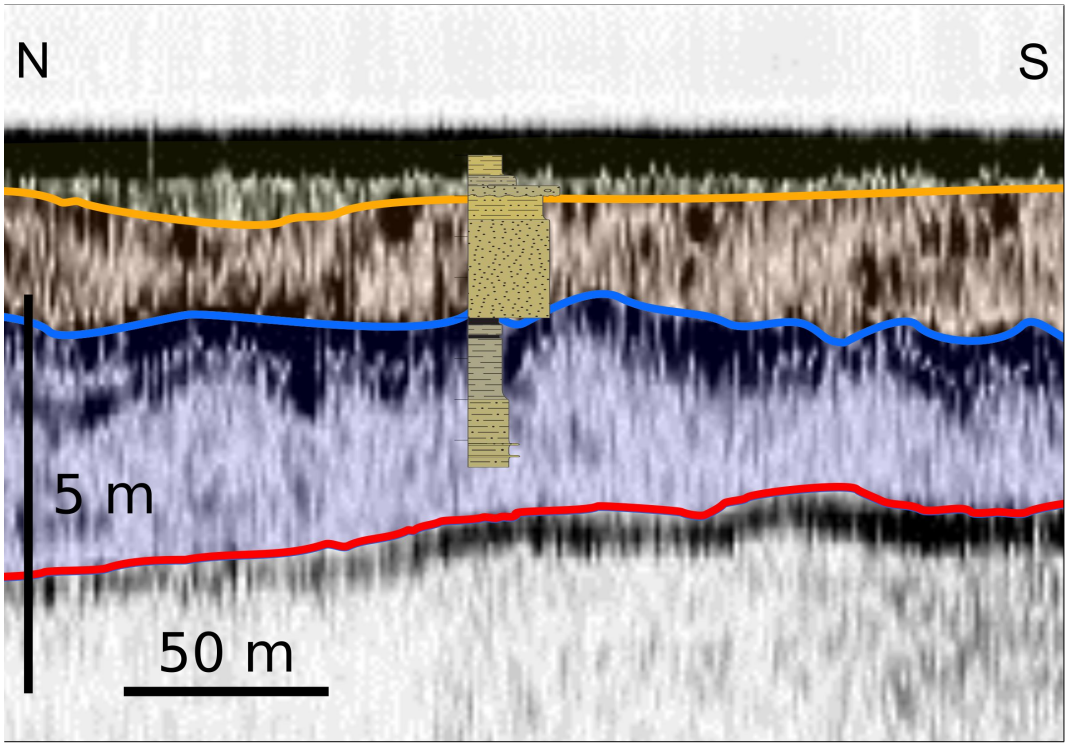

Figure 4.4: Comparison between the stratigraphic log and the CHIRP profile.

[2]The AR00 cruise took place in April 2000, on board the R/V Urania (Correggiari et al., 2011).

Figure 4.5: Picture of the AR00-18 core.

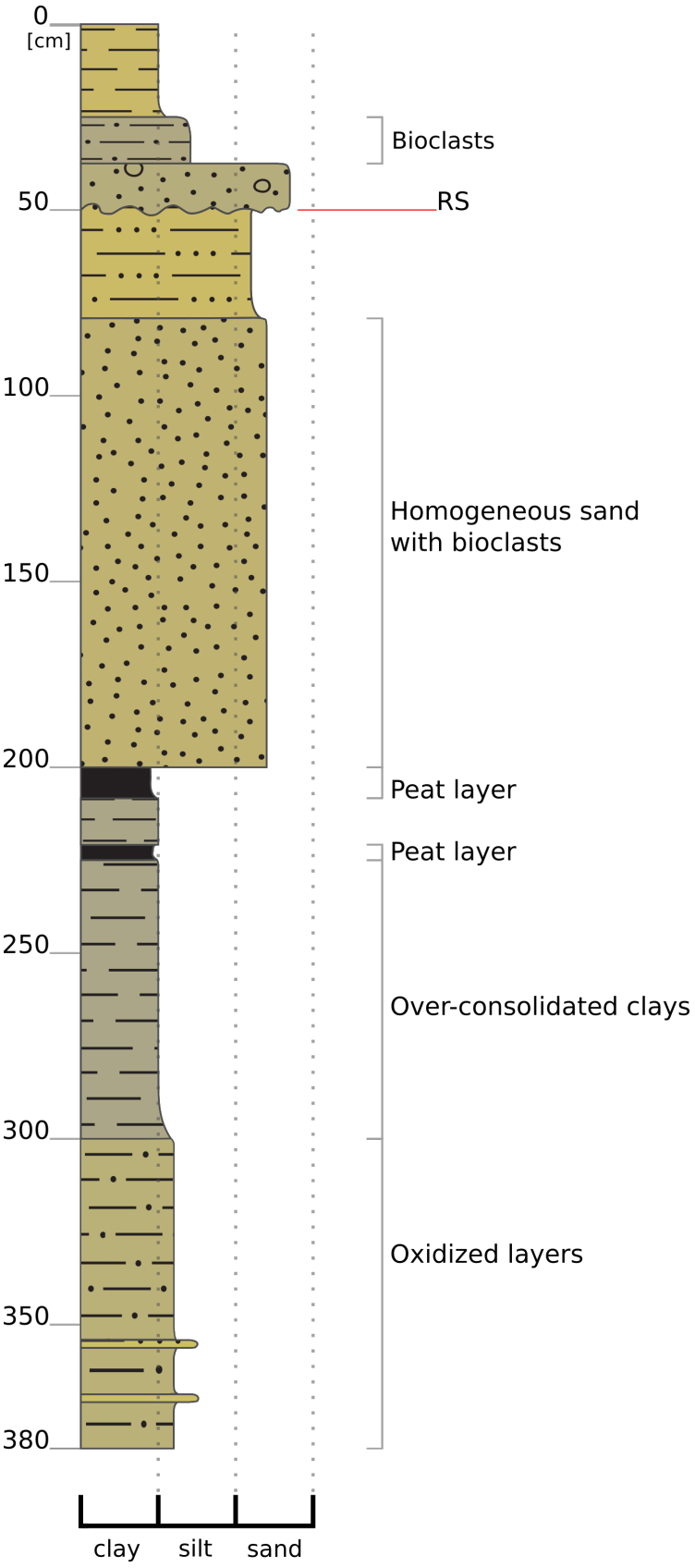

Figure 4.6: Stratigraphic log of the AS00-18 core.

4.4 Reconstructed Surfaces

4.4.1 DEM of the *Transgressive Surface*

The *Transgressive Surface* shows a particular composite pattern and two main morphologies can be distinguished: ridges, linked to a fluvial environment, and an erosional surface, probably linkable to the first marine ingression in this area (Figures 4.7 and 4.8).

The overall difference in elevation is about 4.5 m, ranging from -39.3 m to -34.7 m.

The pattern inferred by the natural levees suggests a preferential E-NE direction, in good accordance to the reconstructed channels of the A and A1 areas (Figure 2.9; Moscon et al., in press), despite the small extent of the area does not allow to make precise evaluation. The well-defined ridge visible in the south-west corner of the area (*A* in figure 4.7) is characterized by a meandering path, with a meander radius of about 500 m, a mean height of 1 m and a channel width of 100 m.

Another interesting example of morphology associated to a fluvial environment is the ridge on the west side of the area (*B* in figure 4.7); this morphology hypothetically corresponds to a meander affected by a crevasse splay and the consequent superimposition of a new ridge which redirected part of the stream in an eastward direction (Figure 4.9). The alluvial plain between the ridges, where not obliterated by the rising sea, gently dips toward east, with a mean gradient of 0.03 - 0.04%.

The erosional surface (*C* in figure 4.7), as already described, is probably the consequence of the marine ingression, and it may have been developed in a tidal flat environment. The recognizable morphology is constituted by a wide eroded sector, located in the east portion of the area, which is connected to a couple of meandering channels with a SW-NE direction, localized in the central and southern portions of the area. The overall erosion reaches a depth of 1 m compared to the alluvial plain described above. The total length of this structure is 6 km; the Width-to-Depth ratio shows a constant value of 7, indicating that the channel probably developed as a marsh creek (cf. D'Alpaos et al., 2005, Hughes, 2012). The north-east portion of the area is also probably characterized by erosion, but the evidences are not as clear as in the other morphologies.

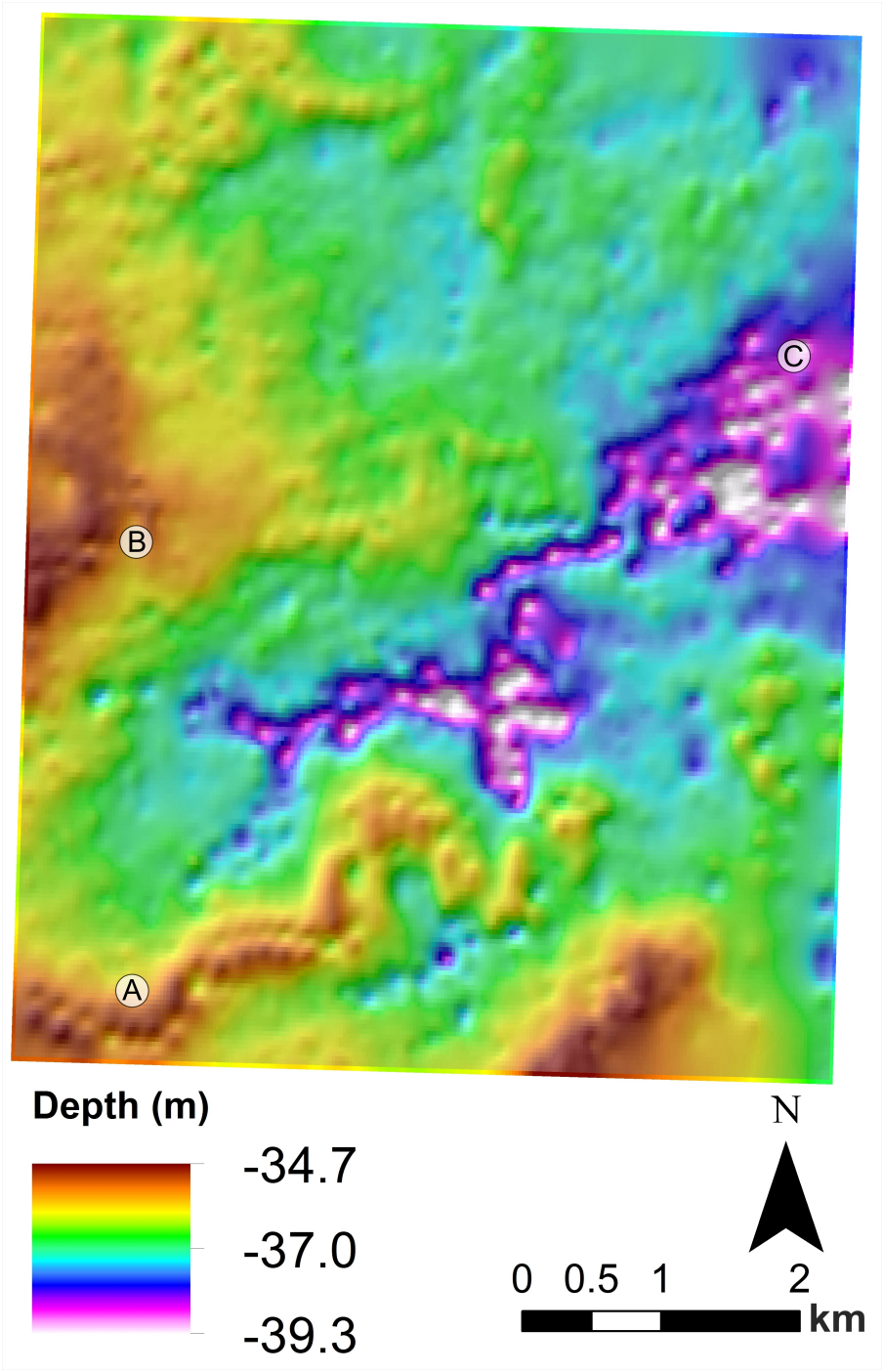

Figure 4.7: Raster image of the *Transgressive Surface*; the hillshade image of the surface was overlapped in transparency (50%) to the raster image in order to improve its readability.

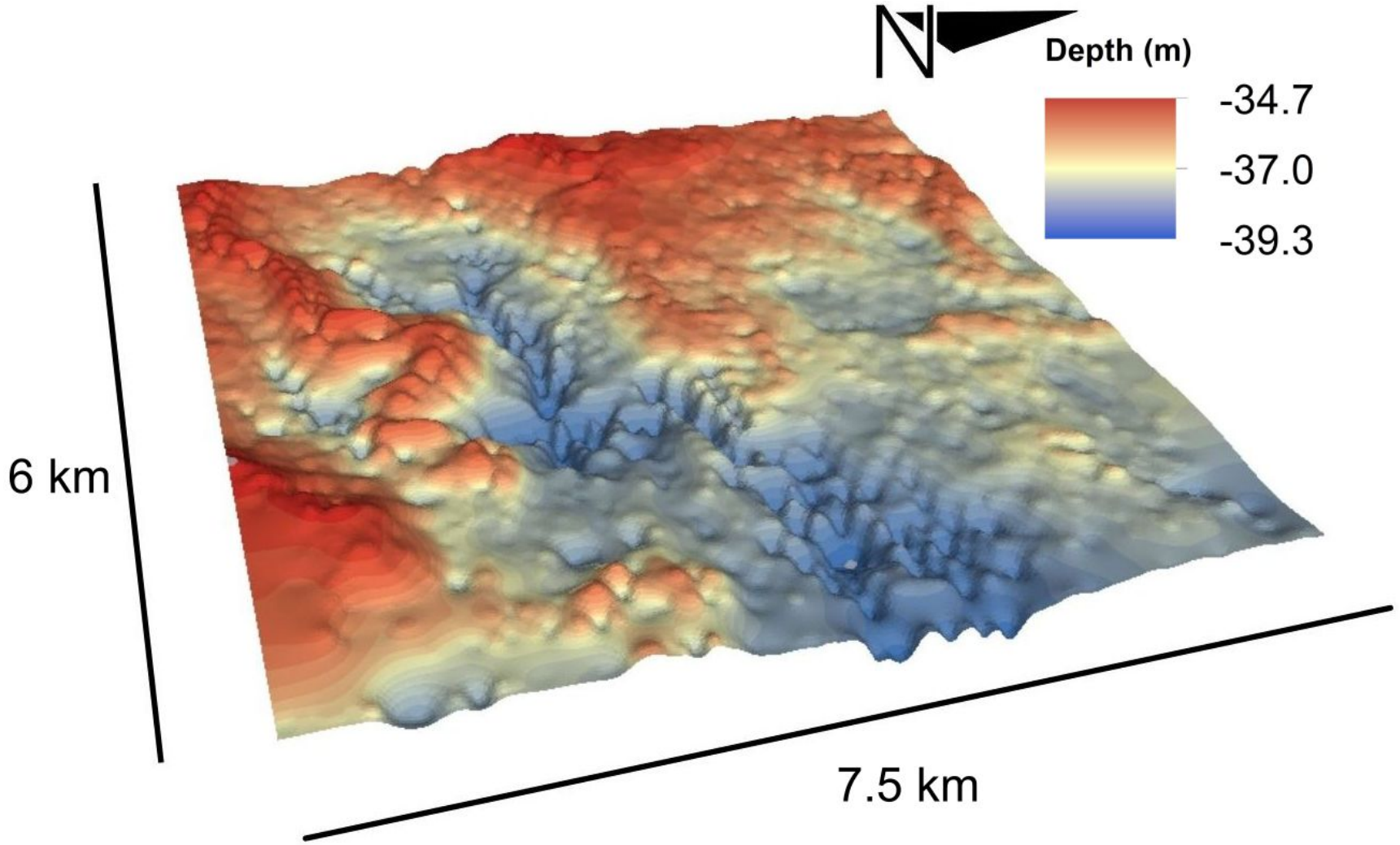

Figure 4.8: TIN image of the *Transgressive Surface*; a vertical exaggeration factor of 100 has been applied in order to enhance the morphologies.

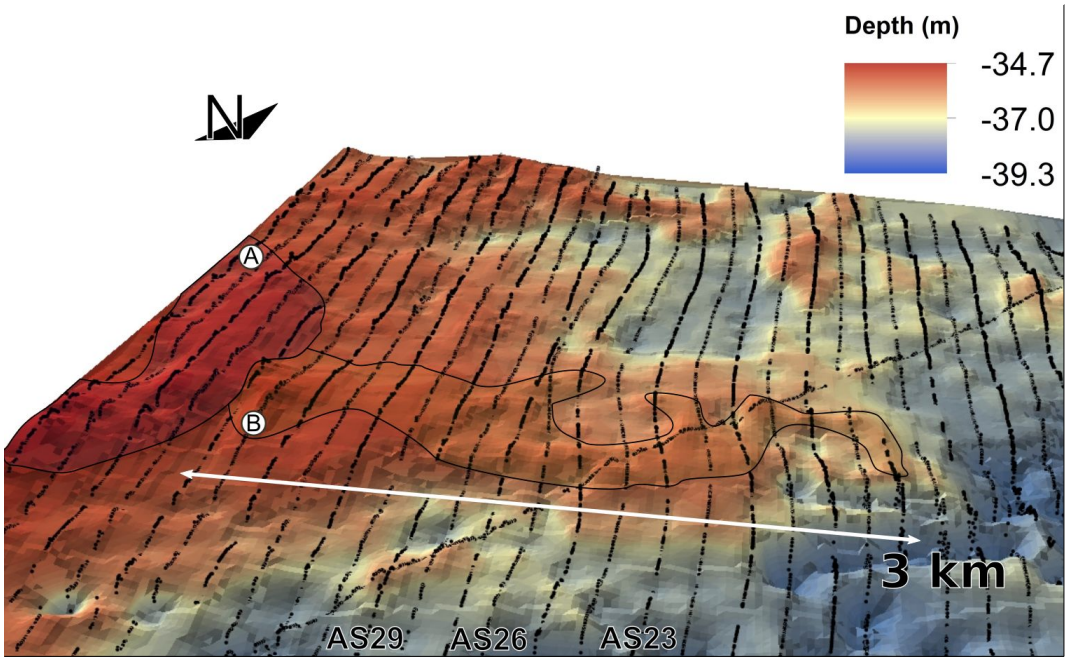

(a) Detail of the crevasse in 3D view. *A* area represents a meander of the main channel, whereas *B* area represents the interpreted crevasse splay ridge.

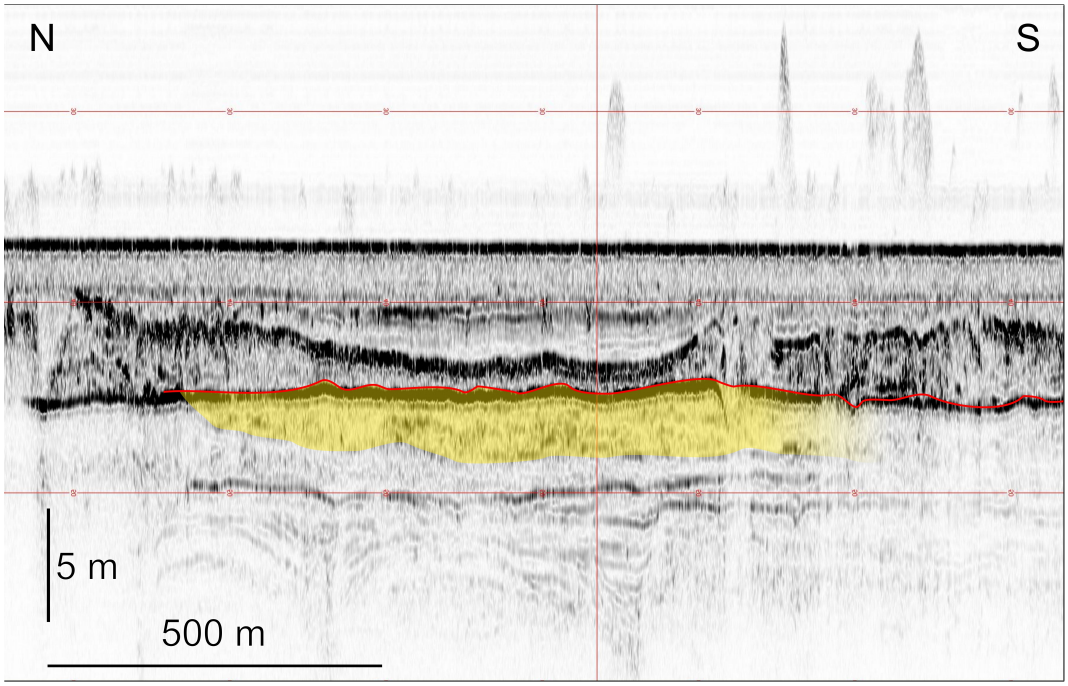

(b) Profile AS26: the yellow area beneath the *TS*, in red, represents the sediment body deposited by the crevasse splay.

Figure 4.9: Crevasse splay morphology and related seismic response.

4.4.2 DEM of the *A Surface*

The *A Surface* shows an emphasized topography compared to the underneath *TS*, with altitudes ranging from -44.8 m to -31.9 m, with a difference in height of about 13 m; if compared to those of the *TS*, the bottom height datum is obviously due to a strong erosion that, if not considered, leads to an overall height difference of 7 ms (Figures 4.10 and 4.11).

The reconstructed topography is mainly made up of fluvial ridges with height that can reach 3 m. The number of visible ridges is greater than that of *Transgressive Surface*, with various interfering channels that delineate small basins. An E-SE channel trend can be inferred by the major fluvial ridges, and this information is still in good agreement with the direction recognized in the A and A1 areas (Figure 2.9; Moscon et al., in press).

A huge cut and fill channel is located in the east portion of the area (*A* in figure 4.10): this channel is characterized by an E-W trend, with a maximum depth of about 10 m and a width up to 430 m. A bifurcation occurs in the western portion of the channel, which shows a maximum length of about 1 km. This erosive feature seems to cut one of the major fluvial ridges, thus connecting two basins. Another minor similar channel is located in the SW area (*B* in figure 4.10); also this channel cuts a ridge and connects two different basins.

This surface is the result of the ongoing transgression, which produced the transgressive deposit which lies between the *TS* and the *A Surface*; by subtracting the *TS* elevation to the *A Surface* elevation the depositional pattern can be inferred, thus highlighting that the raised areas of the *Transgressive Surface* have a good correspondence to the depressed areas of the *A surface* (Figure 4.12). This hypothesizable feature gains here a particular significance by confirming the reliability of the reconstructed surfaces.

Major Channel of the *A Surface*

The erosive surface cuts the whole thickness comprised between the *TS* and the *A* surfaces, but evidence from the CHIRP profiles suggests that this erosive channel is posthumous respect to the *A Surface* and was still active also after its partial burying (Figure 4.13). Thus, this erosive feature separates the depositional body sedimented before the formation of *A Surface* from the one deposited later, that is the channel infill deposit.

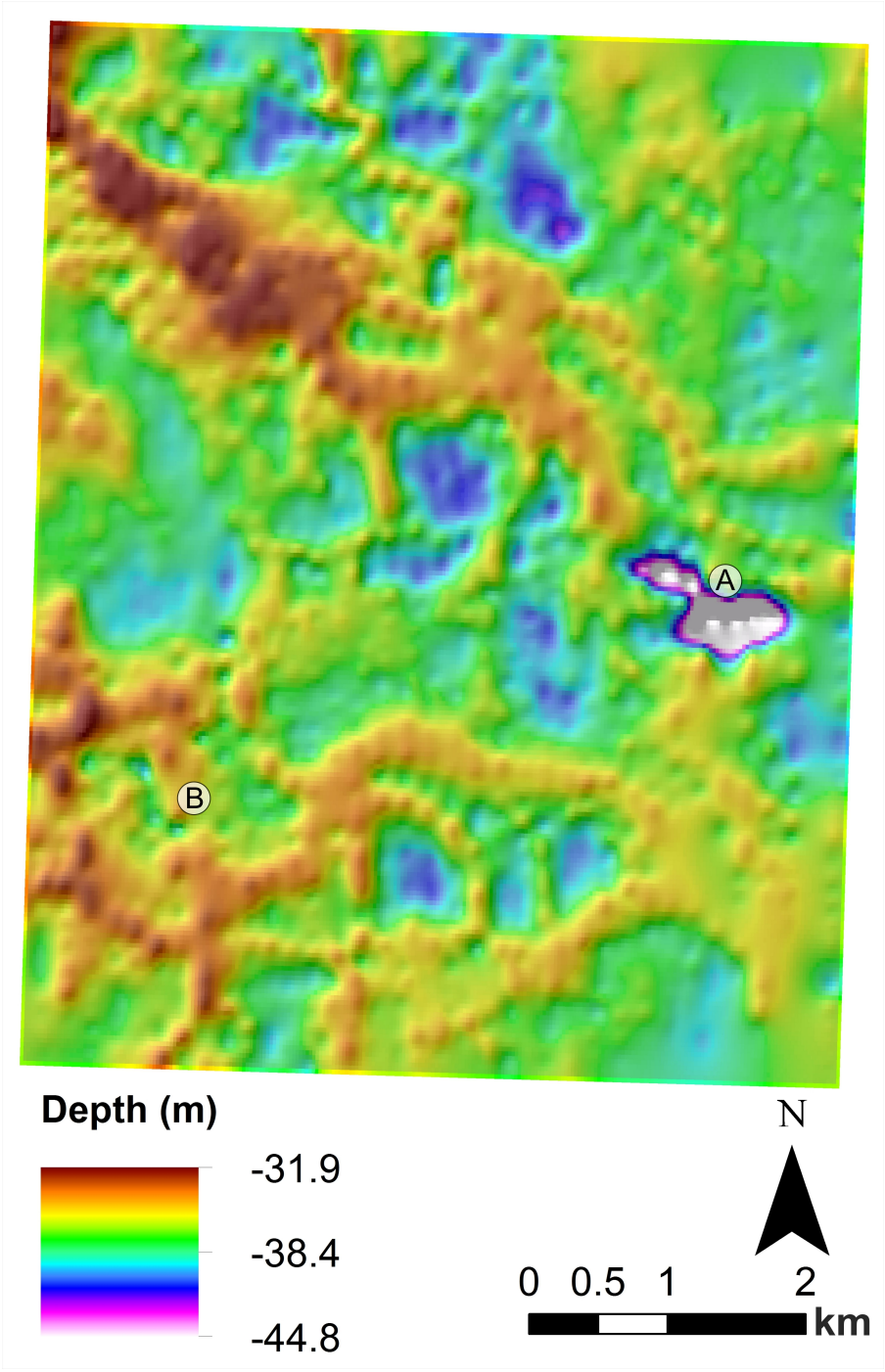

Figure 4.10: Raster image of the *A surface*; the hillshade image of the surface was overlapped in transparency (50%) to the raster image in order to improve its readability.

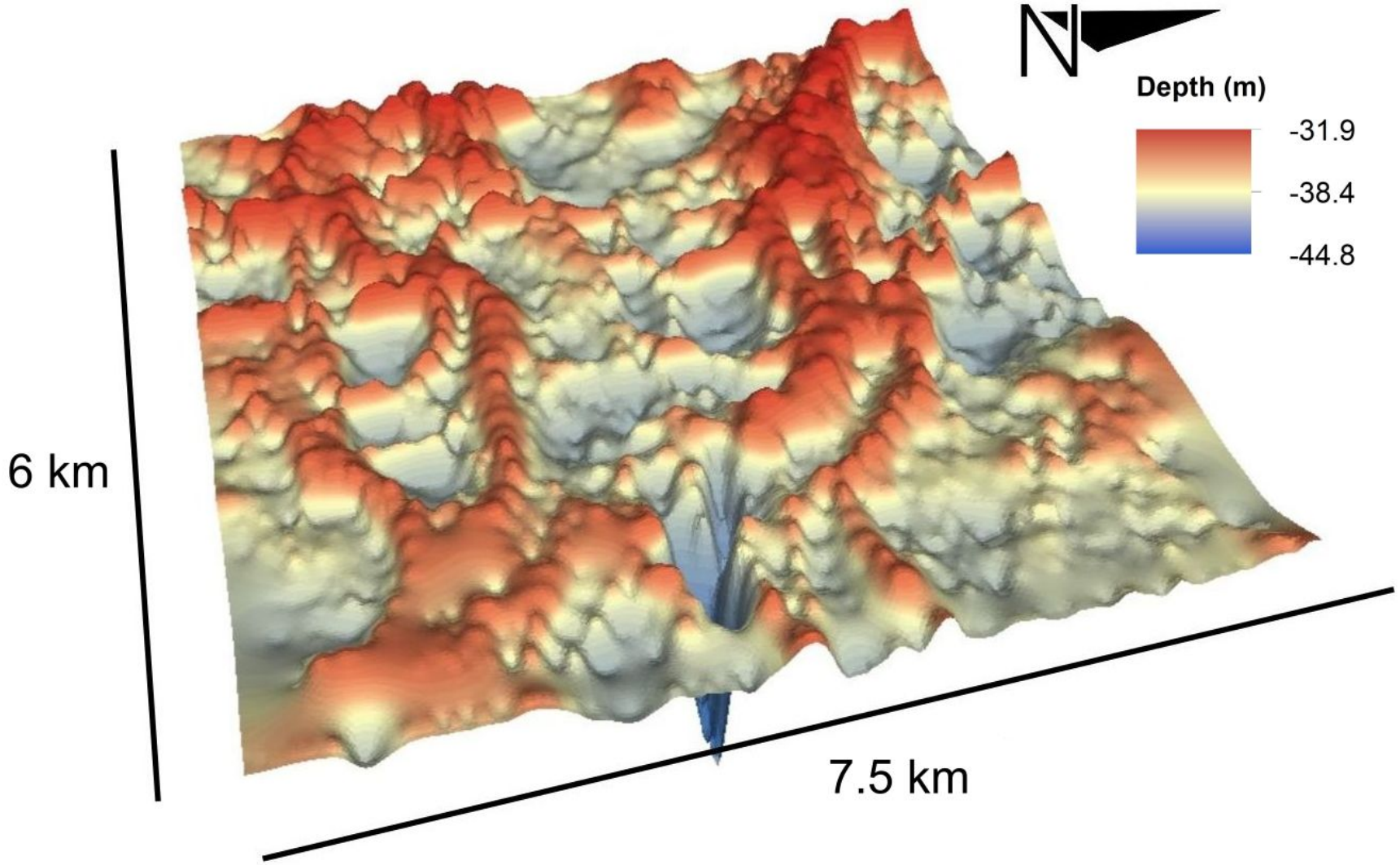

Figure 4.11: TIN image of the *A surface*; a vertical exaggeration factor of 100 has been applied in order to emphasize the morphologies.

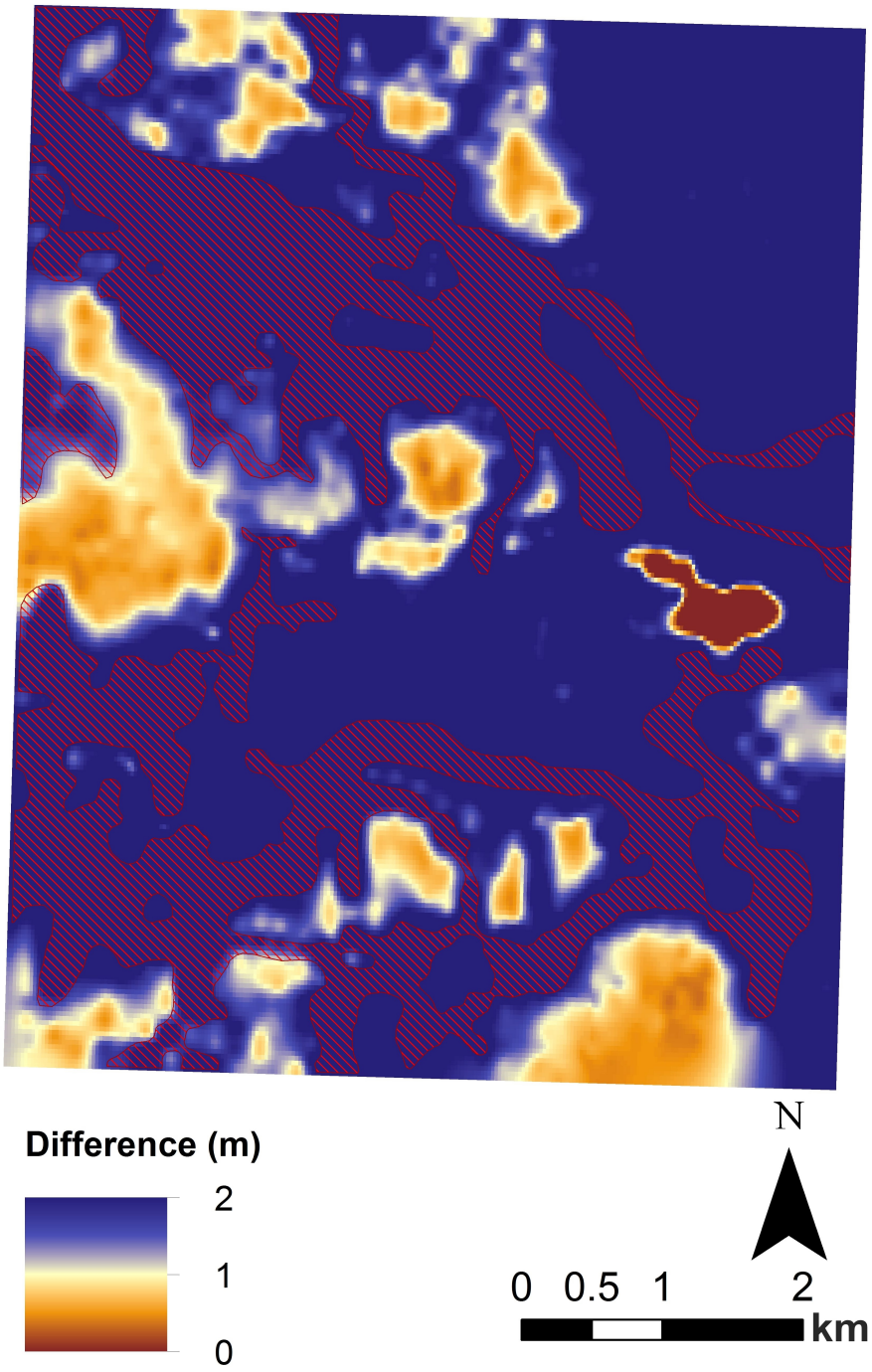

Figure 4.12: The raster image obtained by the difference between the *TS* and the *A* surfaces; the adopted color ramp shows, in a gradation between white and brown, the height differences lower than a meter. The red shape marks the main levees of the *A Surface*.

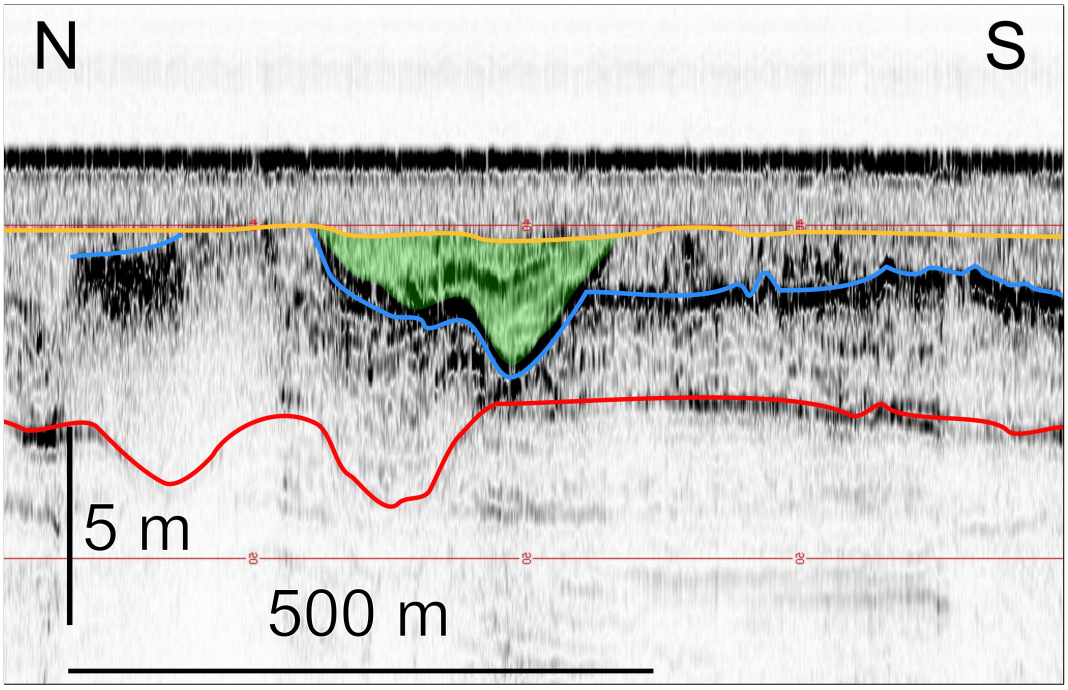

Figure 4.13: Detail from AS14 seismic line; the red line represents the *TS*, the blue line represents the *A Surface*, the orange line represents the *RS*, the green area represents the channel cross section. The development of the channel above the *A Surface* is clearly visible on the northern side.

The choice of including this channel within the *A* surface has been made considering that this feature is intimately related to it; the erosive channel dug a deep scour through the ridge, thus connecting a hypothetical eastern basin (placed beyond the edge of the surveyed area) to the inner low-lying areas comprised among the fluvial ridges. This feature shows a rapid deepening in the seismic profiles, both toward the sea and toward the coast (Figure4.14).

This erosive feature marks a scour also in the deposits beneath the *Transgressive Surface*, but in this case it has been chosen to interpolate the surface and obliterate the scour, considering that nothing seems to connect, at least strongly, the *TS* with this channel.

The environment inferred through the morphology and the sedimentary features is a tidal channel (the evidence will be explain in 4.5.3), thus the bodies placed at the western limit of the channel may be associated to a flood delta (Figure 4.15).

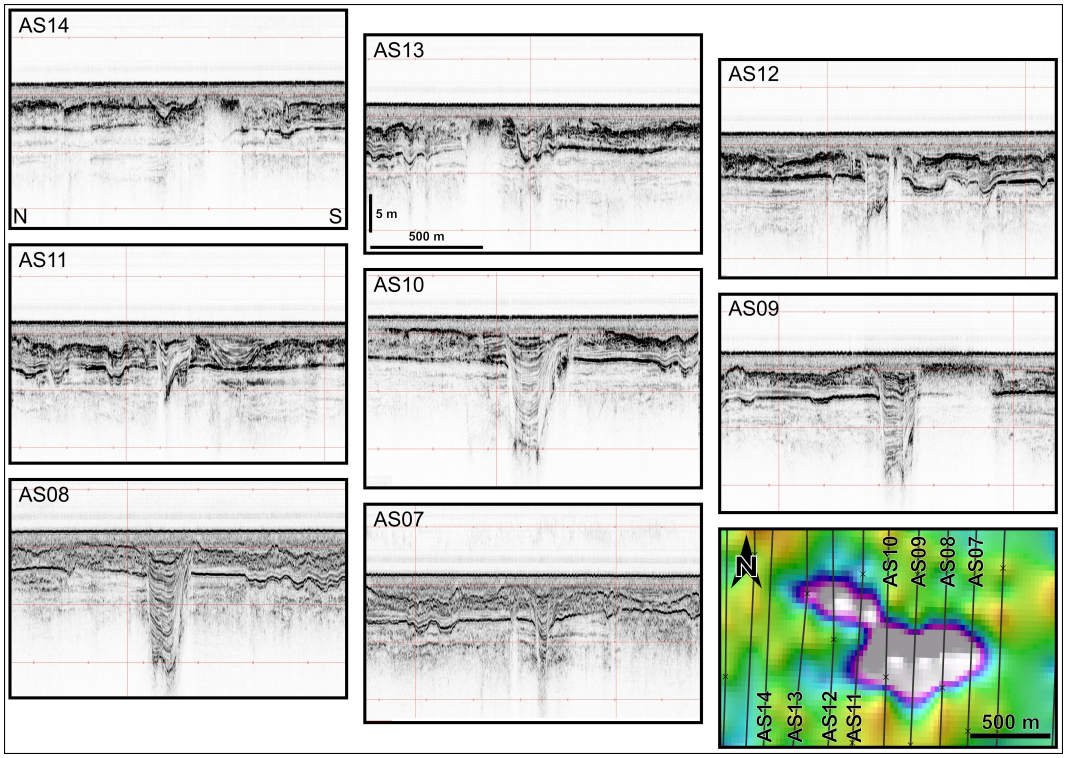

Figure 4.14: Scheme of the tidal inlet trend; the channel completely develops in less than a kilometre, fading very rapidly at its far ends. All the profiles present the same scale and the same orientation.

4.4.3 DEM of the *Ravinement Surface*

The *Ravinement Surface*, as expected, does not show particular morphologies, except for a gentle eastward dip (0.02 - 0.03%) toward east; the overall height difference is of 3 m, ranging from -34 to -31 m (Figures 4.16 and 4.17).

The observable structures are linked to the underlying morphologies of the *A Surface*: some elevations are due to the *A* highs, where the previous topography opposed against the erosive action of the waves, whereas some depressions are probably due to the differential subsidence.

The *Ravinement Surface* is less defined and also less rough than the other two surfaces, therefore a lower number of points has been picked. The digitalization of key surfaces along profile AS41, the only one in diagonal direction (SW-NE), is very sensitive to slight height variations. This occurs because of the small number of picked points if compared to the other profiles. Due to this situation, it was decided not to consider line AS41 in the interpolation process, which otherwise produces a well-defined diagonal stripe through the raster image.

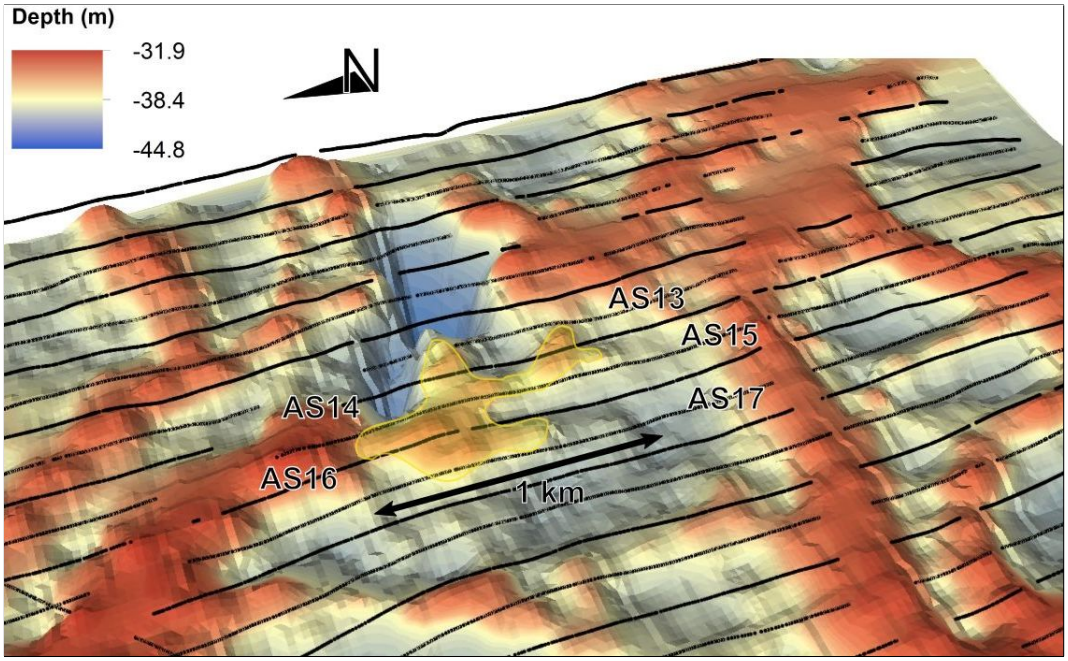

(a) 3D view of the area where the existence of a tidal flood delta was interpreted.

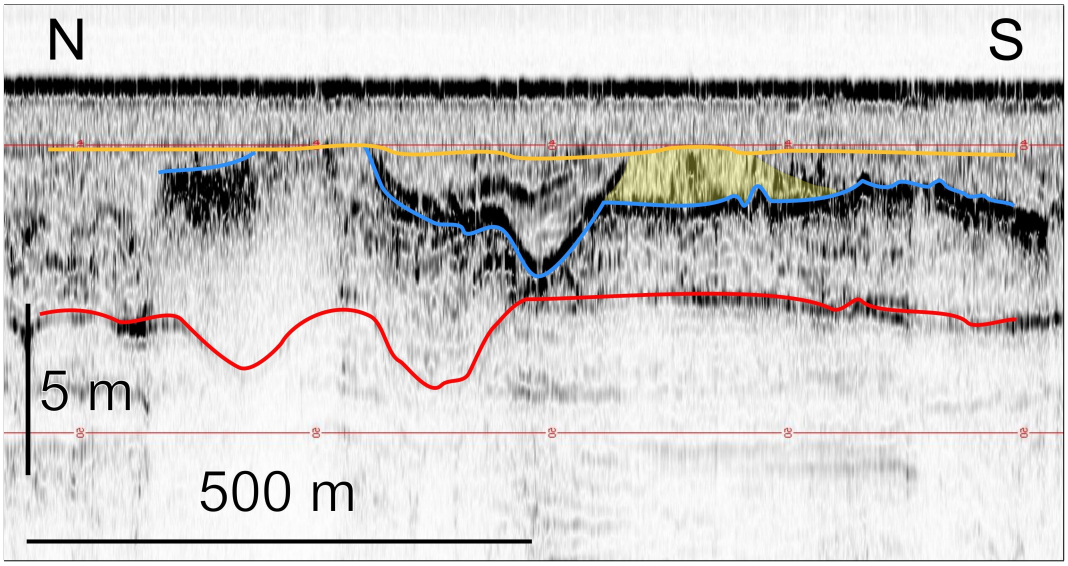

(b) Profile AS14: detail of the flood delta deposit highlighted by the yellow surface.

Figure 4.15: Flood delta evidence.

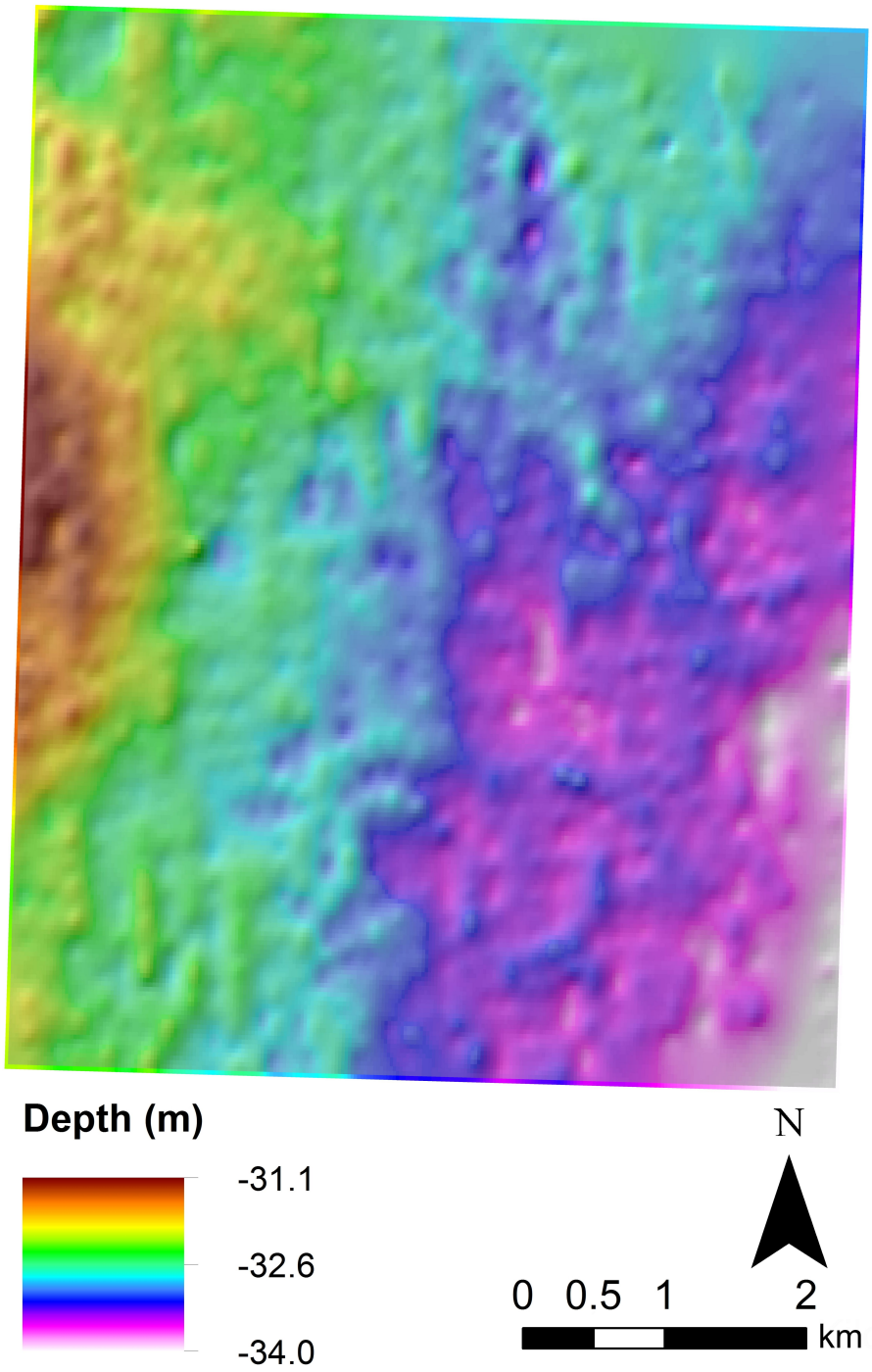

Figure 4.16: Raster image of the *Ravinement Surface*; the hillshade image of the surface was overlapped in transparency (50%) to the raster image in order to improve its readability.

Figure 4.17: TIN image of the *Ravinement Surface*; a vertical exaggeration factor of 100 has been applied in order to enhance the morphologies.

4.5 Sedimentary Facies Interpretation

The described morphologies were compared to the sedimentary structures visible in the seismic traces in order to interpret the depositional environment linked to every surface.

4.5.1 *Transgressive Surface*

The structures which lie beneath the *TS* are quite blurred and only occasionally strong reflectors are visible, therefore it is difficult to link the morphologies to specific sedimentary structures.

The typical sedimentary pattern of the ridges (Figure 4.18) consists in a series of stratified reflectors, but the layers that constitute the levees structures are often difficult to perceive (Figure 4.19).

These channels may be described as meandering due to the peculiar sedimentary pattern visible in the CHIRP profiles: the levee in the inner bank of the meander always shows a chaotic pattern, which may be considered indicative of the meander accretion, whereas the outer bank levee shows a well layered pattern, indicative of the still preserved older plain (Figure 4.19).

The meandering nature is also confirmed by the morphology, which is characterized by outer bank levees higher than the corresponding inner bank levees (Figure 4.18).

The erosive structures often show a partial obliteration of the peaty layer, and tend to truncate the underneath structures (Figure 4.20a).

The hypothetical sedimentary environment that characterized the area was a distal alluvial plain which has been suddenly flooded by a sea water body, which turned the environment to a tidal flat.

The *TS* is dated approximately 11 000 cal. a BP (Moscon et al., in press), after the Melt Water Pulse 1B (Fairbanks, 1989), which corresponds to a relative sea level rise of 0.9 cm/year (Correggiari et al., 1996).

The slope inferred by the areas not affected by erosion, combined to the relative sea rise, indicates a rate of marine ingression of 20 m per year; a tidal range of 1 meter would have also produced a cyclical marine ingression of 2.5 km.

These erosive scours were infilled by a layered deposit that will be described in the following paragraph, as a portion of the transgressive sedimentary body.

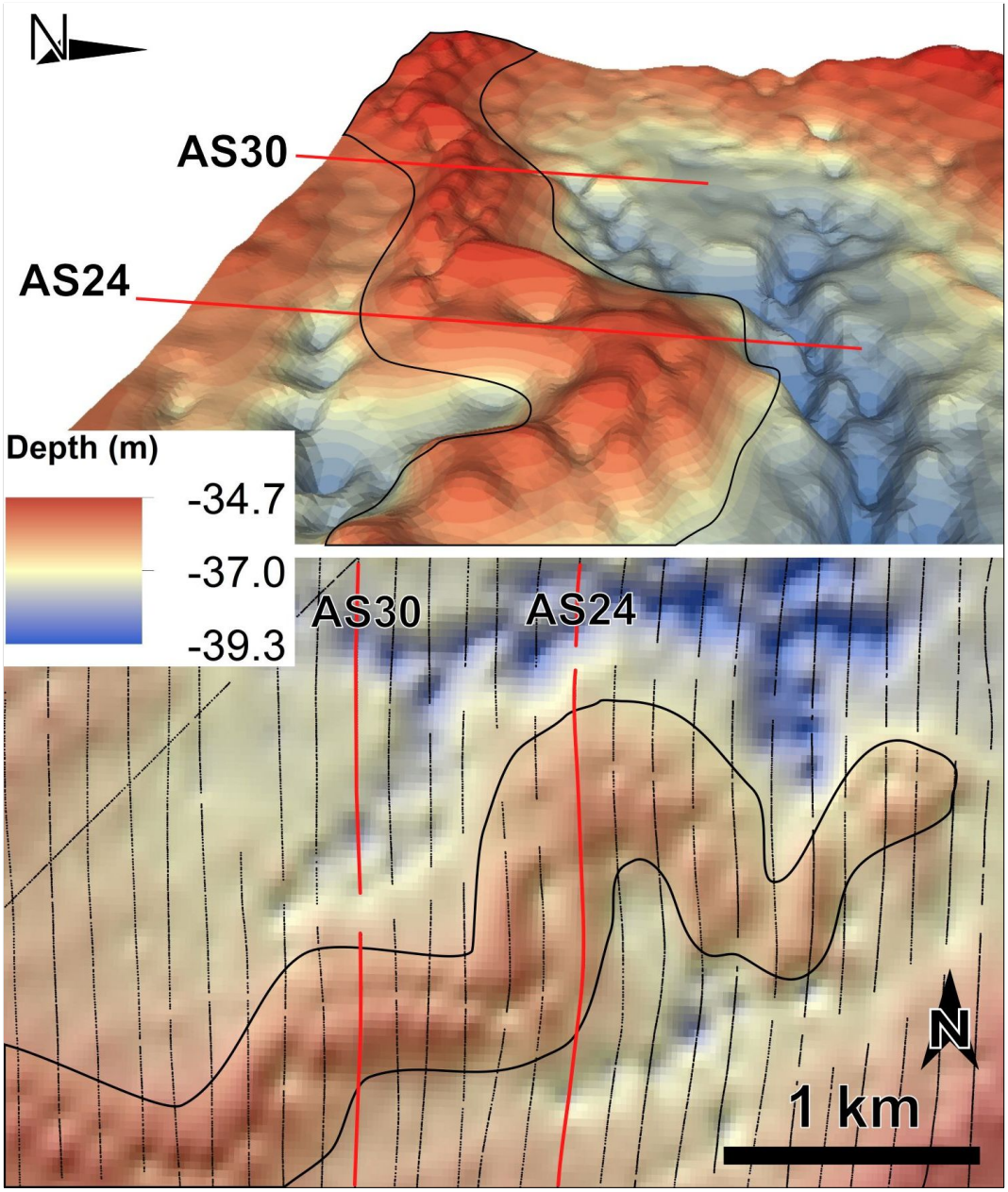

Figure 4.18: Detail of the SW ridge in 3D view; The asymmetric profile of the ridge is clearly visible. The highlighted CHIRP lines correspond to the figures in 4.19.

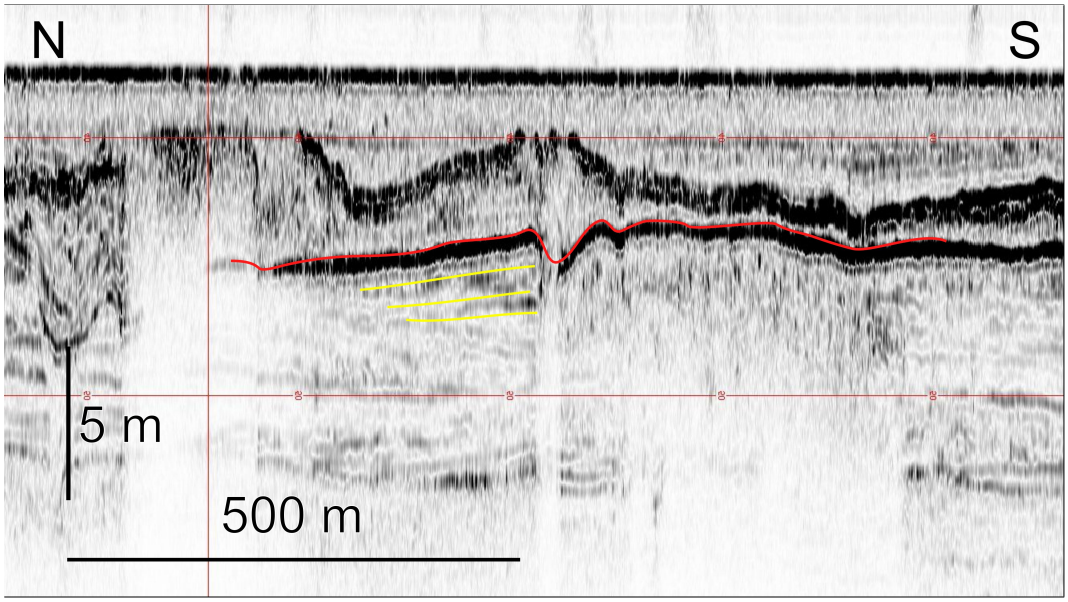

Figure 4.19: Profile AS24: detail of the stratigraphy of the fluvial ridge shown in 4.18. The red line tracks the *TS* and highlights the asymmetry between the levees of the ridge. There is a clear difference in the sedimentary pattern on the two sides of the channel: the northern levee, placed in the outer zone of the meander, shows a layered structure, whereas the southern levee does not show a clear structure, probably due to the meander migration.

The *Transgressive Surface* is therefore lying above the LGM alluvial plain, which has been affected by aggradation during the first phase of marine transgression and by erosional processes in the first moments of the marine ingression in this area. The deposits linked to the LGM plain are only occasionally visible in the seismic profiles and therefore they cannot be traced. The recognizable features can be associated to fluvial ridges and deep erosive scours.

4.5.2 *T1*

The transgressive body beneath the *A Surface* is here called *T1*. The correlation between the morphologies and the sedimentary structure is simpler here due to the clearness of the reflector of the *T1*.

The lower type of deposit can be linked to the erosive channels of the underlying *TS*: the interbedded transparent facies, described in the paragraph 4.2, occupy the erosive scours of the *Transgressive Surface* and in some cases also the adjacent areas; the tendency of the layers of these deposits to trace the underlying topography is probably due to occurrence of differential subsidence

(Figures 3.15 and 4.20b).

The natural levees deposits are characterized by a quite chaotic seismic response, with semi-transparent bodies alternated to strong reflectors; only occasionally the stratification is well defined. The major fluvial ridges are characterized by a transparent body which marks the river axis; these deposits are interpreted as the sand bodies which are deposited at the bottom of the channel. These morphologies are indicative of a pensile fluvial channel (Figures 3.15, 4.21 and 4.22).

The seismic analysis, combined to the DEM, underlines that the ridges developed in different time spans, with at least two different generations (Figures 3.15 and 4.23a).

The seismic profiles clearly show that in some cases the fluvial ridges are overlapped on the tidal channel deposits, whereas in other cases the latter are overlapped on the previous ones (Figure 4.23b); this fact suggests that a first generation of ridges developed simultaneously to the infilling of the tidal channel scour, then a second generation of ridges superimposed over these morphologies.

The environment inferable by these observations is that of a tidal flat which gradually switches to a distal alluvial plain; the erosive features recorded by this surface can be ascribed to the further evolution of the area and will be described in the next paragraph.

The causes of the switch between the tidal flat and the alluvial plain could not be inferred from the analyzed area: they may be caused by a transformation of the paleogeography on a major scale, such as the isolation of the sea ingression produced by a sandspit, or by a higher rate of sedimentary load.

4.5.3 *T2*

The transgressive body between *A* and *ravinement* surfaces is here called *T2*; it is mainly formed by semi-transparent bodies which occupy the lower areas of the pre-existing topography, and in some cases are superimposed also on the ridges. Also in this case the layers pattern is probably due to differential subsidence (Figure 4.24).

These deposits are directly connected to the erosive channel which is as well infilled by the deposit that has been just described above. The contact between the channel and the transgressive body beneath the *A Surface* is markedly

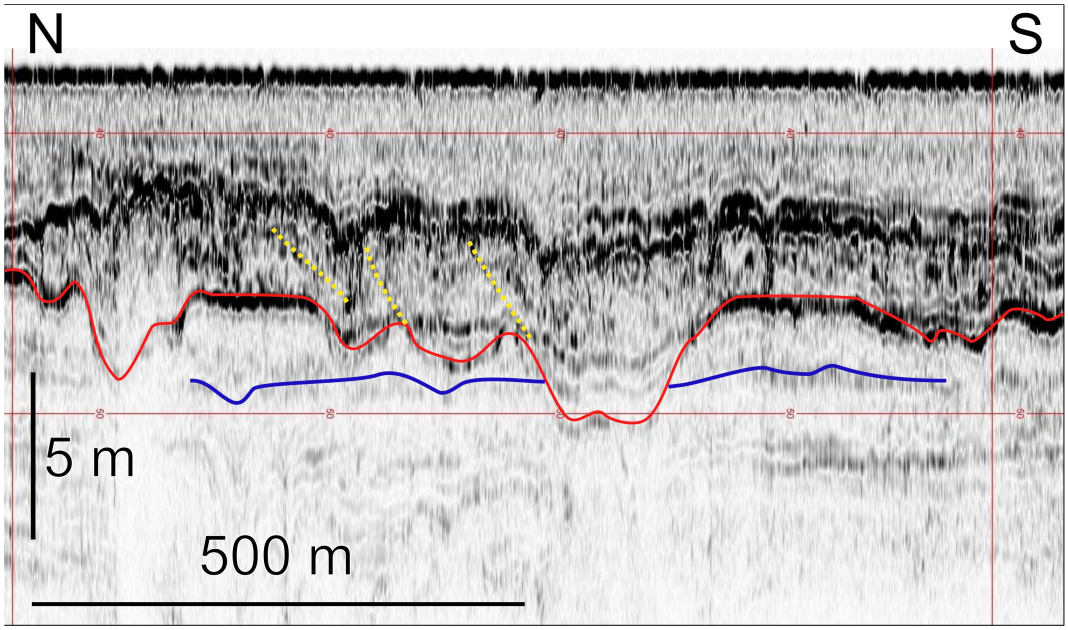

(a) Profile AS17: detail of the eroded surface. The blue line marks a layer interrupted by the erosion. The dotted yellow lines mark the migration of the tidal channel toward south.

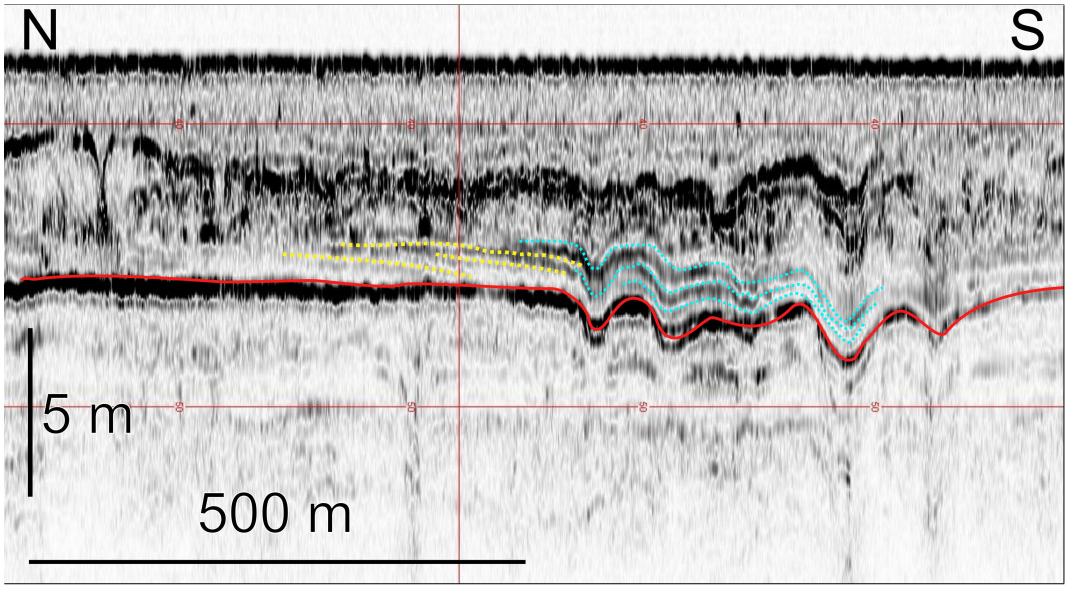

(b) Profile AS13: detail of the layered deposit. The dotted cyan lines likely mark the differential subsidence. The gently dipping layers, highlighted by the dotted yellow lines, may suggest a migration of the tidal channel.

Figure 4.20: The erosive tidal channels and the connected deposits of the *TS*.

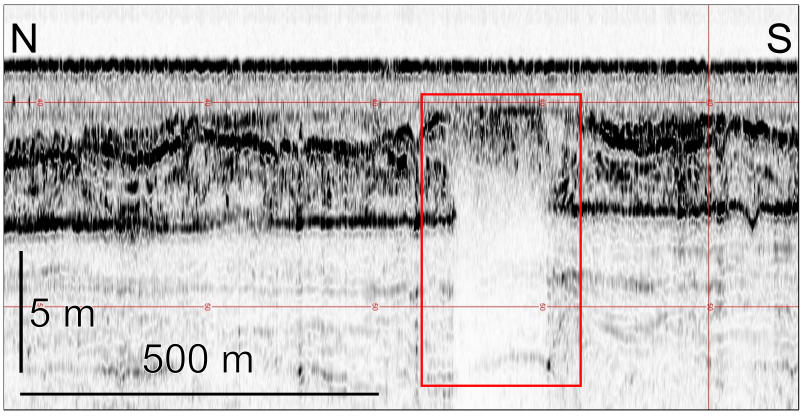

Figure 4.21: Profile AS13: typical response of a sand deposit. The acoustic blanking is the product of the scattering of the acoustic signal induced by the fluids which saturate the porous bodies.

erosive, as a confirmation of the erosive nature of the channel (Figure 4.25).

The environment inferred by these observations is that of a lagoon connected to an eastern basin by a tidal inlet; differently from the tidal plain of the *TS*, here there is no evidence of erosion except for the tidal inlet. A semi-transparent body, with no appreciable structure, can be found above these deposits; this body is truncated, along with the other intersecting morphologies, by the *Ravinement Surface*. This body probably formed after the drowning of the lagoon, in a foreshore - upper shoreface environment.

4.5.4 *H1*

The depositional body of the highstand phase is here called *H1*. This last sedimentary body is comprised between the *Ravinement Surface* and the sea floor and it is made up of a semi-transparent body lacking structures. This body can be ascribed to the highstand system tract and has been probably deposited in an offshore transition to offshore environment.

4.6 Volumes of Sedimentary Bodies

The volumes comprised between the surfaces were calculated with an ArcGIS tool as explained in paragraph 3.2.5. The calculated volumes are here reported (Table of figure 4.27) both as deposited and removed; the only relevant sediment removal occurs in correspondence with the tidal inlet. It must be evidenced

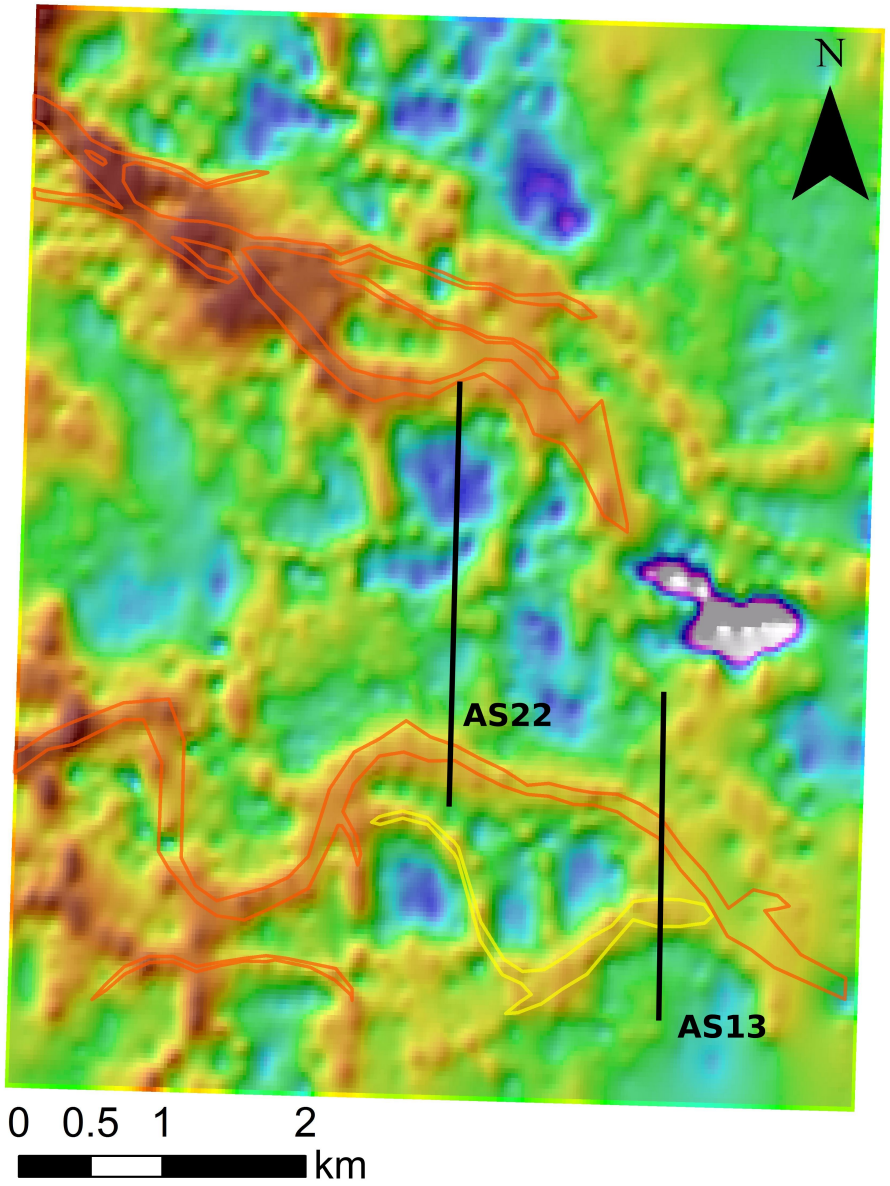

Figure 4.22: The reconstructed sand deposits; these shapes were drawn on the basis of Figure 4.2. The yellow shape has been differentiated because the related ridge is superimposed on the adjacent ridge.

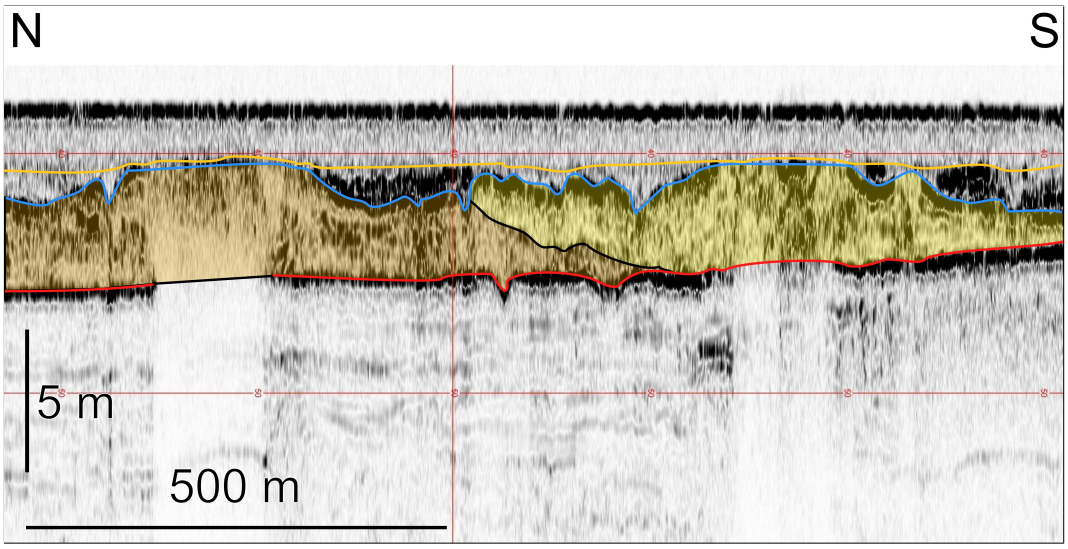

(a) Profile AS13: detail of the superimposition of two levees. The used colours correspond to the colours used in figure 4.22.

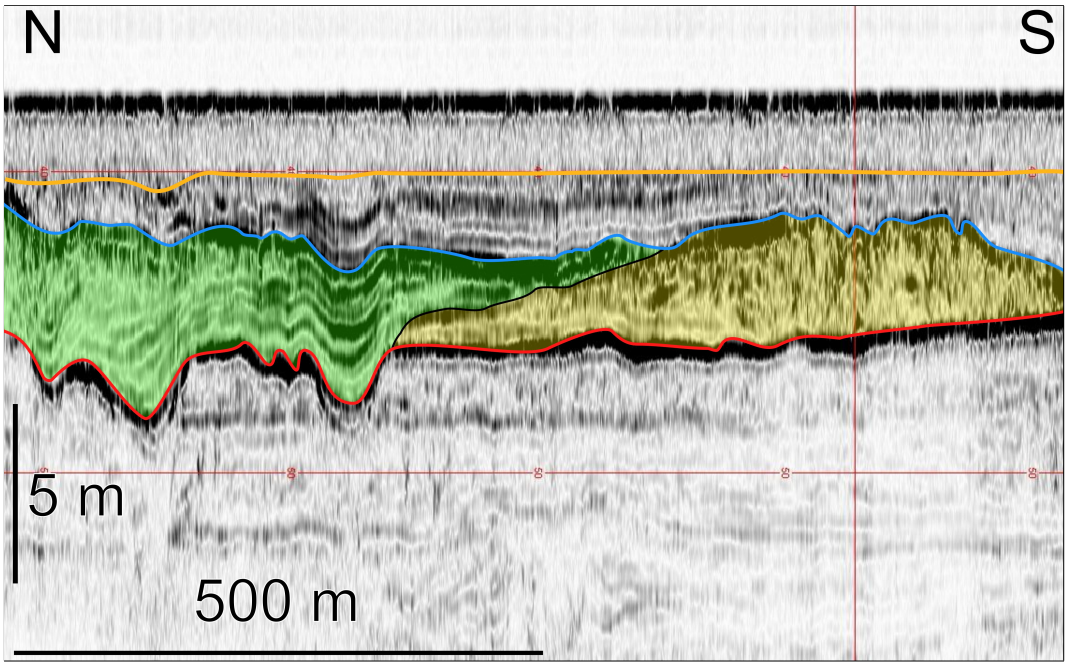

(b) Profile AS22: detail of the superimposition of the lagoon deposits onto a fluvial ridge.

Figure 4.23: Stratigraphic relations between the deposits of the transgressive body.

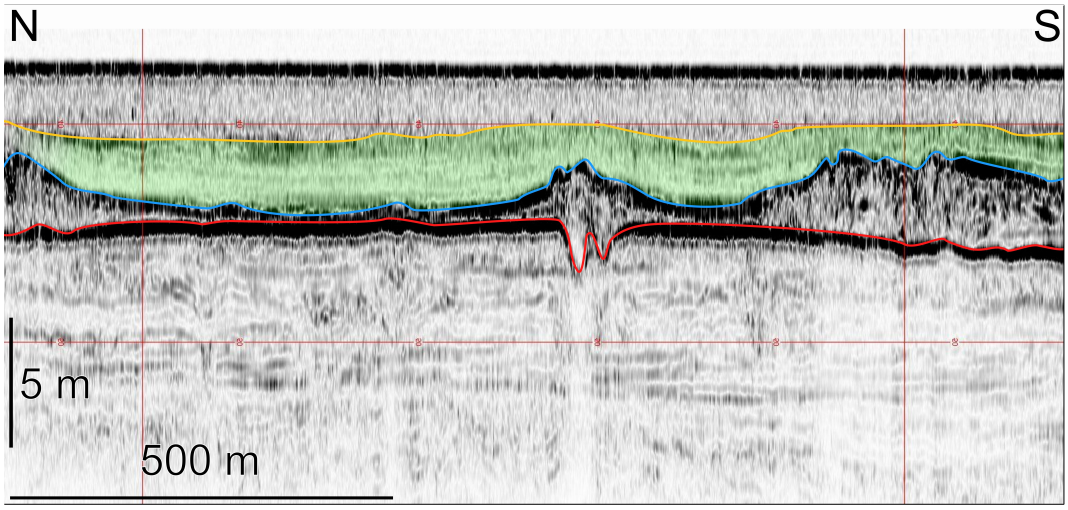

Figure 4.24: Profile AS22: typical appearance of a low-energy layered deposit interpreted as the product of lagoon sedimentation.

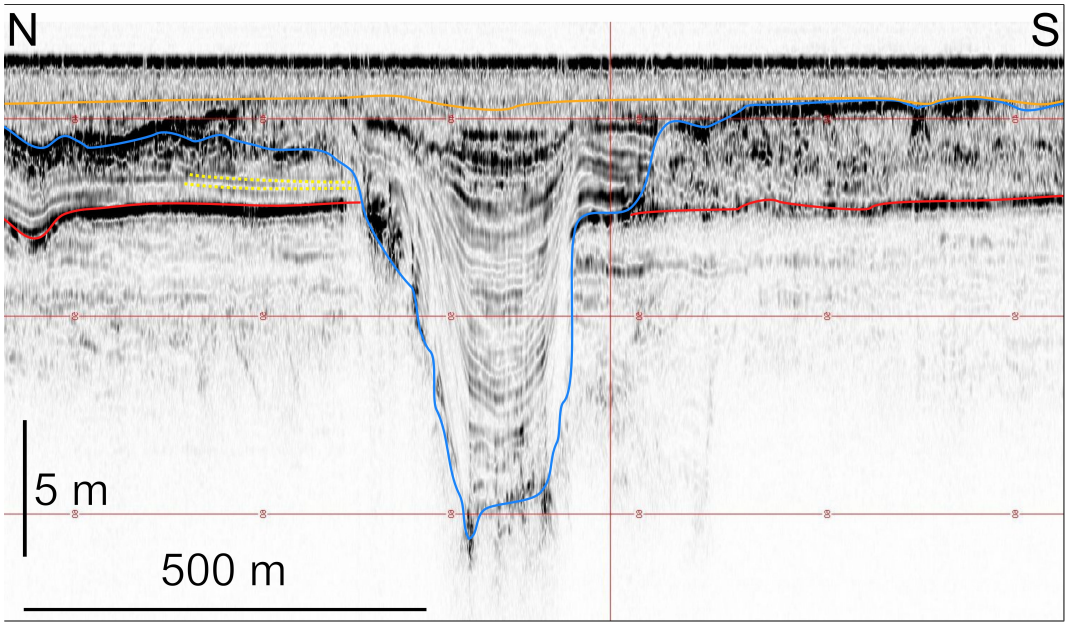

Figure 4.25: Profile AS10: example of the erosive surface between the channel and the transgressive body; the yellow dotted layers on the northern side are clearly truncated by the channel, whereas, on the southern side, there is a strong difference between the channel infill and the ridge deposit.

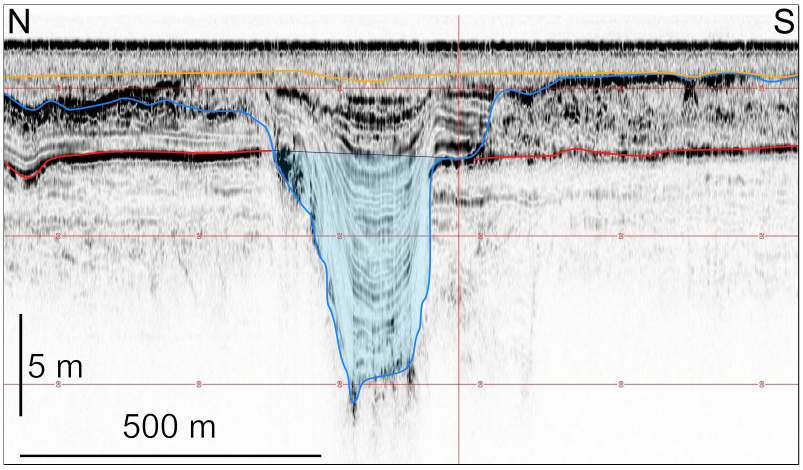

Figure 4.26: The effective volume represented by the calculated datum refers only to the colored area.

	Deposited volume (m^3)	Removed volume (m^3)
RS - A	67 700 000	0
A - TS	105 300 000	661 000

Figure 4.27: Deposited and removed sediment volumes.

that this result underestimates the real volume of the tidal inlet, because it only considers the intersection between *TS* and *A* (Figure 4.26).

A more specific analysis was performed in the calculation of the ridge volumes of the *A Surface*; the following data (Table of figure 4.28) only represent the volume comprised between the *A* and the *TS* surfaces in the correspondence of the major fluvial ridges individuated in the Figure 4.29.

	Volume (m^3)
N levee (A)	20 800 000
W levee (B)	1 700 000
S levee (C)	20 800 000
Total	43 300 000

Figure 4.28: Volumes of the ridges of the *A Surface*; the letters correspond to the fluvial ridges represented in figure 4.29.

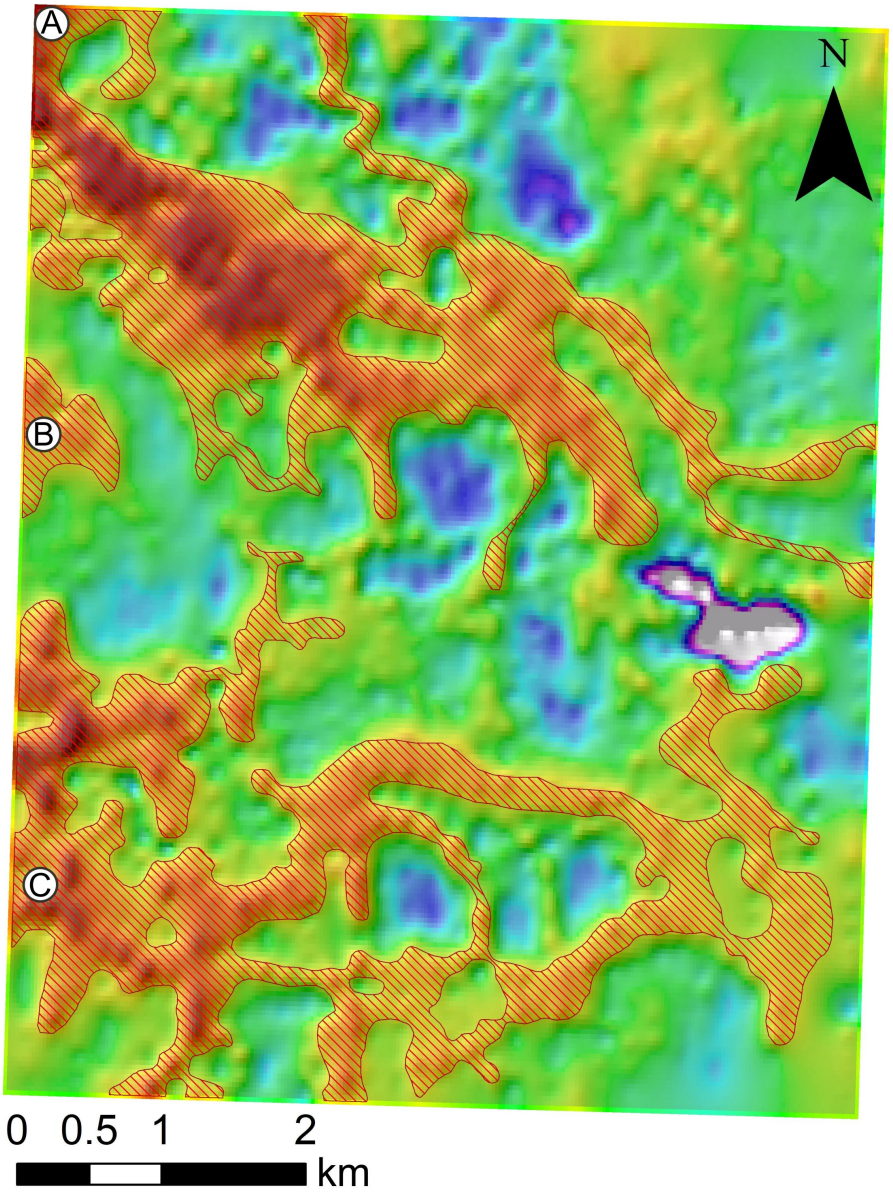

Figure 4.29: The red shapes roughly mark the limits of the ridges; they were used in order to calculate the volumes of these features.

Chapter 5

Discussion

5.1 Sea-level Rise and Lambeck's Model

The identification of deposits related to lagoons-brackish swamps environments, which are connected to the tidal inlet, suggests an interesting datum of the paleo sea-level position, which can be reasonably placed at the same level of the upper deposits.

Dating these features is of particular interest due to the implications of a known sea-level rise rate on a coastal environment. The lack of dated cores in this area leads to the use of sea-level rise models for the Adriatic Sea, in order to obtain a reasonable age estimate for these deposits; the obtained dates were then compared to the reference data.

In order to obtain an age datum, the depth of the top of the layered deposits lying onto the *A Surface* (Figure 5.1) was compared to the Adriatic sea-level rise curve from Correggiari et al., (1996). The obtained date was then compared to the Lambeck's model.

5.1.1 Adriatic Sea-Level Rise Curve

The sea-level rise curve for the northern Adriatic Sea (Figure 2.6) represents the known relative sea-level rise of the last 20 000 years without any correction for subsidence; the age of the top of the lagoon is easily obtained by entering a depth datum in this curve (Figure 5.4).

The depth of 33.1 m, which is considered representative for the top of the lagoon-brackish marsh deposits placed above the *A Surface* (Figure 5.1), was obtained by averaging several depths taken from different CHIRP lines; in order

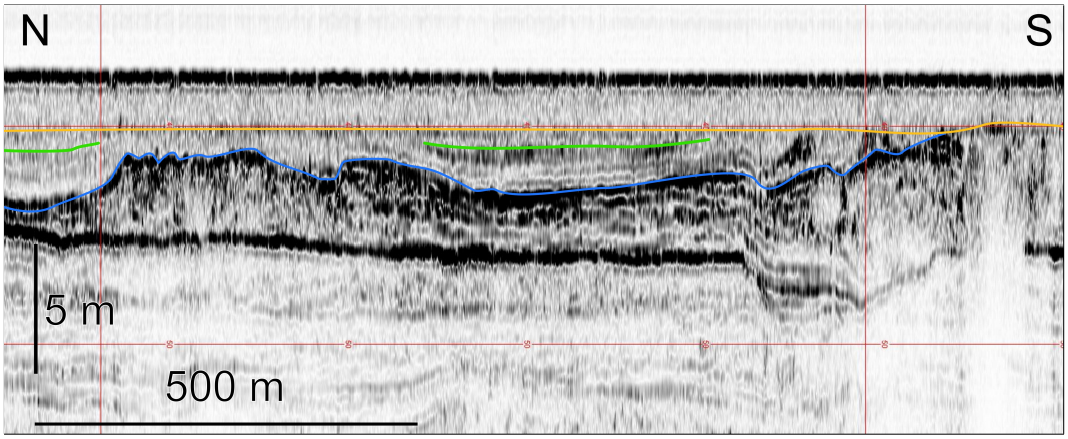

Figure 5.1: The green lines represent the tops of the typical lagoon-brackish marsh deposits; the related depth was compared with the curve build on the observed points in order to obtain an age datum.

to represent the error committed during the selection of the uppermost layer of the lagoon unit, the first and the third quartiles will be displayed, along with the averaged depth datum (Table of figure 5.2). The obtained data are well comparable to the ages inferred by ^{14}C dating on a near core (Moscon et al., in press) (Figure 5.3).

	Depth (m)	cal. a BP
I quartile	-33.2	9 853
Average datum	-33.1	9 831
III quartile	-32.8	9 798

Figure 5.2: Depths and relative calculated ages.

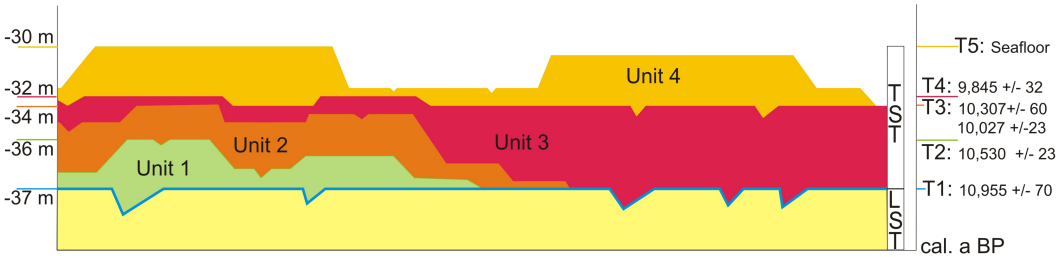

Figure 5.3: Estimated dates for the main surface of the area analyzed in Moscon et al., (in press), which is situated roughly 10 km eastward compared to the position of the tidal inlet; the T4 surface corresponds to the *Ravinement Surface* of this work. Modified from Moscon et al., in press.

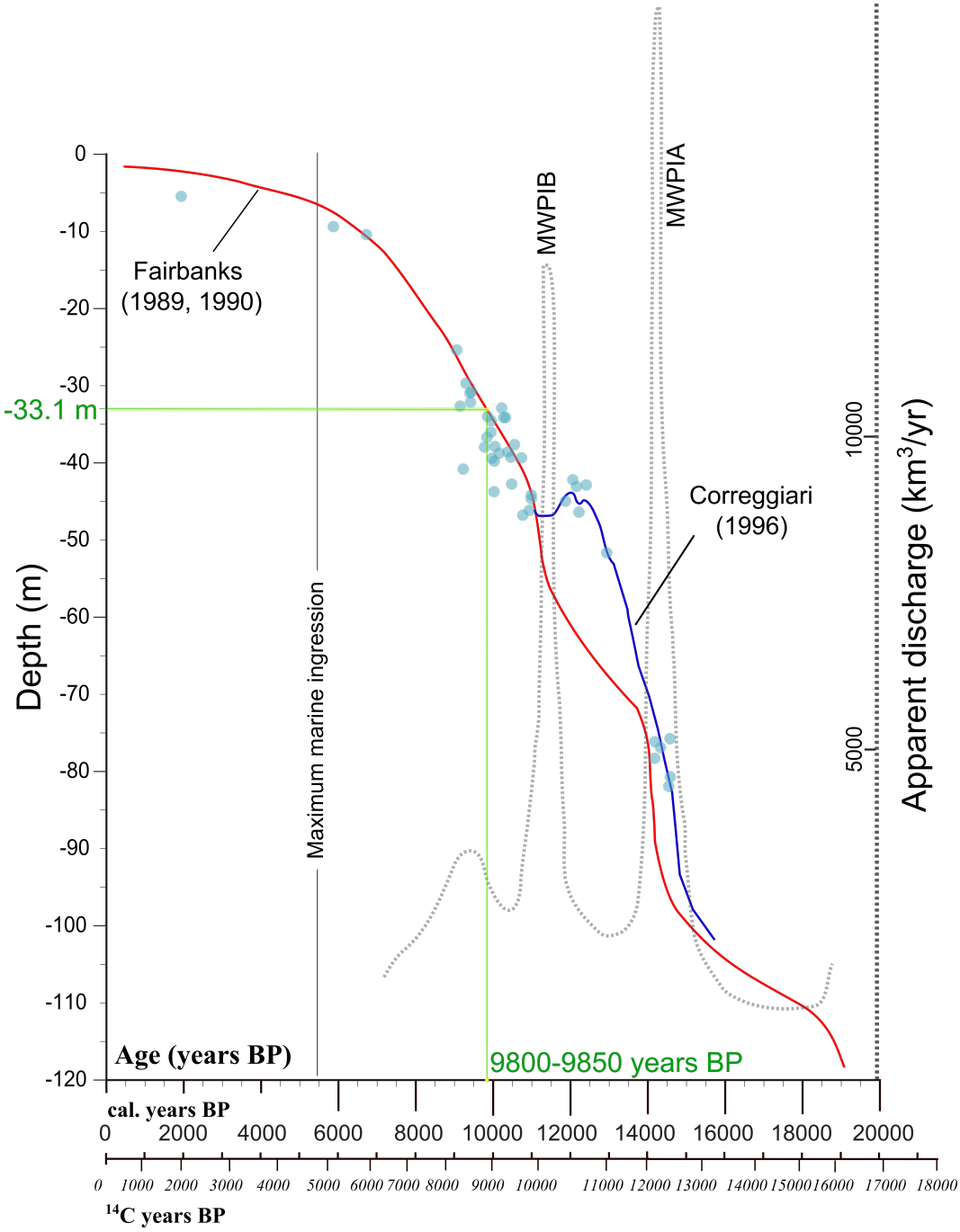

Figure 5.4: Lagoon deposits depth projected on the sea-level curve for the northern Adriatic Sea. The thickness of the green line represents the range between the first and the third quartiles, evidencing that the possible associated error is almost negligible. Modified from Correggiari et al., 1996.

5.1.2 Lambeck's Model

The Lambeck's model (its complete identification number is K33_j1b_WS9_6) (Lambeck et al., 2004, Antonioli et al., 2009, Lambeck et al., 2011) provides a series of sea-level rise curves for different sites; these curves are built with a geophysical model which does not take account for the subsidence or tectonic vertical movements. The sites used here are the sites 31 and the 32, corresponding to Ravenna and the mouth of the Po River near Porto Tolle (Figures 5.7 and 5.8), due to their proximity to the study area; the depths shown in the tables of figures 5.5 and 5.6 were calculated with these curves from the age datum deduced in the previous section.

The depth difference between the Adriatic sea-level curve and the Lambeck's model may be caused by the subsidence of the area, which can be easily inferred by dividing the depth difference by the numbers of years BP elapsed since their sedimentation.

	Calculated depth (m)	Inferred subsidence ($cm/year$)
I quartile	-34.6	0.015
Averaged datum	-35.0	0.020
III quartile	-35.3	0.023

Figure 5.5: Study area subsidence inferred with the *site 31* curve (Ravenna).

	Calculated depth (m)	Inferred subsidence ($cm/year$)
I quartile	-33.9	0.009
Averaged datum	-34.4	0.013
III quartile	-34.7	0.016

Figure 5.6: Study area subsidence inferred with the *site 32* curve (Porto Tolle).

Considering the predicted curve for *site 31*, which is the closest to the study area, the obtained subsidence shows a good accordance with the datum presented in paragraph 2.6.3, thus providing a validation for this analysis. Notwithstanding this good result, this analysis should be matched to a core, in order to better select the depth of the uppermost lagoon-brackish marsh deposits and thus removing the intrinsic error due to the manual selection of the top lagoon layer. A core would be also useful in order to precisely

date the lagoon deposits, thus supplying a datum which may be compared to the Adriatic sea-level curve and the Lambeck's model, which here must be considered efficient without the chance to testing it with a known datum.

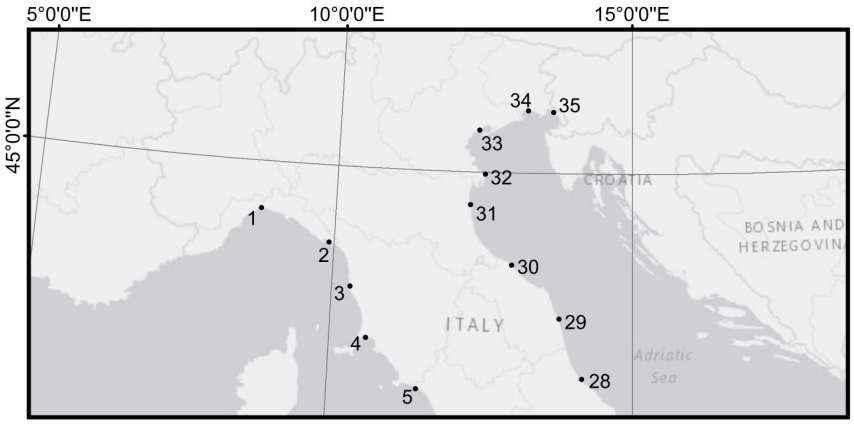

Figure 5.7: Sites available for the Lambeck's model. Modified from Lambeck et al., 2011.

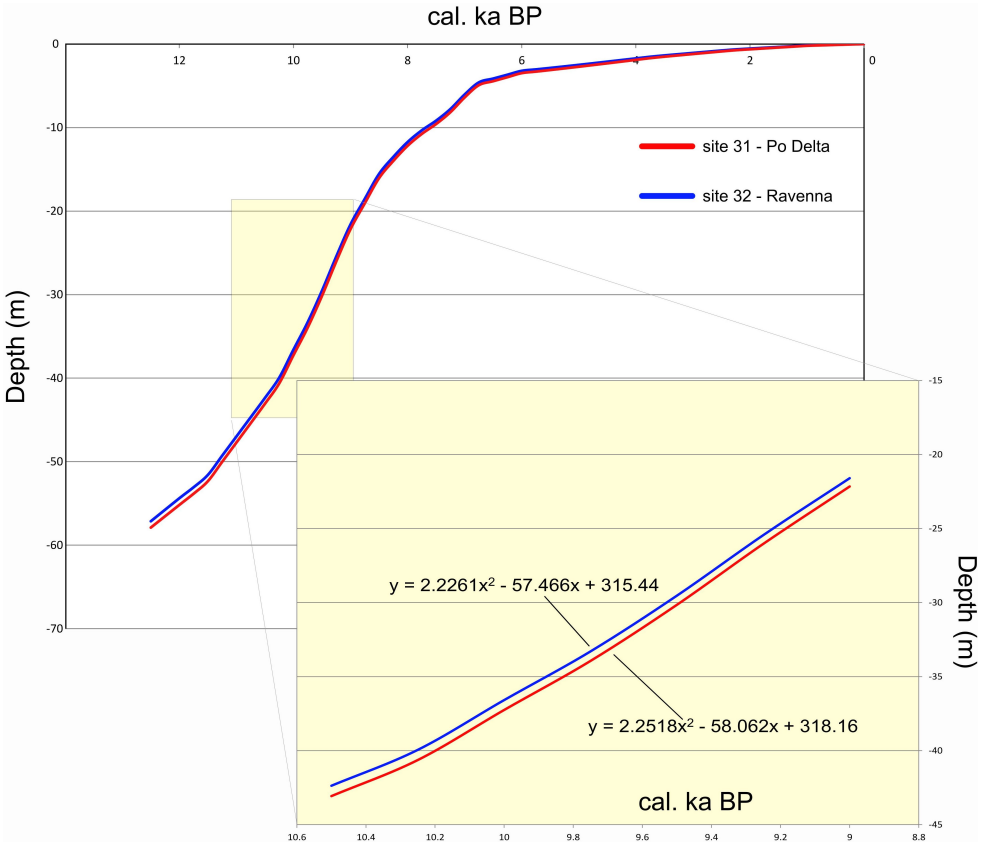

Figure 5.8: Sea-level rise curves for the sites 31 and 32; the relations shown in the detail were obtained with a polynomial regression.

5.2 Coring Proposal

The absence of cores in the study area did not allow to check directly some stratigraphic ground truths for the seismic analysis. In this chapter three sites for an hypothetical future coring are proposed (Figure 5.9), along with the synthetic log of these cores; all the proposed logs have a length of 6 meters, in the hypothesis of a complete penetration of the corers described in the Methods chapter.

Core_1

The first hypothetical core is situated within the tidal inlet (Figure 5.10a); this core should provide data to interpret the depositional facies of the infilling and for a geochronological dating (Figure 5.11).

Core_2

The second hypothetical core is placed in correspondence to the lagoon/brackish swamp deposit (Figure 5.10b). This core may provide a precise dating for the peaty layers, which can be compared to the dating inferred by the sea-level rise curve; it should also provide a further proof on the nature of these deposits (Figure 5.12).

Core_3

The position of the last core has been chosen in order to intercept two fluvial ridges, one pertaining to the *A Surface* and one to the *TS* (Figure 5.10c); this core may provide interesting data on the nature of the sediments which constitute these morphologies (e.g. grain size, composition) and may also sample peaty layers useful for dating the surfaces (Figure 5.13). This core is the only one which may reach the first centimeters under the *Transgressive Surface*.

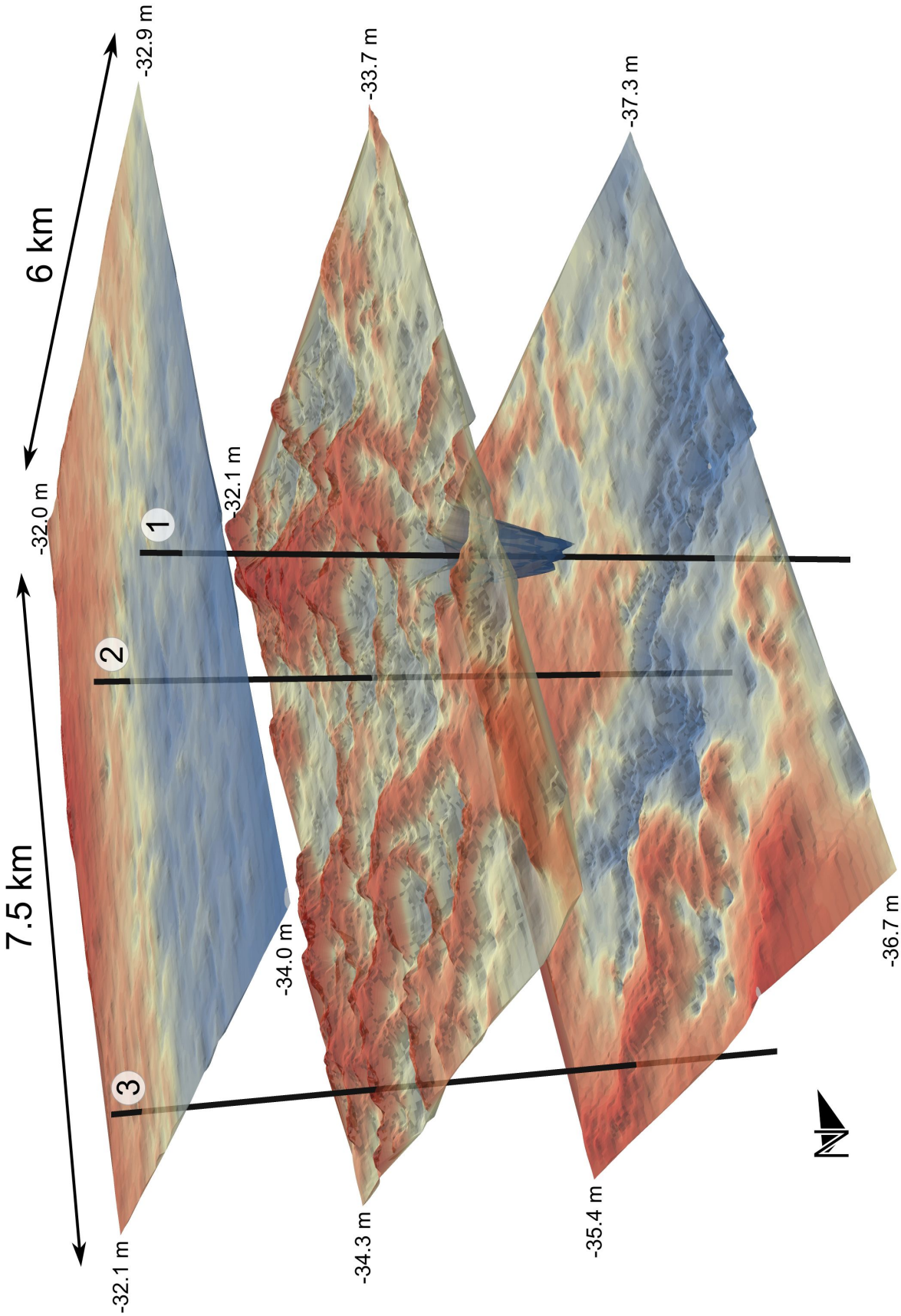

Figure 5.9: Location of the proposed cores in 3D view.

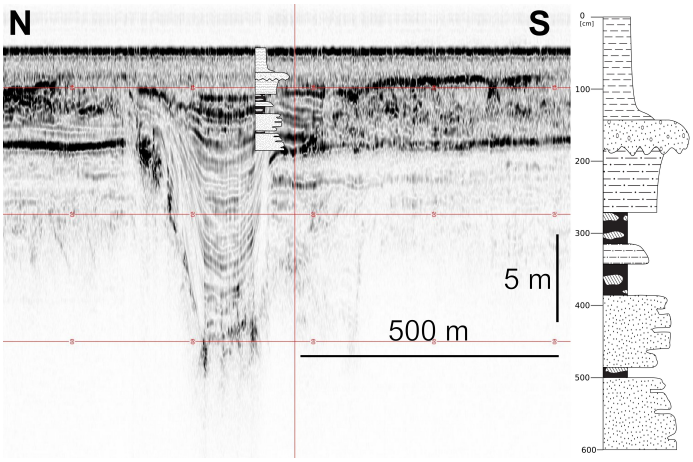

(a) Representation of the Core_01 in the AS10 seismic profile.

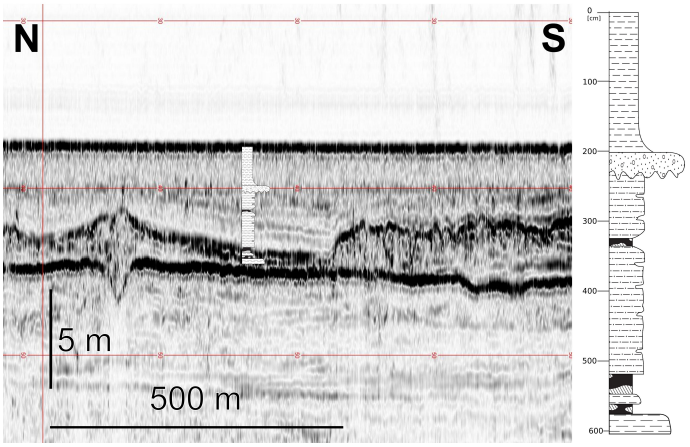

(b) Representation of the Core_02 in the AS23 seismic profile.

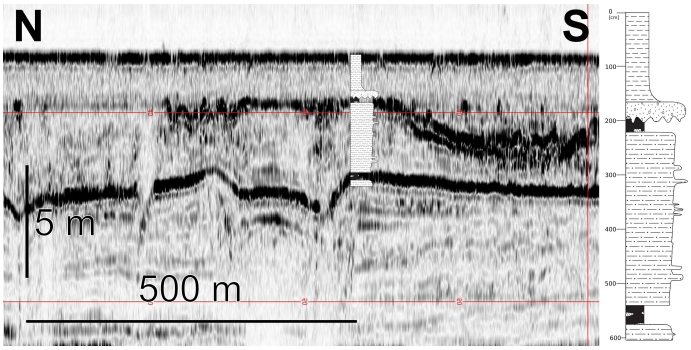

(c) Representation of the Core_03 in the AS32 seismic profile.

Figure 5.10: Comparison between the stratigraphic logs and the seismic responses.

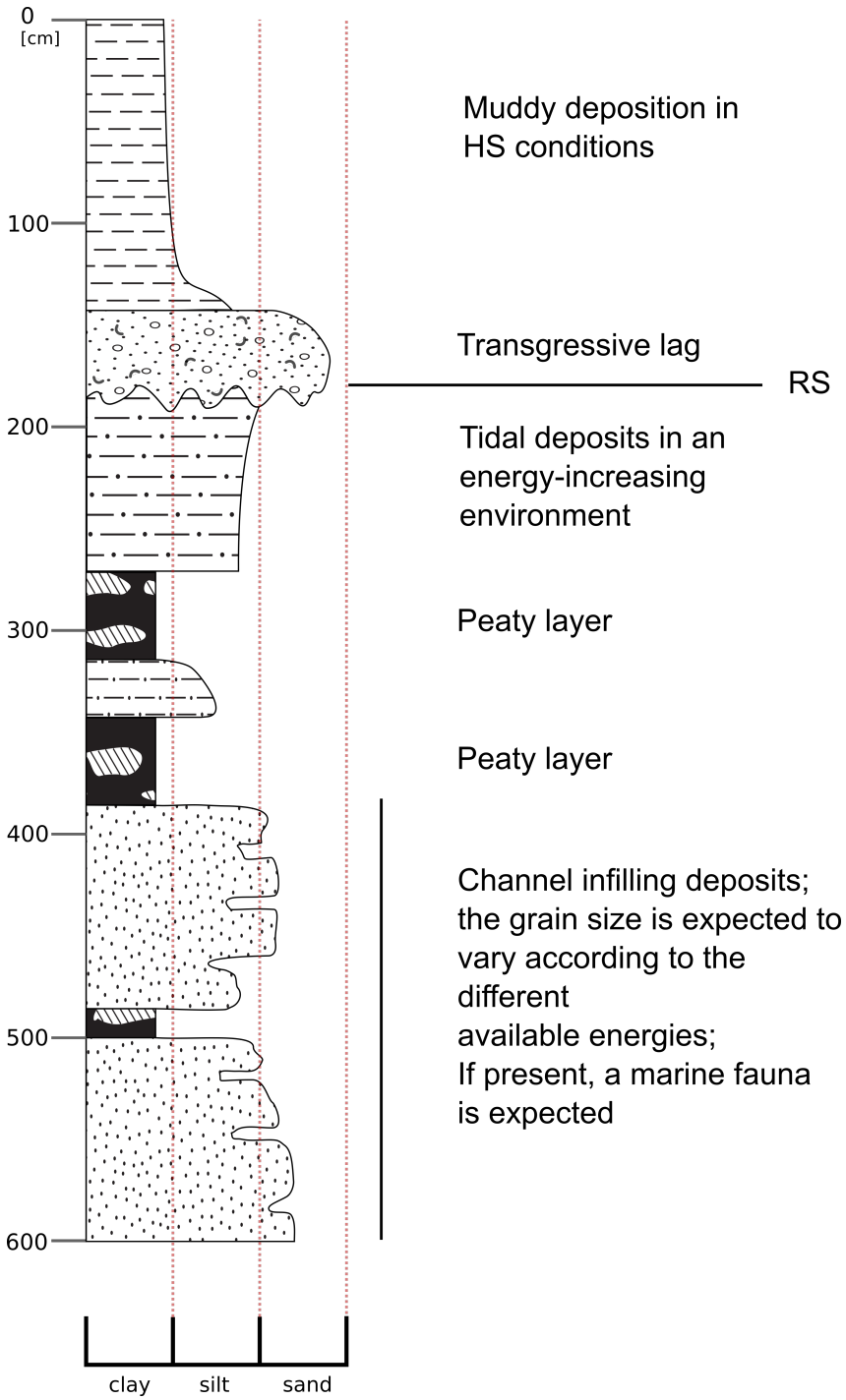

Figure 5.11: Synthetic stratigraphic log of the Core_01.

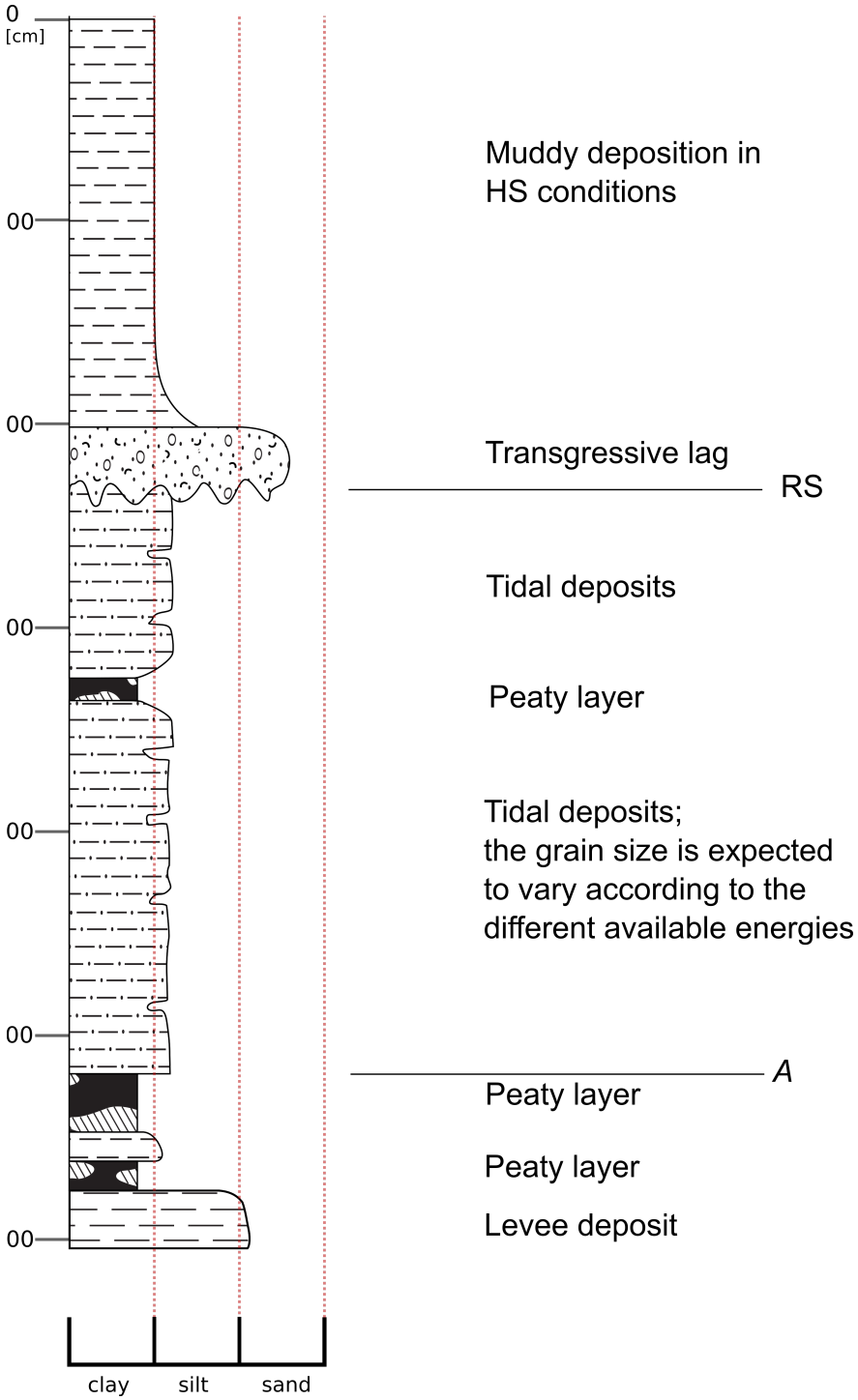

Figure 5.12: Synthetic stratigraphic log of the Core_02.

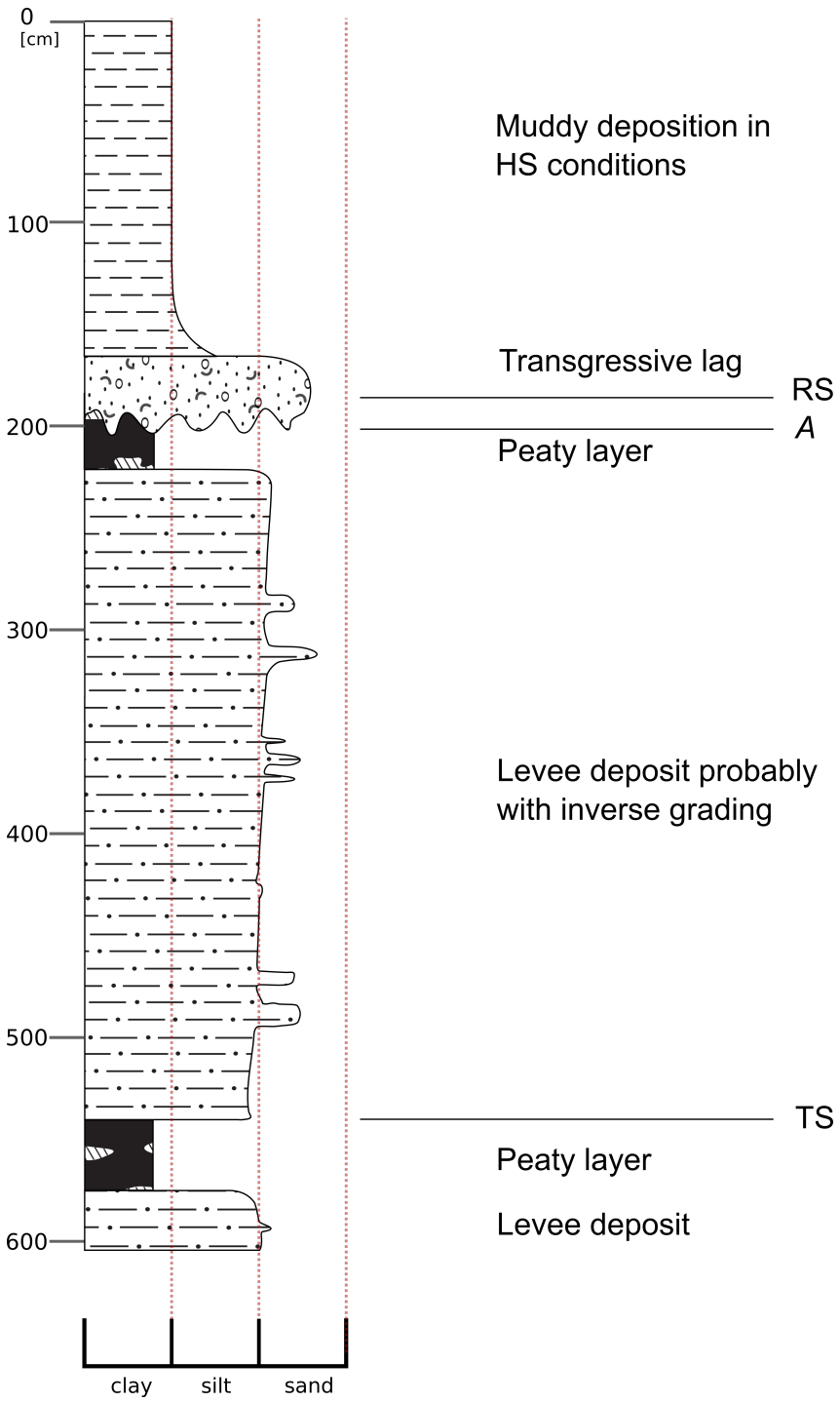

Figure 5.13: Synthetic stratigraphic log of the Core_03.

5.3 Geomorphological and Stratigraphic Analogues

The comparison between the study area with other present coastal areas, were similar morphological and geological features are present, supplies interesting information for different points of view:

- Current analogous environments provide a huge data basin, which is exploitable in order to gain information on the forcing conditions which constrained the studied morphologies during their evolution;
- The knowledge of the evolution of the paleo-morphologies in the framework of the forcing factors that affected these processes can help to predict the short and long term evolution of the current environments, thus helping a conscious management of the coastal resources.

The stratigraphy of the study area represents another interesting topic to be compared to some similar cases already studied in the Adriatic and other basins:

- The study area can be linked to other areas with similar stratigraphy and a well-known evolutionary history. This process may supply a validation to the evolution hypothesis presented in this thesis;
- Linking the stratigraphy of a recent and easily accessible succession, such as the one of the study area, to a more ancient one may supply interesting hints in the developing of its evolutionary model and in the definition of its depositional characteristics; the study case discussed in this thesis may be of particular interest due to its peculiarities, such as the low gradient of the former alluvial plain on which the analyzed morphologies have been formed, and the rapid sea-level rise which affected the area. This approach may be useful both in the academic research and in the research related to fluid extraction (e.g. water and oil). This subject, which needs further in-depth analysis, will not be discussed in this work.

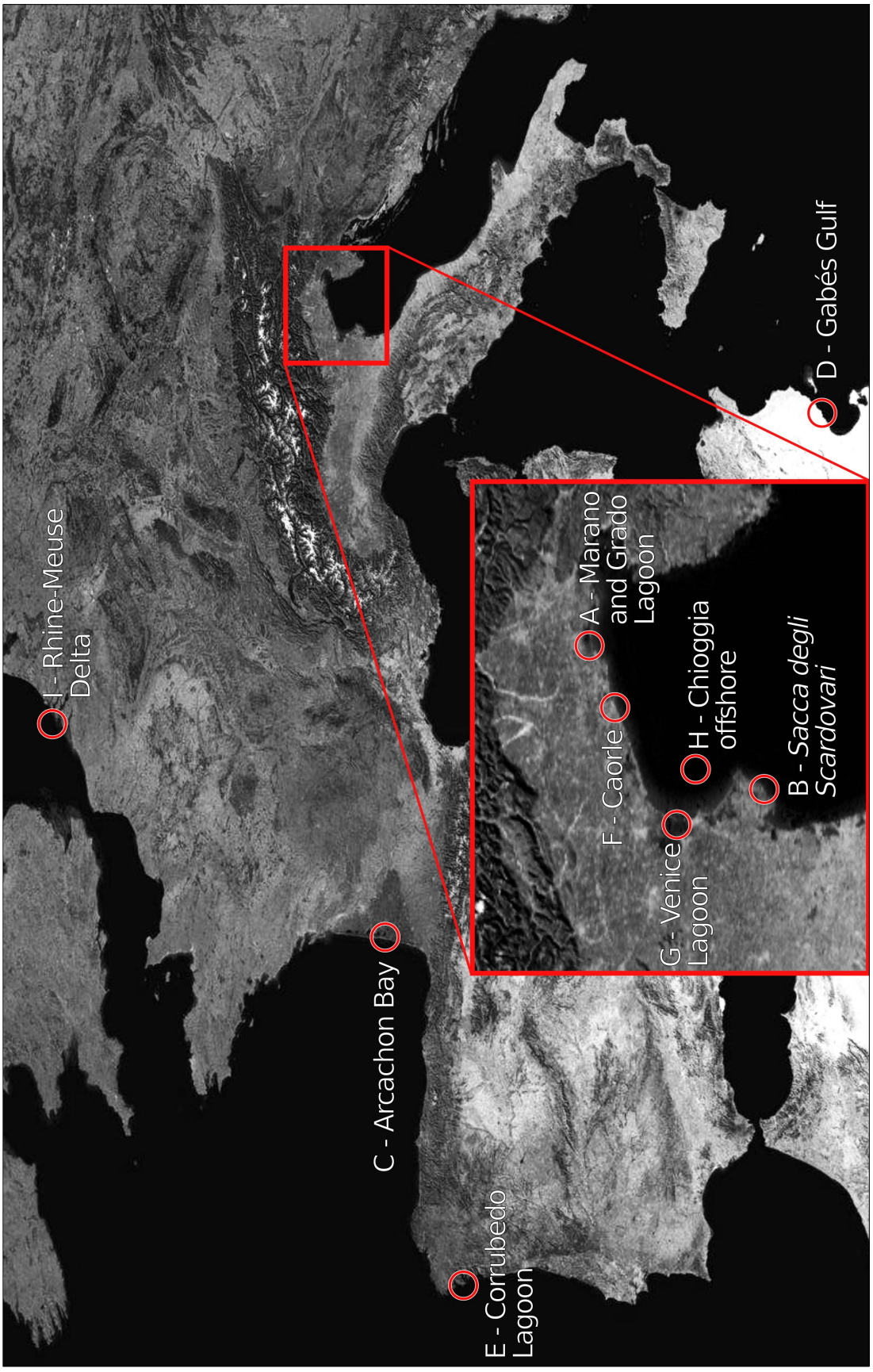

Figure 5.14: Overview of the location of the analogues introduced in the 5.3.1 and 5.3.2 paragraphs.

5.3.1 Geomorphological Analogues

Marano and Grado Lagoon

A well-fitting analogous can be found in the Marano and Grado lagoon, situated in the northern portion of the Adriatic Sea (A in figure 5.14); the current oceanographic characteristics (e.g. tidal range, shelf slope) may be considered quite similar to those involved during the formation of the study area (Storms et al., 2008). This lagoon, which covers an area of 160 km^2, is characterized by a well-developed, dendritic shaped tidal channel network, with three main tidal inlets that can reach a depth of 12 meters. These depths are due to an anthropic excavation of the inlets, in order to allow the circulation of large ships inside the lagoon; the natural depths would be around 6 m (Figure 5.15) (Fontolan et al., 2007, 2012).

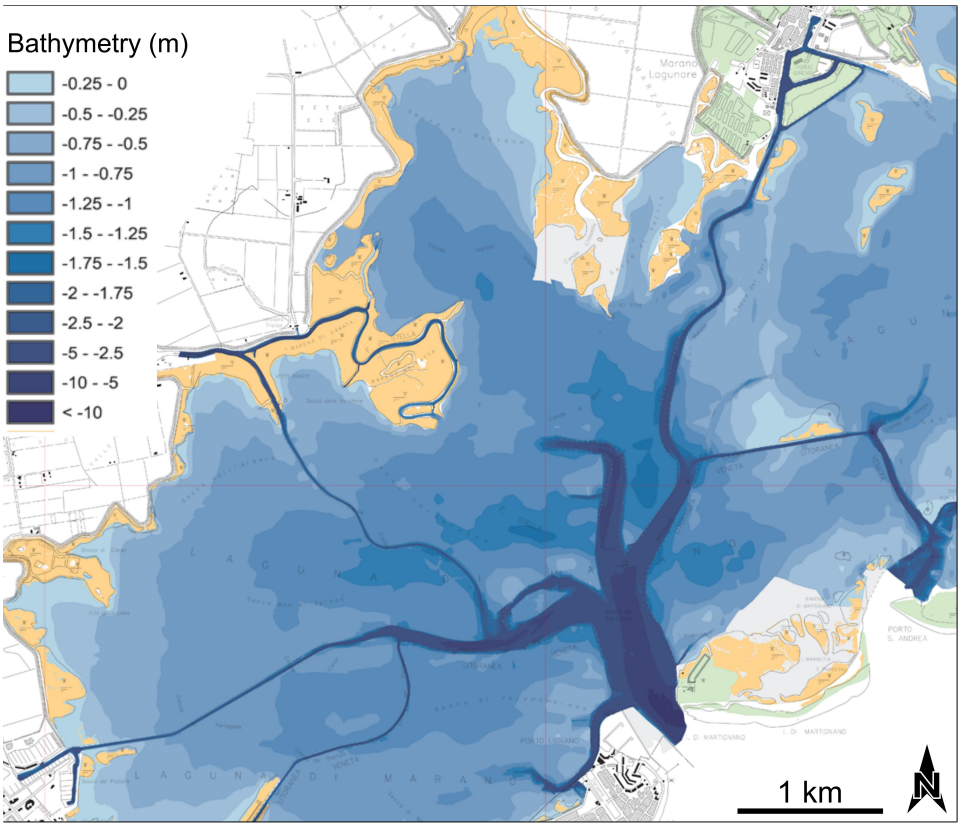

Figure 5.15: Bathymetry of the Lignano inlet of the Marano and Grado Lagoon; the depths of this tidal inlet is comparable to that of the study area. Modified from Carta batimetrica della Laguna di Marano e Grado, 2011.

Sacca degli Scardovari, Po Delta

Another analogous from the northern Adriatic is the *Sacca degli Scardovari* Lagoon, located in the Po Delta (B in figure 5.14) and genetically related to its progradation. The *Sacca degli Scardovari* Lagoon is confined between the *Gnocca Po* westward and the *Tolle Po* eastward. This lagoon covers an area of 30 km^2 and is characterized by two tidal inlets; the main one can reach a depth of 8 m. The bathymetry map does not show any evidence of a further tidal channelization (Figure 5.16). It must be notice that the progradation of the two deltaic branches which enclosed the lagoon occurred in the span of few tens of years, between the nineteenth and the twentieth century (Stafani & Vincenzi, 2005). Thus, the evolution of this lagoon area has been strongly influenced by the anthropogenic activity that boosted the total sedimentary load of the river.

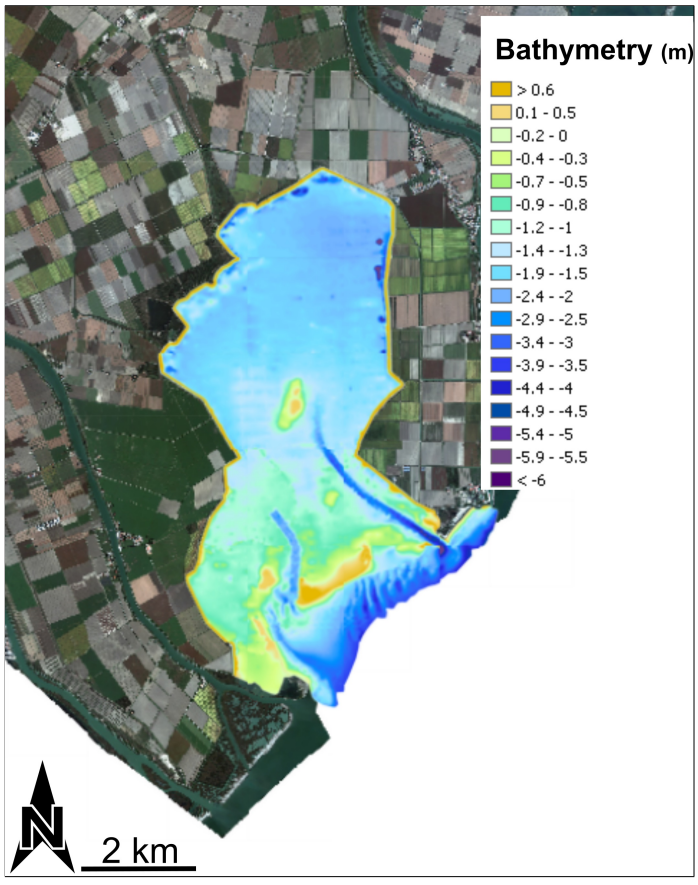

Figure 5.16: Bathymetry map of the*Sacca degli Scardovari* Lagoon. Images from *http://sil.deltapo.it/web/?portfolio=evoluzione-dei-fondali-lagunari*.

Arcachon Bay, France

An example from the Atlantic Ocean coasts is the Arcachon Bay (160 km[2]), situated in southern France, at the outlet of the Eyre River (C in figure 5.14). In this case the environmental conditions are quite different from the study area (the tidal range reaches 4 meters at Cap Ferret) but the main inlet channel can reach depths of more than 10 meters, thus displaying a morphology quite comparable to the tidal inlet recognized in the study area; the inner basin is characterized by a tidal channelization with an anastomosing trend (Figure 5.17) (Verger, 2005).

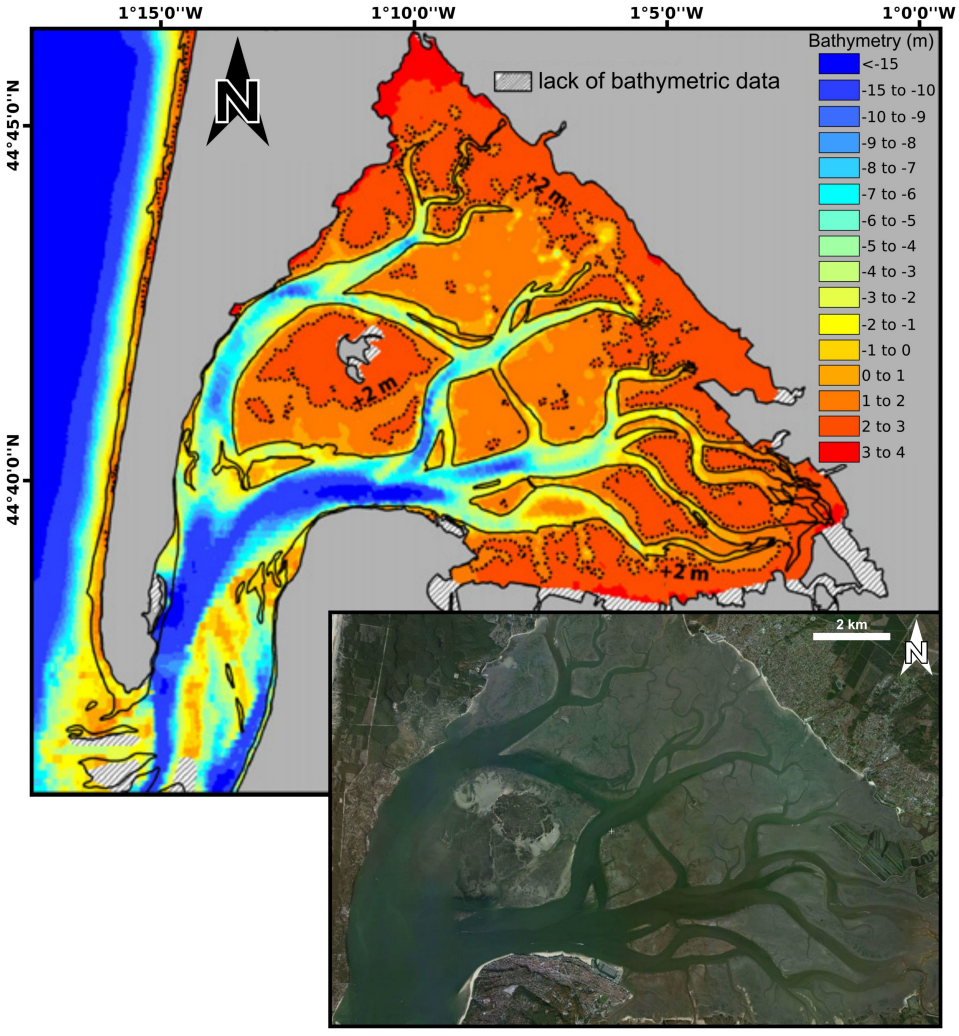

Figure 5.17: Bathymetry of the Arcachon basin; modified from Allard et al., 2009.

Gulf of Gabés Tidal Flat, Tunisia

An example of tidal flat developed under conditions similar to those of the study area may be found in Tunisia, in the Gulf of Gabés (D in figure 5.14); a well-developed, meandering-anastomosing shaped channelization characterized the area, which is not enclosed by any barrier. This morphology may be associated to the tidal channels visible on the *TS* (Figure 5.18).

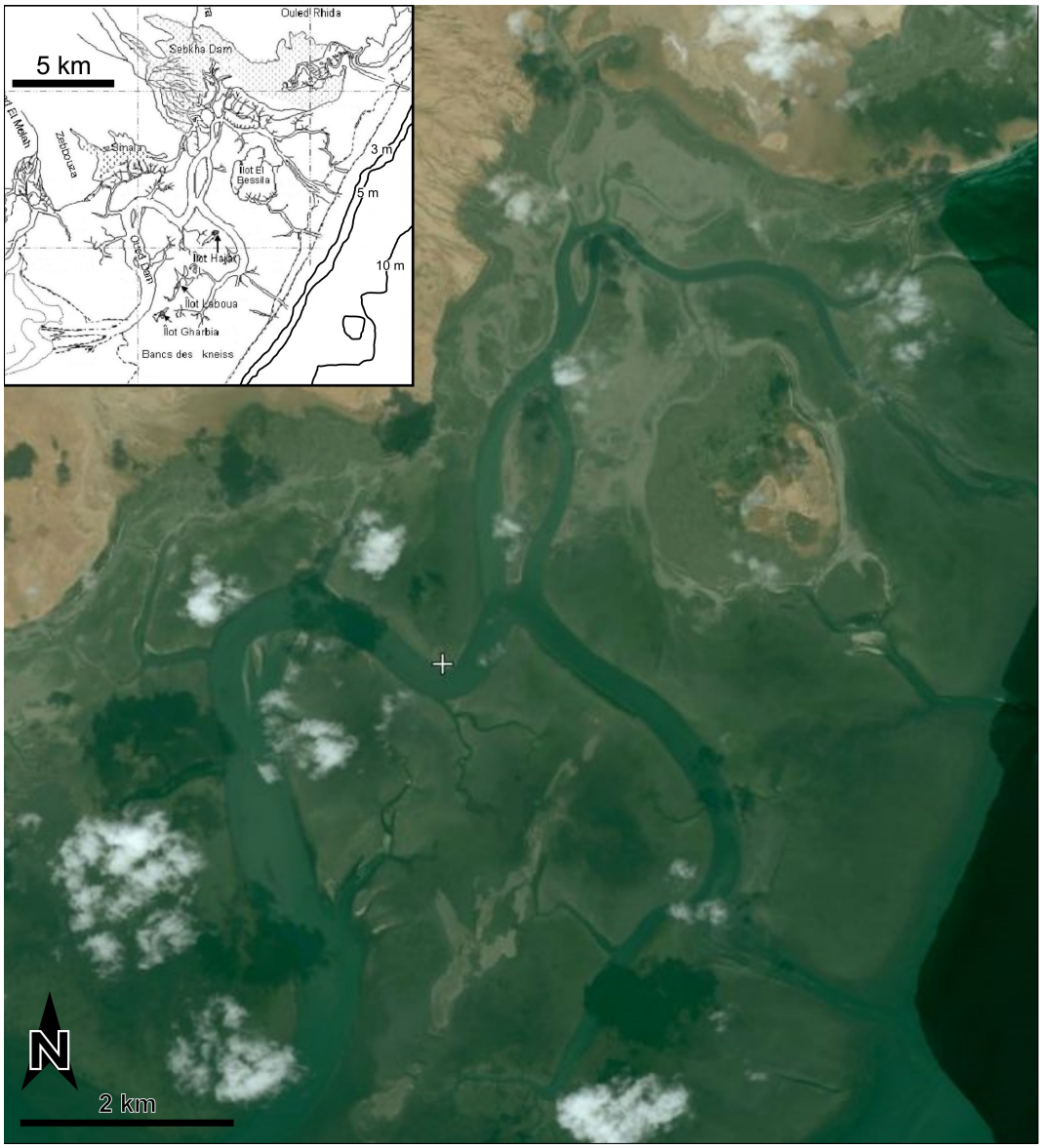

Figure 5.18: Satellite picture of the Gabés tidal flat. In the box on the corner is represented the bathymetry of the area, modified from Bali & Gueddari, 2011.

Corrubedo Lagoon, Spain

Another example from the Atlantic Ocean can be found in the north-east Spain coasts, in the Corrubedo beach-lagoon complex (E in figure 5.14). Once again the environmental conditions do not completely match with those of the study area (the mean tidal range reach 3 meters). The Corrubedo Lagoon is almost infilled and a unique tidal inlet connects it to the ocean (Figure 5.19); the tidal inlet is 450 m long and 610 m wide, and reaches a depth of 4 m (Vilas et al., 1988) with a meandering path. These characteristics link this area to the erosive channel of the *Transgressive Surface*.

Figure 5.19: Satellite picture of the almost infilled Corrubedo Lagoon.

5.3.2 Analogous Stratigraphy

Caorle coast

A transect based on a series of cores taken along the Caorle coast (F in figure 5.14) clearly shows an erosive feature with a depth at least of 10 m (the cores were not deep enough to reach the bottom of the erosive channel). This structure may be interpreted as a tidal inlet, probably active during the sea-level transgression and now completely sealed by the overlying coastal deposits (Figures 5.20 and 5.22) (Bondesan et al., 2008).

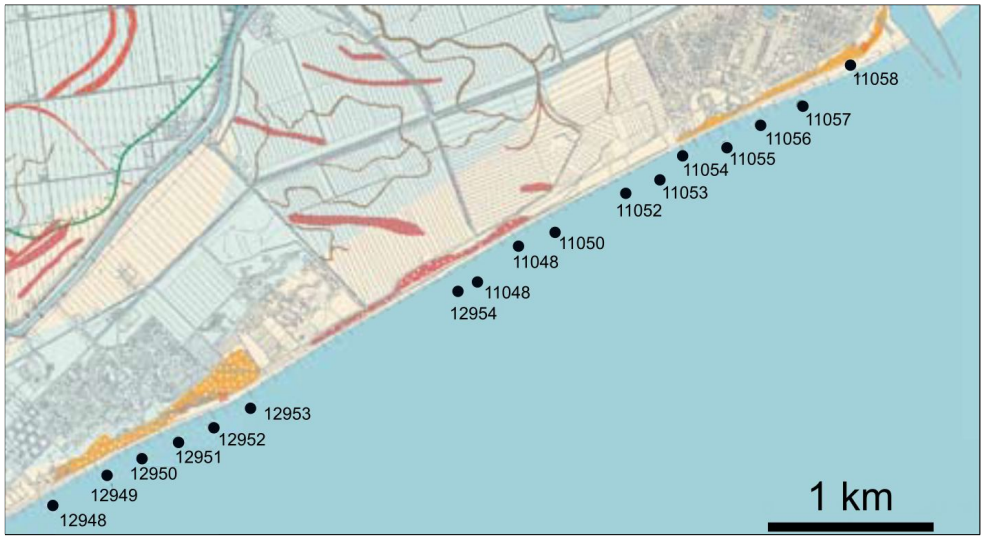

Figure 5.20: Location of the cores used for the cross section visible in 5.22. From Bondesan et al., 2008

Venice Lagoon

Seismic surveys carried out in the Venice Lagoon (G in figure 5.14) have evidenced some filled erosive scours comparable to the tidal inlet of the study area. These features may be therefore associated to paleo tidal inlets of the Venice Lagoon, now completely sealed by sediments and substituted by the tidal inlets of the present lagoon (Figure 5.21).

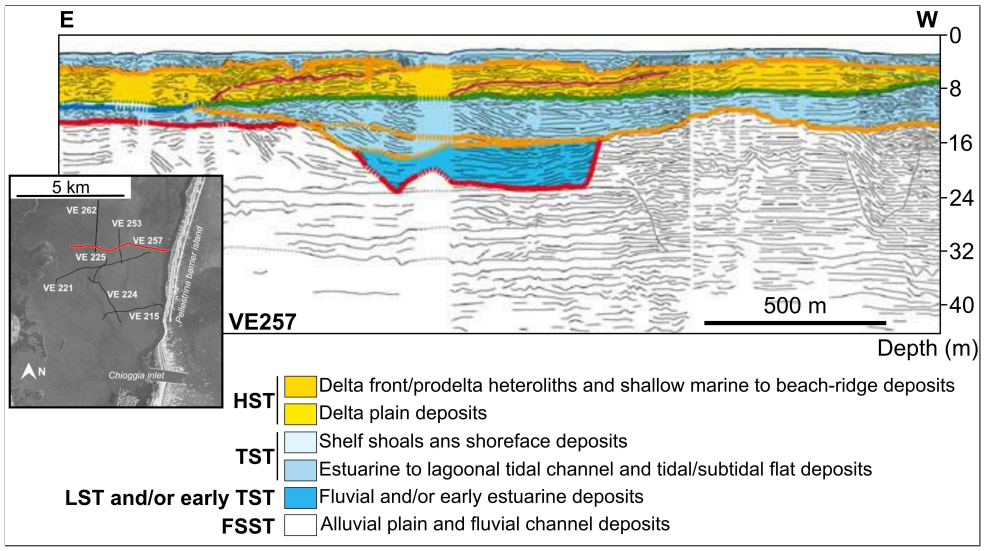

Figure 5.21: Longitudinal section of a paleo tidal inlet of the Venice Lagoon; it shows a length of about 500 m, a width of 200 m and a maximum depth of 10 m. Modified from Zecchin et al., 2009.

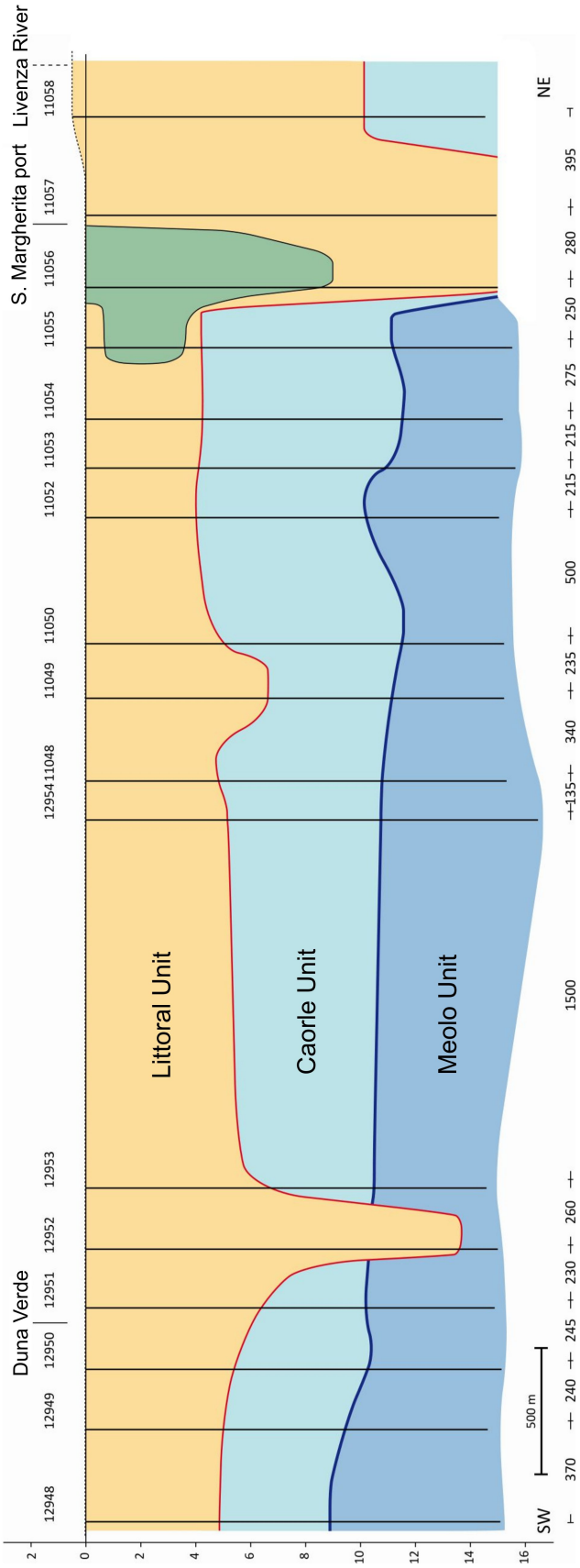

Figure 5.22: Inferred cross section of the deposits offshore the Caorle coast; the erosive channel interpreted as a tidal inlet is placed in the norther side of the section. From Bondesan et al., 2008.

Chioggia Offshore

In the area offshore Chioggia (H in figure 5.14) a deep erosive scour has been individuated by a seismic line; this incision shows a width of less then a kilometer and a depth up to 30 m and it has been interpreted as an infilled paleo valley (Figures 5.23 and 5.24) (Trincardi et al., 2011). The whole northern Adriatic area is characterised by several similar structures, which may be compared to the tidal inlet of the study area, both under the morphological and stratigraphic points of view. Therefore, these features may be reinterpreted in light of the work developed in this thesis.

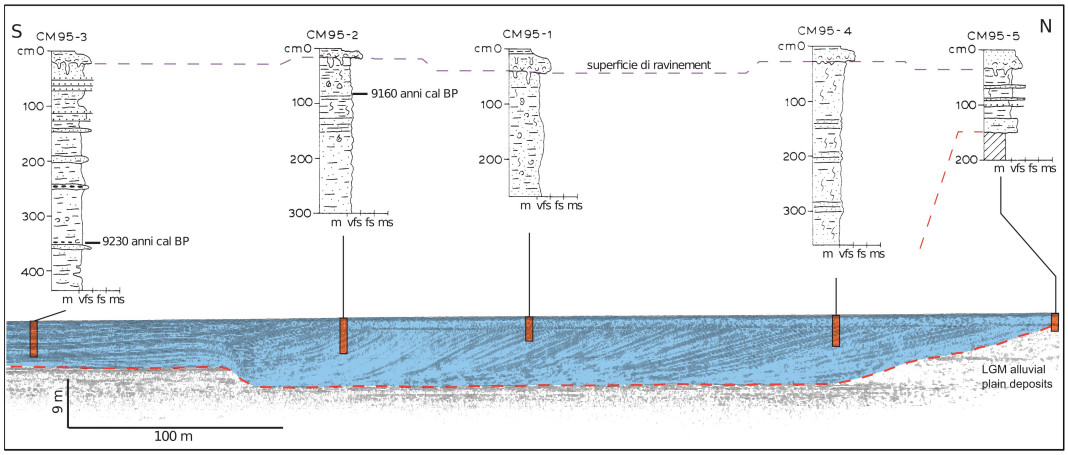

Figure 5.23: Cross section of the erosive scour offshore Chioggia. The cores highlight a fine grained infilling with a *Cerastoderma glaucum* fauna, typical of estuarine and lagoon environments. The sedimentary pattern shows a transition from downlap to onlap. From Trincardi et al., 2011.

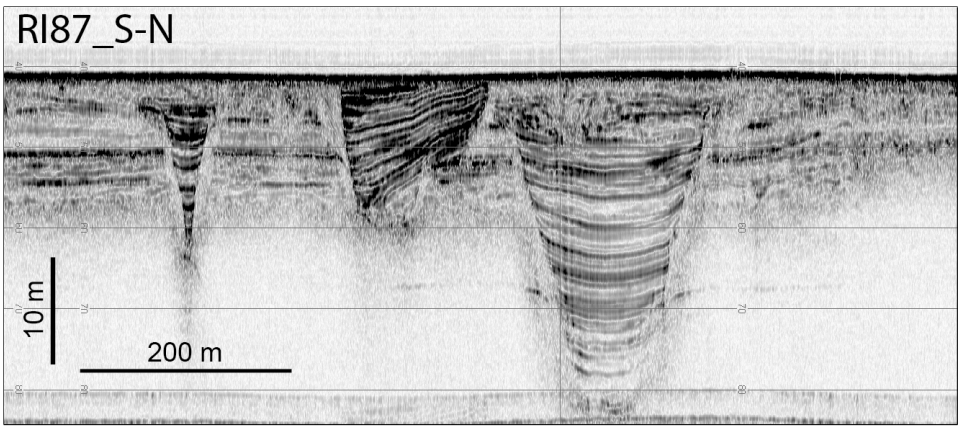

Figure 5.24: CHIRP line of the area offshore Chioggia; different generations of erosive channels are visible.

Rhine-Meuse Delta, Netherlands

Seismic lines realized along the Netherland coast, NE of the Rhine-Meuse mouth (I in figure 5.14), show particular erosive structure (Figures 5.25) interpreted as tidal channels (Hijma et al. 2010); the evolution of the back-barrier basin linked to these tidal channels was strongly influenced by the evolution of the Rhine-Meuse mouth and by the sea-level rise. The infilling of these channels started between 8.3 and 7.4 ka BP, in conjunction to a decrease rate of both sea-level rise and tidal-amplitude increasing, and a shifting of the Rhine distributary northward; these events lead to a decrease of the tidal prism, with a subsequent progressive size decrease of the tidal channels (Hijma et al. 2010).

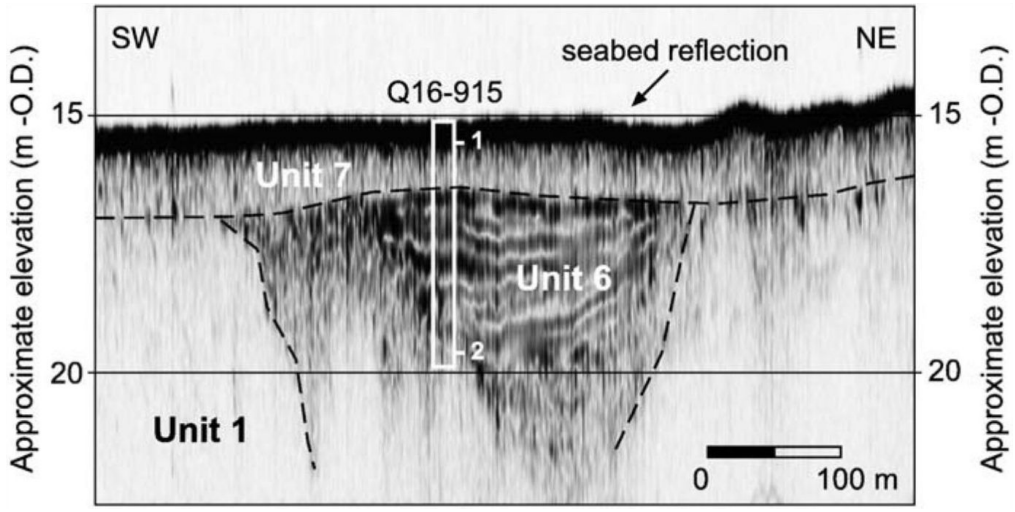

(a) CHIRP profile of a tidal inlet; the seismic response is strongly similar to that of the analyzed tidal inlet.

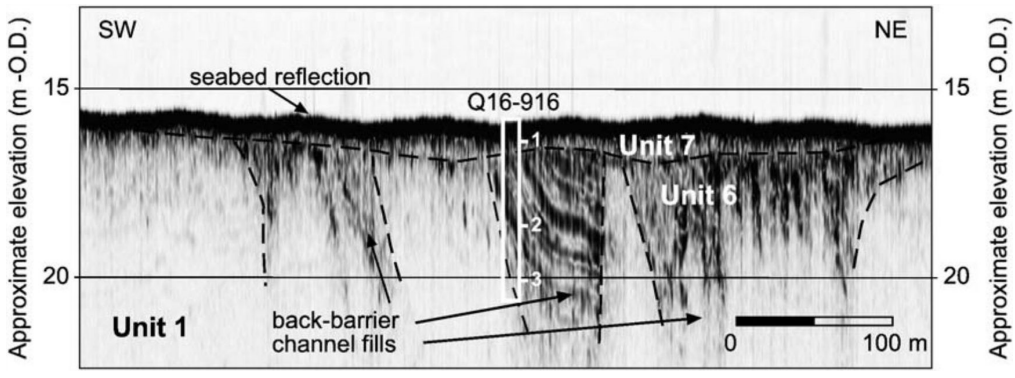

(b) CHIRP profile of a tidal-channel system showing a slight lateral migration.

Figure 5.25: Seismic records of a tidal system situated on the NE of the Rhine-Meuse delta; from Hijma et al. 2010.

Chapter 6

Conclusions

This work shows the potential of the very-high resolution analysis performed with the CHIRP sonar, which, if combined to core analysis, allows detailed reconstruction of the paleo geomorphology, of the stratigraphy and of the evolutionary history of an area; the method presented in this work can be easily applied to large submerged areas, therefore improving the knowledge of the processes which regulated the evolution of the Adriatic basin (e.g. climatic changes, response of the depositional systems).

The inferable evolutionary history of the study area began after the Last Glacial Maximum: the previous LGM alluvial plain gradually aggraded during the sea-level rise induced by the melting of the ice caps. At that moment (i.e. $10\,955 \pm 225$ cal. a BP) the area was characterized by meandering rivers with low ridges (about 1 m above the related floodplain) and an overall NE direction.

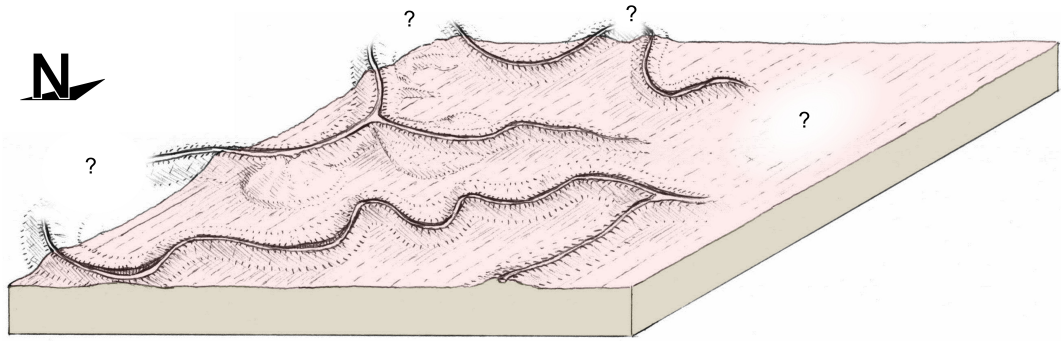

The alluvial plain was then intercepted by the transgressive shoreline which left a meandering erosive scour, probably due to tidal dynamics.

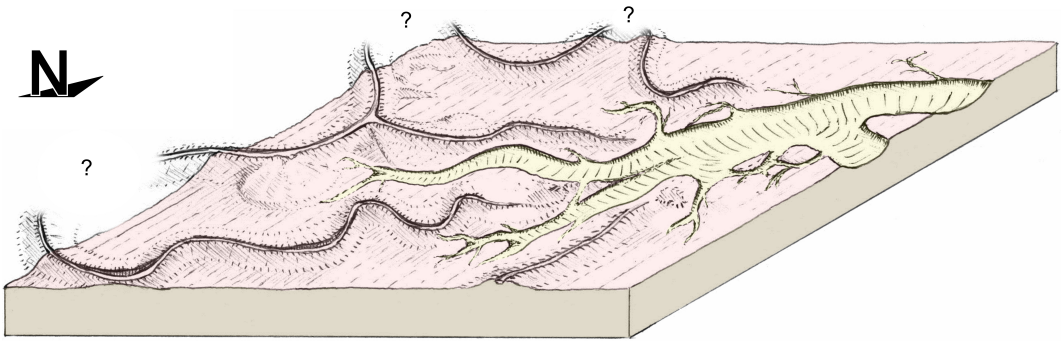

After this first ingression, the seismic lines show the overlapping of a pensile river network with ridges up to 3 meters and an overall SE direction; in the A area, situated roughly 5 km eastward from the analyzed area (Figure 2.9), the top of this unit is dated at $10\,307 \pm 115$ cal. a BP. The return to a continental depositional environment was probably induced by slight morphological changes, such as the isolation of the sea-loch induced by a sand spit.

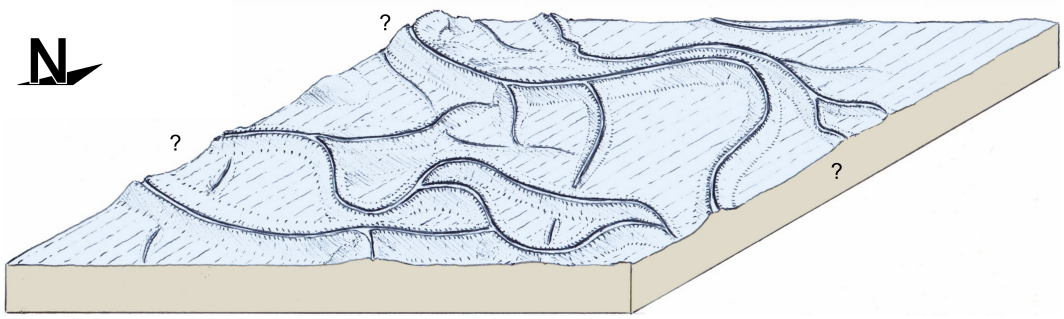

This ridge network was then occupied by the sea and likely transformed into a lagoon; in the eastern zone of the area a tidal inlet was dug by the rising sea, with a maximum depth of 10 meters in comparison with the *A Surface*.

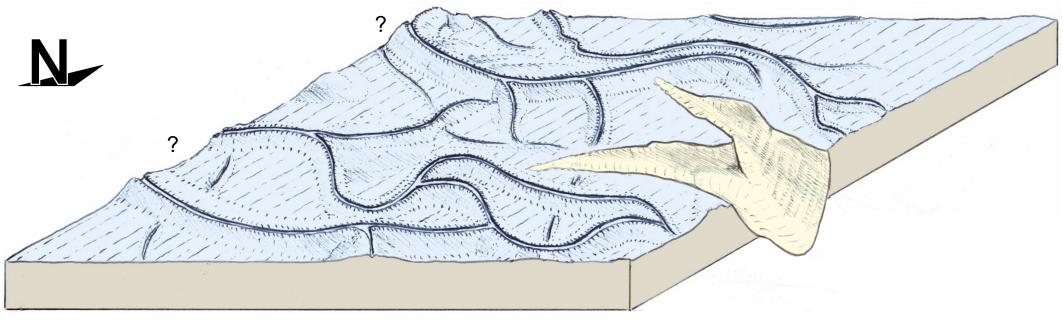

An attempt to dating the lagoon deposits has been made (Section 5.1) considering the relative sea-level curve for the Adriatic Sea from Correggiari et al., (1996). The inferred age for the top of these deposits lays between 9 800 and 9 850 cal. a BP. This date should coincide with the overstepping of the

lagoon (Green et al., 2013).

After the overstepping, these deposits were flattened by the ongoing sea-level rise, which marks the *Ravinement Surface* ($9\,845 \pm 115$ cal. a BP). At that moment the study area was completely submerged and the sea-level kept rising; the area then gradually shifted to the offshore position which still occupies.

Another interesting datum is provided by the attempt of estimating the subsidence of the area; this computations were carried out by the comparison between the sea-level rise curve from Correggiari et al., (1996) and the sea-level rise model for the northern Adriatic from (Lambeck et al., 2011). The obtained datum, 0.2 to 0.3 mm/year, is well comparable to the subsidence rates inferable by other published works (e.g. Antonioli et al., 2009).

The reconstructed 3D environments were also used in order to estimate the volumes of the sedimentary bodies enclosed between key surfaces or which constitute the main fluvial ridges.

The most important result achieved by this work is the identification of the tidal inlet nature of the deep erosive scour, which fixes the position of the 9.8 ka sea-level at -33 m on the MSL[3]. Several similar features, characterized by absence of continuity and rapid deepening, are spread in the whole northern Adriatic Holocenic geological record (Trincardi et al., 2011), and they are generally interpreted as segments of paleovalley systems (cf. Blum et al., 2013). These morphologies are well comparable with the tidal inlet of this work, which completely developed in about 800 m, between -34 m and -44 m, thus reaching a maximum incision of 10 m; this work provides the basis for a new interpretation of these features as tidal inlets. Tidal inlets are precious indicators of the paleo sea-level position and are characterized by a well-recognizable seismic response in the CHIRP profiles. This thesis thus suggests a way to further improve the knowledge of the Holocenic sea-level evolution for the Adriatic basin.

[3]The error estimate for this datum varies between -2 m and +0.5 m. The position of the lagoon deposits may not be the same of the paleo sea-level, thus producing this uncertainty range. Other minor errors are induced by problems in the measurements and in the bathymetry (e.g. dGPS, tidal range, atmospheric pressure).

References

Allard J., Chaumillon E., Féniès H. (2009) - *A synthesis of morphological evolutions and Holocene stratigraphy of a wave-dominated estuary: The Arcachon lagoon,SW France.* Continental Shelf Research, 29, 957 - 969,

Allen P. A., Allen J. R. (2005) - *Basin Analysis - Principles and applications, second edition.* Blackwell publishing.

Amorosi A., Fontana A., Antonioli F., Primon S., Bondesan A. (2008) - *Post-LGM sedimentation and Holocene shoreline evolution in the NW Adriatic coastal area.* GeoActa, Bologna, 7, 41 - 67.

Antonioli F., Ferranti L., Fontana A., Amorosi A., Bondesan A., Braitenberg C., Dutton A., Fontolan G., Furlani S., Lambeck K., Mastronuzzi G., Monaco C., Spada G., Stocchi P. (2009) - *Holocene relative sea-level changes and vertical movements along the Italian and Istrian coastlines.* Quaternary International, 206, 102 - 133.

Argnani A., Frugoni F. (1997) - *Foreland deformation in the Central Adriatic and its bearing on the evolution of the Northern Apennines.* Annali di geofisica, XL, 3, 771 - 780.

Asioli A., Trincardi F., Lowe J. J., Aritzegui D., Langone L., Oldfield F. (2001) - *Sub-millennial scale climatic oscillations in the central Adriatic during the Lateglacial: palaeoceanographic implications.* Quaternary Science Reviews, 20, 1201 - 1221.

Bali M., Gueddari M. (2011) - *Les chenaux de marée autour des îles de Kneiss, Tunisie: sédimentologie et évolution.* Hydrological Sciences Journal, 56, 498 - 506.

Bard E., Hamelin B., Fairbanks R. G. (1990) - *U-Th ages obtained by mass spectrometry in corals from Barbados: sea level during the past 130,000 years.* Nature 346, 456 - 458.

Berendsen H. J. A., Stouthamer E. (2001) - *Palaeogeographic development of the Rhine-Meuse delta, The Netherlands.* Koninklijke Van Gorcum, Assen.

Bernoulli D. (2001) - *Mesozoic-Tertiary carbonate platforms, slopes and basins of the external Apennines and Sicily.* Anatomy of an Orogen - The Apennines and Adjacent Mediterranean Basins, Springer, 307 - 325.

Bertotti G., Casolari E., Picotti V. (1999) - *The Gargano Promontory: a Neogene contractional belt within the Adriatic plate* Terra Nova, 11, 168 - 173.

Blanchon P., Shaw J. (1995) - *Reef drowning during the last deglaciation: Evidence for catastrophic sea-level rise and ice-sheet collapse.* Geology, 23, 4 - 8.

Blum M. D., Törnqvist T. (2000) - *Fluvial responses to climate and sea-level change: a review and look forward.* Sedimentology, 47, 2 - 48.

Blum M., Martin J., Milliken K., Garvin M. (2013) - *Paleovalley systems: Insights from Quaternary analogs and experiments.* Earth-Science Reviews, 116, 128 - 169.

Bondesan, M., Castiglioni, G.B., Elmi, C., Gabbinelli, G., Marocco, R., Pirazzoli, P.A., Tomasin, A., (1995) - *Coastal areas at risk from storm surges and sea-level rise in Northeastern Italy.* Journal Coastal Research, 11, 1354 - 1379.

Bondesan A., Bassan V., Bertani B., Fontana A., Fontolan G., Furlanetto P., Magri S., Meneghel M., Mozzi P., Primon S., Rosselli R., Vitturi A. (2004) - *Note illustrative della carta geomorfologica della provincia di Venezia.* Provincia Di Venezia, Ufficio Difesa del Suolo.

Bondesan A., Abbà T., Bassan V., Bisazza A., Fagarazzi E., Fontana A., Francese R., Furlanetto P., Mazzuccato A., Mozzi P., Piovan S., Primon S., Stefani C., Vitturi A. (2008) - *Le unitá geologiche della provincia di Venezia.* Provincia Di Venezia, Servizio Geologico e Difesa del Suolo.

Triches A., Pillon S., Bezzi A., Lipizer M., Gordini E. (2011) - *Carta batimetrica della Laguna di Marano e Grado. Note illustrative*. Arti Grafiche Friulane / Imoco spa (Ud).

Castellarin A. (2001) - *Alps-Apennines and Po Plain-frontal Apennines relations*. Anatomy of an Orogen - The Apennines and Adjacent Mediterranean Basins, Springer, 177 - 195.

Cattaneo A., Correggiari A., Langone L., Trincardi F. (2003) - *The late-Holocene Gargano subaqueous delta, Adriatic shelf: Sediment pathways and supply fluctuations*. Marine Geology, 193, 61 - 91.

Catuneanu O. (2006) - *Principles of sequence stratigraphy*. Elsevier, 105 - 234.

CNR, Consiglio Nazionale delle Ricerche. (1990-1992) - *Structural model of Italy. Scale 1:500.000, sheets I-II-III-IV*. S.EL.CA. Publisher, Firenze.

Correggiari A., Roveri M., Trincardi F. (1996) - *Late Pleistocene and Holocene evolution of the north Adriatic Sea*. Il Quaternario, 9(2), 697 - 704.

Correggiari A., Cattaneo A., Trincardi F. (2001) - *The modern Po Delta system: Lobe switching and asymmetric prodelta growth*. Marine Geology, 222 - 223, 49 - 74.

Correggiari A., Aguzzi M., Remia A., Preti M (2011) - *Caratteristiche sedimentologiche e stratigrafiche dei giacimenti sabbiosi in Mare Adriatico Settentrionale utilizzabili per il ripascimento costiero*. Studi costieri, 19, 11 - 31.

D'Alpaos A., Lanzoni S., Marani M. (2005) - *Tidal network ontogeny: Channel initiation and early development* Journal of Geophysical research, 110, F02001.

Deschamps P., Durand N., Bard E., Hamelin B., Camoin G., Thomas A. L., Henderson G. M., Okuno J., Yokoyama Y. (2012) - *Ice-sheet collapse and sea-level rise at the Bølling warming 14,600 years ago*. Nature, 483, 559 - 564.

Fairbanks R.G. (1989) - *17.000-year glacio-eustatic sea level record: influence of glacial melting rates on the Younger Dryas event and deep-ocean circulation*. Nature, 342, 637 - 642.

Ferranti, L., Antonioli, F., Mauz, B., Amorosi, A., Dai Pra, G., Mastronuzzi, G., Monaco, C., Orrù , P., Pappalardo, M., Radtke, U., Renda, P., Romano, P., Sansò, P., Verrubbi, V., (2006) - *Markers of the last interglacial sea level highstand along the coast of Italy: tectonic implications*. Quaternary International, 145 - 146, 30 - 54.

Fleming K., Johnston P., Zwartz D., Yokoyama Y., Lambeck K., Chappell J. (1998) - *Refining the eustatic sea-level curve since the Last Glacial Maximum using far- and intermediate-field sites*. Earth and Planetary Science Letters, 163, 327 - 342.

Fontana A., Mozzi P., Bondesan A. (2008) - *Alluvial megafans in the Venetian-Friulian Plain (north-eastern Italy): Evidence of sedimentary and erosive phases during Late Pleistocene and Holocene*. Quaternary International, 189, 71 - 90.

Fontana A., Correggiari A., Juračić M. (2014) - *Il Mare Adriatico dall'ultima glaciazione a oggi: evoluzione geomorfologica e aspetti paleoambientali*. Adriatico senza confini, via di comunicazione e crocevia di popoli nel 6000 a.C. Guida della mostra in Udine, 13/10/2014 - 22/2/2015, Museo Friulano Storia Naturale, Udine, 18 - 23.

Fontana A., Mozzi P., Marchetti M. (2014) - *Alluvial fans and megafans along the southern side of the Alps*. Sedimentary Geology, 301, 150 - 171.

Fontolan G., Pillon S., Delli Quadri S., Bezzi A. (2007) - *Sediment storage at tidal inlets in northern Adriatic lagoons: Ebb-tidal delta morphodynamics, conservation and sand use strategies*. Estuarine, Coastal and Shelf Science, 75, 261 - 277.

Fontolan G., Pillon S., Bezzi A., Villalta R., Lipizer M., Triches A., D'Aietti A. (2012) - *Human impact and the historical transformation of saltmarshes in the Marano and Grado Lagoon, northern Adriatic Sea*. Estuarine, Coastal and Shelf Science, 113, 45 - 56.

Gasperini L., Stanghellini G. (2009) - *An interactive computer program for processing and interpretation of high-resolution seismic reflection profiles*. Computers & Geosciences, 35(7), 1497-1507.

Green A. N., Cooper J. A. G., Leuci R., Thackeray Z. (2013) - *Formation and preservation of an overstepped segmented lagoon complex on a high-energy continental shelf.* Sedimentology, 60, 1755 - 1768.

Hanebuth T. J. J., Stattegger K., Bojanowski A. (2008) - *Termination of the Last Glacial Maximum sea-level lowstand: The Sunda-Shelf data revisited.* Global and Planetary Change, 66, 76 - 84.

Hengl T., Reuter H. I. (2009) - *Geomorphometry: concepts, software, applications.* Developments in Soil Science, 33, Elsevier, 772 pp.

Hijma M. P., van der Spek A. J. F., van Heteren S. (2010) - *Development of a mid-Holocene estuarine basin, Rhine-Meuse mouth area, offshore The Netherlands.* Marine Geology, 271, 198 - 211.

Hughes Z. J. (2012) - *Tidal Channels on Tidal Flats and Marshes.* Principles of Tidal Sedimentology, Springer, 269 - 300.

Contribution of Working Groups I, II and III to the Fifth Assessment Report of the Intergovernmental Panel on Climate Change [Core Writing Team, R.K. Pachauri and L.A. Meyer (eds.)] (2014)- *IPCC, 2014: Climate Change 2014: Synthesis Report.* IPCC, Geneva, Switzerland, 151 pp.

Lambeck K., Antonioli F., Purcell A., Silenzi S. (2004) - *Sea-level change along the Italian coast for the past 10,000 yr.* Quaternary Science Reviews, 23, 1567 - 1598.

Lambeck K., Antonioli F., Anzidei M., Ferranti L., Leoni G., Scicchitano G., Silenzi S. (2011) - *Sea level change along the Italian coast during the Holocene and projections for the future.* Quaternary International, 232,250 - 257.

Liker M., Lučić M., Barišić B., Repanić M., Grgić I., Bašić T. (2008) - *Analysis of Recent Global Geopotential Models Over the Croatian Territory* Gravity, Geoid and Earth Observation, International Association of Geodesy Symposia, 135, 281 - 288.

Martinson D.G., Pisias N.G., Hayes J.D., Imbrie J., Moore T.C., Shackleton N.J. (1987) - *Age dating and the orbital theory of the ice ages-development of a high-resolution 0 to 300,000 year chronostratigraphy.* Quaternary Research, 27, 1 - 29.

Maselli V., Trincardi F., Cattaneo A., Ridente D., Asioli A. (2010) - *Subsidence pattern in the central Adriatic and its influence on sediment architecture during the last 400 kyr*. Journal of Geophysical Research, 115, B12106, doi:10.1029/2010JB007687.

Miola A., Bondesan A., Corain L., Favaretto S., Mozzi P., Piovan S., Sostizzo I. (2006) - *Wetlands in the Venetian Po Plain (northeastern Italy) during the Last Glacial Maximum: Interplay between vegetation, hydrology and sedimentary environment*. Review of Palaeobotany and Palynology, 141, 53 - 81.

Morley C. K. (1986) - *A classification of thrust fronts*. AAPG Bull., 70, 371-378.

Moscon G., Correggiari A., Stefani C., Fontana A., Remia A. (in press) - *Very-high resolution reconstruction of a transgressive deposit in the northern Adriatic Sea (Italy)*. Alpine and Mediterranean Quaternary, 28(2).

Orange D., Garcia-Garcia A., Lorenson T., Nittrouer C., Milligan T., Miserocchi S., Langone L., Correggiari A., Trincardi F. (2005) - *Shallow gas and flood deposition on the Po Delta*. Marine Geology, 222 - 223, 159 - 177.

Rossato S. (2009) - *Geomorfologia dell'Alto Adriatico: il contributo della missione oceanografica SomRISA09*. Quaderni di dottorato, Dipartimento di Geografia "G. Morandini", 4, 213 - 219.

Roveri M., Boscolo Gallo A., Rossi M., Gennari R., Iaccarino S. M., Lugli S. (2005) - *The Adriatic foreland record of Messinian events (Central Adriatic Sea, Italy)*. GeoActa, 4, 139 - 157.

SeaBeam Instruments (2000) - *Multibeam sonar, theory of operation*.

Stefani M., Vincenzi S. (2005) - *The interplay of eustasy, climate and human activity in the late Quaternary depositional evolution and sedimentary architecture of the Po Delta system*. Marine Geology, 222 - 223, 19 - 48.

Stoker M. S., Pheasant J. B., Josenhans H. (1997) - *Seismic methods and interpretation*. Glaciated continental margins, Springer, 9 - 26.

Storms J. E. A., Weltje G. J., Terra G. J., Cattaneo A., Trincardi F. (2008) - *Coastal dynamics under conditions of rapid sea-level rise: Late Pleistocene to*

Early Holocene evolution of barrier - lagoon systems on the northern Adriatic shelf (Italy). Quaternary Science Reviews, 27, 1107 - 1123.

Syvitski J. P. M., Kettner A. J. (2007) - *On the flux of water and sediment into the Northern Adriatic Sea.* Continental Shelf Research, 27, 296 - 308.

Tir M., Rožić N., Razumović I. (2013) - *The quality of the croatian height reference system.* 13th SGEM GeoConference on Informatics, Geoinformatics And Remote Sensing, 2, 487 - 494.

Trincardi F., Argnani A., Correggiari A., Foglini F., Rovere M., Angeletti L., Asioli A., Campiani E., Cattaneo A., Gallerani A., Piva A., Remia A., Ridente D., Taviani M.(2011) - *Note illustrative della carta geologica dei mari Italiani alla scala 1:250.000, foglio Venezia.* ISPRA.

Asioli A., Bortoluzzi G., Cattaneo A., Correggiari A., Fabbri A., Gamberi F., Ligi M., Penitenti D., Roveri M., Taviani M. (2011) - *Note illustrative della carta geologica dei mari Italiani alla scala 1:250.000, foglio Ravenna.* ISPRA.

Trincardi F., Campiani E., Correggiari A., Foglini F., Maselli V., Remia A. (2014) - *The bathymetry of the Adriatic Sea: the legacy of the last eustatic cycle and the impact of modern sediment dispersal.* Journal of Maps, 10(1), 151 - 158.

Vai G. B., Martini I. P. (2001) - *Geomorphologic Setting.* Anatomy of an Orogen - The Apennines and Adjacent Mediterranean Basins, Springer, 1 - 4.

Verger F. (2005) - *Marais et estuaires du littoral français.* Belin, Paris.

Vilas F., Sopena A., Rey L., Ramos A., Nombela M. A., Arche A. (1988) *The Corrubedo tidal inlet, Galicia, N. W. Spain: sedimentary processes and facies.* P.L. de Boer et al. (eds.), Tide-Influenced Sedimentary Environments and Facies, 183 - 200.

Zecchin M., Brancolini G., Tosi L., Rizzetto F., Caffau M., Baradello L. (2009) - *Anatomy of the Holocene succession of the southern Venice lagoon revealed by very high-resolution seismic data.* Continental Shelf Research, 29, 1343 - 1359.

List of Figures